Protein Interaction Partners of ASAP1 and Their Role in Metastasis

DISSERTATION

Submitted to the

Combined Faculties for the Natural Sciences and for Mathematics

Of the Ruperto-Carola University of Heidelberg, Germany

For the degree of

Doctor of Natural Sciences

Anna Poletti

2012

Referees:

Univ.-Prof. Dr. Jonathan P. Sleeman

Centrum für Biomedizin und Medizintechnik Mannheim (CBTM)

Univ.-Prof. Dr. Uwe Strähle

Forschungszentrum Karlsruhe, Institut für Toxikologie und Genetik

INDEX

ZUSAMMENFASSUNG

Die Metastasenbildung ist das letzte, lebensgefährliche Stadium eines Tumors. Deswegen ist es wesentlich zu verstehen, wie dieser Prozess reguliert wird, um einen therapeutischen Eingriff zu ermöglichen. ASAP1 (Arf-GAP mit SH3-Domänen, Ankyrin-repeat Proteinen and PH-Domänen) wurde während eines unvoreingenommenen genetischen Screenings von Genen entdeckt, die an der Metastasenbildung beteiligt sind. Anschließend wurde gezeigt, dass dieses Protein die Motilität und Invasivität von Tumorzellen fördert. In einem Pankreaskarzinom-Modell wurde durch „loss-of-function“ und „gain-of-function“ Versuche bewiesen, dass ASAP1 eine funktionelle Rolle bei der Regulation der Metastasierung spielt. Die Expression von ASAP1 in Patienten mit kolorektalem Karzinom korreliert stark mit einer kurzfristigen Überlebensrate ohne Metastasenbildung und einer schlechten Prognose. Auf molekularer Ebene zeigten Koimmunpräzipitationsexperimente, dass ASAP1 sowohl h-prune als auch Nm23-H1 (nicht-metastatisches Protein 23-H1) binden kann, die beide auch in die Regulation des metastatischen Prozesses involviert sind. Zielsetzung meiner Arbeit war es, durch die Verwendung der hochmetastasierenden Brustzelllinie MDA MB 231, die ASAP1, Nm-23H1 und h-prune endogen exprimiert, zu untersuchen, wie ASAP1 zur Metastasenbildung beiträgt. Dabei habe ich folgende Aspekte analysiert: a) den Einfluss von ASAP1 und seiner Interaktionspartner bei der Internalisierung von EGF; b) den Einfluss von Proteinkomplexen, die ASAP1 enthalten, auf die Zellmotilität; c) weitere mögliche Interaktionspartner, die die Aktivität von ASAP1 beeinflussen könnten. Meine Ergebnisse haben gezeigt, dass weder Nm23-H1 noch h-prune, trotz ihrer Rolle bei der Regulation der Motilität und der Metastasenbildung, den Einfluss von ASAP1 auf die Zellmigration beeinflussen. Außerdem wirken sich diese beiden Proteine auch nicht auf die Fähigkeit von ASAP1 aus, die Internalisierung von EGF zu regulieren. Ich habe dann meinen Schwerpunkt auf andere mögliche Proteine gelegt, die zur ASAP1-vermittelten Metastasenbildung beitragen könnten. Dafür habe ich ein Screening zur Findung potentieller Interaktionspartner durchgeführt, die SH3- Domänen besitzen, da die SH3-bindende Domäne von ASAP1 äußerst wichtig für seine motilitätsfördernde Aktivität ist. Dadurch habe ich SLK (Ste–20 Like Kinase) als einen neuen Interaktionspartner von ASAP1 ermittelt und seine Effekte auf die Funktion von ASAP1 analysiert. Obwohl SLK mit

ASAP1 koimmunpräzipitierte und selbst in die Regulation der Zellmotilität involviert ist, konnte dieses Protein nicht die zellmotilitätsfördernde Aktivität von ASAP1 beeinflussen. Insgesamt zeigen meine Ergebnisse die Rolle von ASAP1 sowohl bei der Begünstigung der Zellmotilität als auch bei der Förderung der Rezeptorinternalisierung im Kontext von Tumorzellen. Beides sind wichtige biologische Prozesse, die die Metastasierung regulieren.

ABSTRACT

Metastasis formation is the life-threatening end stage of cancer. It is therefore vital to understand how this process is regulated so that therapeutic intervention becomes possible. ASAP1 (Arf-GAP with SH3-domains, Ankyrin-repeats and PH-domains) was discovered in an unbiased genetic screen for genes that are involved in metastasis formation. Subsequently it was shown that this protein promotes tumor cell motility and invasiveness. Loss and gain of function experiments in a pancreatic carcinoma model demonstrated a functional role for ASAP1 in regulating metastasis. In human colorectal cancer patients ASAP1 expression strongly correlates with short metastasis-free survival and poor prognosis. At the molecular level, co-immunoprecipitation experiments have shown that ASAP1 binds to both h-prune and Nm23-H1 (Non-Metastatic protein 23-H1), proteins that are also involved in the metastatic process. Using the highly metastatic breast cell line MDA-MB-231 that endogenously expresses ASAP1, Nm-23H1 and h-prune, in my PhD thesis I aimed to characterize how ASAP1 contributes to metastasis by addressing the following issues: a) the influence of ASAP1 and its interaction partners on the internalization of EGF; b) effects of ASAP1-containing protein complexes on cellular motility; c) further possible interaction partners that may modulate ASAP1 activity. My results showed that, despite their role in regulating motility and metastasis formation, neither Nm23-H1, nor h-prune influence the effects of ASAP1 on cell migration. Moreover, these two proteins also do not affect the ability of ASAP1 to regulate the internalization of EGF. I then focused my attention on other possible proteins that might contribute to ASAP1-mediated metastasis by screening for potential SH3 domain-bearing interaction partners, because the SH3 binding domain of ASAP1 is crucial for its motility-promoting activity. I thereby identified SLK (Ste-20 Like Kinase) as a new interaction partner of ASAP1, and analyzed its effects on ASAP1 function. Although SLK co-immunoprecipitated with ASAP1, and is itself involved in the control of cell motility, this protein did not affect the motility-promoting activity of ASAP1. Together, my results demonstrate the role of ASAP1 in promoting both cell motility and receptor internalization in the context of tumor cells, important biological processes that regulate metastasis formation.

1. INTRODUTCION

1.1 Cancer

1.1.1 General features

The terms neoplasia, tumor and cancer all refer to a common pathological state, namely the aberrant growth of a mass of proliferating cells that have been transformed, caused by a variety of stimuli. Although many of the triggering events that lead to cellular transformation have been identified, including certain viral and bacterial infections, chemical compounds and radiation, the etiology of the majority of tumors is still unknown. There are, nevertheless, several proved risk factors, such as age, gender, life style, race and the environment. Our scarce knowledge in this pathology is reflected by the fact that cancer is one of the leading causes of death in developed countries, counting for approximately 25% of all deaths in 2008 (Jemal et al., 2008).

In 2000 Hanahan and Weinberg proposed a way to characterize cancer in "six hallmarks of cancer", which include the features the tumor acquires during its development, and distinguishes it from healthy tissues (Hanahan and Weinberg, 2000). These are:

- Sustaining proliferative signalling
- Evading growth suppressors
- Resisting cell death
- Enabling replicative immortality
- Inducing angiogenesis
- Activating invasion and metastasis

The first version of the hallmarks of cancer has now been revised to take into consideration that a tumor mass is not composed of just tumor cells, but is a complex interaction between the transformed cells and recruited cells, the primary tissue and the host environment (Hanahan and Weinberg, 2011). These hallmarks have been integrated with the concept of "enabling characteristics" that are required for tumor development. Two of these enabling characteristics are genomic instability and

mutation of cancer cells, and tumor-promoting inflammation. Some authors even consider inflammation as the seventh hallmark of cancer (Colotta et al., 2009). To complete the scenario, other factors have been included, namely two additional "emerging hallmarks": reprogramming energy metabolism, and evading immune destruction (*Figure 1*).

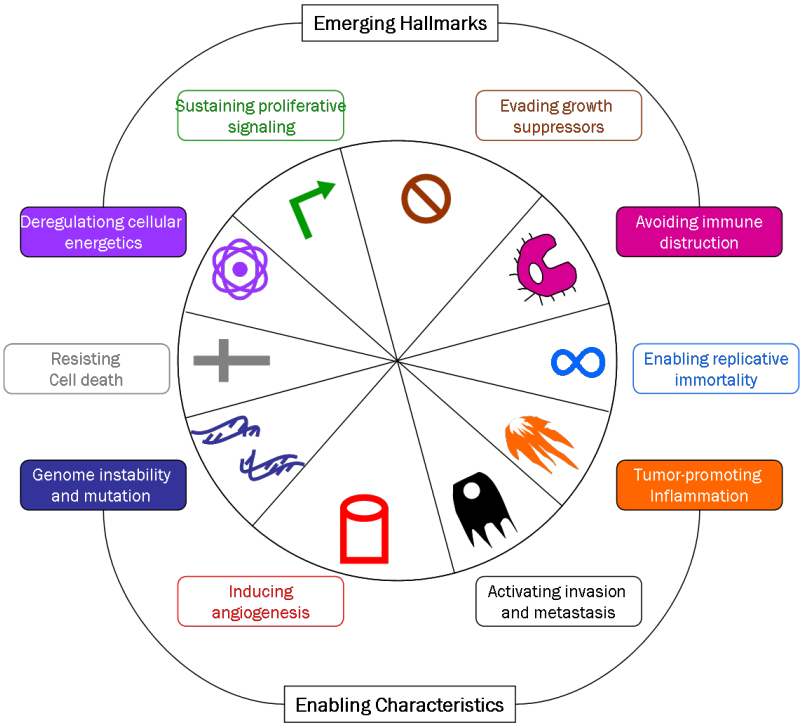

Figure 1: **Hallmarks and enabling characteristics of cancer development** (adapted from Hanahan and Weinberg, 2011).

Alterations to cellular metabolism have also been proposed as hallmark of cancer by Cairns, Harris and Mak (2011), who argue that the final aim of many oncogenic pathways is the adaptation of the tumor cell metabolism in order to sustain rapid growth and survival. Indeed, as early as 1930 Warburg observed that tumor cells undergo a glycolytic switch, and limit their metabolism to glycolysis even in the presence of oxygen ("aerobic glycolysis"), avoiding oxidative phosphorylation in the mitochondria (Warburg, 1926).

Finally, new findings have shown the importance in tumor biology of the tumor microenvironment, which includes not only several cell types, but also biological characteristics such as pH variations and hypoxia. Tumor cells have a constant signal exchange with the microenvironment during development. Cancer-associated

fibroblasts (CAFs), pericytes, endothelial cells and bone marrow-derived cells (BMDC) all participate in a complex signalling environment, which changes during tumor progression and eventually promotes metastasis formation (Hanahan and Weinberg, 2011). In recent years, tumor-associated macrophages (TAMs), myeloid-derived suppressor cells (MDSC) and mesenchymal stem cells (MSC) have often been correlated with tumor growth and malignant progression in a variety of studies (Joyce and Pollard, 2009).

1.1.2 Activating invasion and metastasis

1.1.2.1 General concepts

The main threat to cancer patient survival is the development of metastatic potential (Talmadge and Fidler, 2010). The survival rate for cancer patients whose primary tumors have begun to spread drops dramatically. Metastasis is defined as the spread of cancer cells from the primary site to other parts of the body. It is characterized by several distinct steps, the first (after initial transformation and angiogenesis) being local invasion *(Figure 2).* This process includes changes in the adhesive properties of the cell, and the activation of proteolysis, which is necessary for the cells to create a protrusion (Wang et al., 2005). Here, matrix metalloproteinases (MMPs) remodel the surrounding matrix and allow tumor cells to cross non-permissive tissue barriers. Examples include MMP2, 9 and 14 (Gialeli et al., 2010). These proteins are produced not only by the tumor cells, but also by the surrounding fibroblasts in response to paracrine stimuli coming from the tumor (Murphy et al., 2008). In general, the primary tumor itself secretes factors that promote the migration of tumor cells in both an autocrine and paracrine manner. Cells from the immune system, bone marrow derived cells, endothelial cells and fibroblasts that infiltrate the tumor tissue produce a variety of factors such as EGF, HGF, TGFβ, HGF and CCL5, that activate the migration machinery (Christofori, 2006).

Cancer cells that invade into the surrounding tissue can reach either blood or lymph vessels where they will intravasate, entering either the blood stream or the lymphatic circulation as circulating tumor cells (CTCs). According to the parallel progression model, this spreading of CTC can happen already at very early stages of tumorigenesis, even before the clinical appearance of the disease (Klein, 2009). Many CTCs are apoptotic because they have lost contact with their substrate, or die due to the shear

forces in the circulation (Sleeman et al., 2011). The few CTCs that survive will eventually arrest in capillaries and extravasate into the new tissue. There the disseminated tumor cells (DTCs) may start to proliferate and induce angiogenesis, in order to supply nutrients and oxygen to the rapidly growing mass (Talmadge and Fidler, 2010). Every step in this process includes many rate limiting obstacles for metastasis formation. The process of metastasis is thus inefficient, seldom exceeding 0.01% (Fidler, 1970).

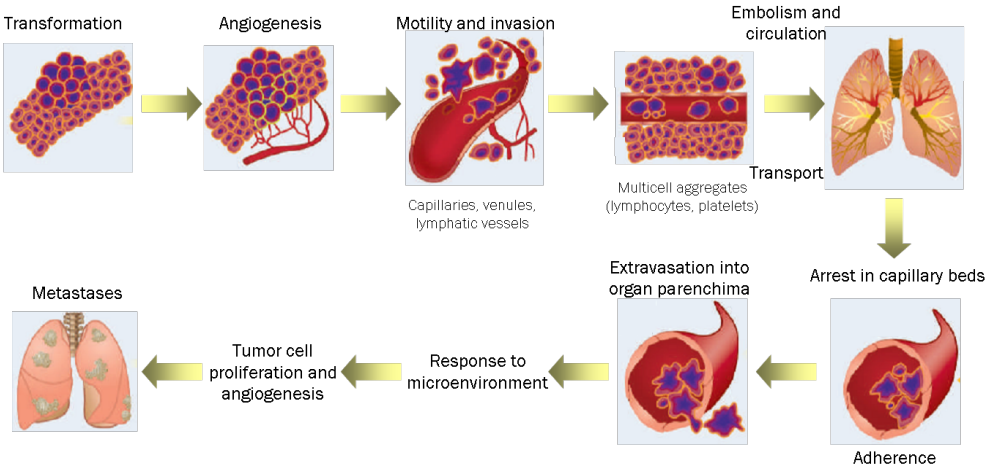

Figure 2: **The invasion-metastasis cascade** (adapted from Talmadge and Fidler, 2010)

Not all tumor cells acquire the ability to give rise to metastasis, and only those that have undergone "advantageous" genetic changes seem to be the ones able to locally invade the tissue, as described by the clonal selection model (Fidler and Kripke, 1977). However, this model has now been re-evaluated, as genomic instability and epigenetic changes may be necessary but not sufficient for the development of metastasis. An interaction with the stroma and the stromal cells, including remodeling of the ECM, induction of angiogenesis, local hypoxia and inflammatory conditions, is essential for the further progression of the tumor (Sleeman et al., 2012).

1.1.2.2 Role of the macrophages

Not every tumor cell is able to move away from its primary site and reach the lymphatics or the blood stream. This may be due to the suppressive effect of the immune system cells present at the original location (Hayakawa and Smyth, 2006). However the immune system also has positive effects on tumor progression. The tumor-associated macrophages (TAMs) are recruited and activated from the bone

marrow by tumors through secretion of cytokines such as CCL-2, and can be of two subgroups, M1 and M2. M1 macrophages give an anti-tumoral response by secreting pro-inflammatory cytokines as TNFα and IL-12 (Coghlin and Murray, 2010). In contrast, the M2 subtype secretes IL-10, VEGF-A and TGFβ, which rather promote angiogenesis and exert immunosuppressive functions (Solinas et al., 2009). Moreover, macrophages can also secrete proteases that contribute to the extravasation process (Kessenbrock et al., 2010). M2 TAMs are most frequently found in later stages of tumor, whereas the M1 activated macrophages seem to play a role rather at the beginning of tumor development (Biswas et al., 2008). Another subtype of TAM has been recently discovered that expresses Tie-2 and promotes angiogenesis (De Palma et al., 2005).

1.1.2.3 The epithelial-mesenchymal transition (EMT)

Epithelial cells can to loose many of their characteristics and take on mesenchymal features in a complex process termed EMT. This transition results in a more motile phenotype and changes the adhesive properties of the cells, and has therefore been connected with the metastatic process (Thiery, 2002). For example, the loss of epithelial markers such as E-cadherin has been correlated with poor prognosis (Peinado et al, 2004). The EMT process has a pivotal role during embryogenesis, and the very same factors that regulate it in this physiological condition, like SNAI1, Slug and Twist, are also involved in EMT in the tumor context. In fact, changes in the expression of these factors due to genomic instability in tumor cells may be the triggering event for EMT (Thiery and Sleeman, 2006). Growth factors derived from both tumor and stromal cells, including TGFβ, stimulate the expression of these transcription regulators, which act as suppressors of the promoter for E-cadherin. This results in a loss of this protein and thus a loss of cell-cell interactions and a consequent morphological switch to a spindle-like shape (Onder et al., 2008). The loss of E-cadherin is accompanied by the gain of N-cadherin ("cadherin switch"), which confers a mesenchymal phenotype to the cells and enhances migration and invasion (Christofori, 2006). Furthermore, EMT is characterized by the expression of proteases (MMPs), and increased motility and resistance to apoptosis (Hanahan and Weinberg, 2011), typical features of invasive cells (*Figure 3)*.

EMT is often found at the "invasive front" of a tumor, rather than being distributed in the whole mass, underlying its role in promoting metastasis formation. Indeed, EMT-

like features have been associated with metastatic potential (Thompson and Newgreen, 2005). Moreover, recent findings have related the EMT with the presence of the the so-called cancer stem cells (CSC), a tumor cell sub-population which is supposed to be capable of (re-)initiating tumor growth and thus to give rise to a metastasis (Brabletz et al, 2005). In fact, the EMT process increases the stemness of the cells (Mani et al., 2008).

EMT seems to play a role not only in the metastatic process. Cancer cells also may take advantage of this process to avoid oncogene-induced senescence, tumor hypoxia and increased apoptosis, thus giving an escape route to these hurdles (Sleeman et al., 2012).

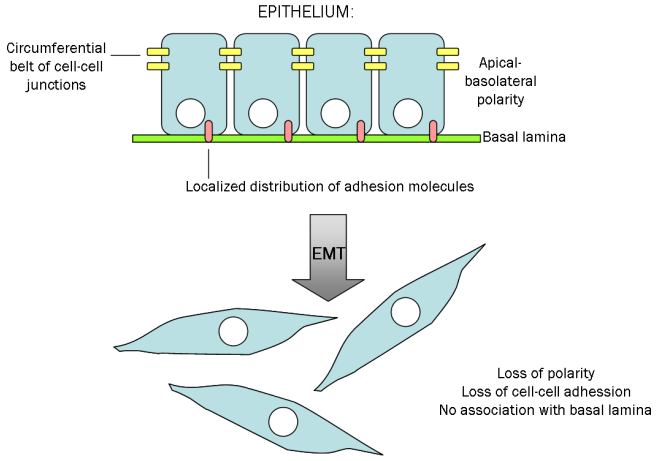

Figure 3: **EMT.** The epithelium is characterized by a thin layer of cells, which have a apical-basolateral polarity and are connected by specialized junctions both to each others and to the basal lamina. Upon EMT the cells change in morphology, loose their polarity as well as their adhesive properties.

1.1.2.4 The premetastatic niche

If a tumor cell manages to survive the harsh flow of the blood stream and extravasate, it still has to face a new and hostile environment that will not necessarily be permissive. This was already clear to Paget in 1889, when he proposed his “seed and soil” theory, which is still wildly accepted. He argued that the metastatic cells (the “seed”) will survive only if they end up in a permissive organ (the “soil”). This concept underscores the importance of the interactions between tumor cells and host tissue, although nowadays the “soil” can include concepts such as the premetastatic niche (Talmadge and Fidler, 2010). CTCs can reach different organs, but may be able to “seed” as DTCs and grow in only few of them. This happens when cancer cells arriving

from a primary site find a microenvironment, which is already permissive and supportive for their colonization. The intrinsic characteristics of the tissue or the effect of factors released by recruited bone marrow-derived cells may help creating the appropriate "soil" (Peinado et al., 2011). Kaplan and colleagues first described the presence of bone marrow-derived (BMD) hematopoietic progenitor cells expressing VEGFR1 prior the arrival of metastatic tumor cells (Kaplan et al., 2005). There are other molecules that have been shown to play a role in creating an appropriate microenvironment that facilitates the outgrowth of a tumor. For example fibronectin, secreted by activated fibroblasts, is able to promote the activation of lysyl oxidase (LOX), which is the staring point for matrix deposition and its cross-linking (Fogelgren et al., 2005). Molecules involved in inflammation, such as members of the S100 family and of the Serum Amyloid A (SAA) acute phase proteins, also contribute to the formation of the niche, for example by recruiting CD11b+ myeloid cells (Lukadinin and Sleeman, 2012). These in turn may secrete factors such as TGFβ that inhibit natural killer cells, B cells and the functional maturation of dendritic cells (Yang and Moses, 2008). In fact, it is believed that myeloid cells recruited at pre-metastatic sites create an "immune sanctuary" that will enable the growth and proliferation of tumor cells (Psaila and Lyden, 2009).

1.1.2.5 Tumor dormancy

A cancer cell that succeeds in reaching and colonizing a secondary site may lie dormant for months or even years before it gives rise to a detectable metastasis. Dormant tumor cells can be characterized by an incapability to turn on the "angiogenic switch", where their proliferation rate is balanced by apoptosis (Almog, 2010). Alternatively, they can be in a prolonged state of G_0, and thus insensitive to chemotherapy that targets actively cycling cells (Uhr and Pantel, 2011). The reactivation of these cells is due both to the influence of the microenvironment, as well to the genotype (e.g. loss of metastasis suppressor genes) and phenotypic characteristics of the dormant cells (Sleeman et al., 2012).

1.2 Cell motility and metastasis

1.2.1 Cell motility in cancer cells

An important first step in metastasis for tumor cells is often the remodelling of their actin cytoskeleton, detachment from the primary tissue and movement towards and invasion into a lymphatic or blood vessel. Similar motile properties are required during extravasation at distant sites. Therapeutic approaches that target cell motility have the potential to prevent the development of systemic metastatic disease, and thus significantly improve cancer treatment (Palmer et al., 2011).

The ability of a cell to move is of fundamental importance in metastasis, as well as in a plethora of physiological events such as development, homeostasis, the immune response and bone remodelling. Therefore cell motility and migration is a tightly regulated process. The movement of a single cell requires the following steps: polarization, protrusion and adhesion, translocation of the cell body and retraction of the rear (Sheetz et al., 1999). An extracellular stimulus is in most cases responsible for polarization, namely the creation of a migrating front and a rear in the cell, which breaks the symmetry (Horwitz and Webb, 2003). In response to a gradient of soluble (chemotactic) or surface bound (hapotactic) stimulus, the cell activates asymmetrically its receptors on the side of the stimulus, such as members of the G-protein coupled receptors (GPCR) superfamily (Cotton and Claing 2009). These give rise to a cascade of activations of downstream effectors, such as phosphoinositide 3-kinase (PI3K), which induce secondary messengers like phosphoinositol-trisphosphate (PIP_3), that rapidly accumulates at the leading edge (Kölsch et al., 2008). This asymmetric accumulation activates Rho family GTPases, in particular Rac and Cdc42, that eventually affect the *de novo* polymerization of actin, leading to the formation of the structures responsible for filopodia, lamellipodia and lamellae formation (*Figure 4)*.

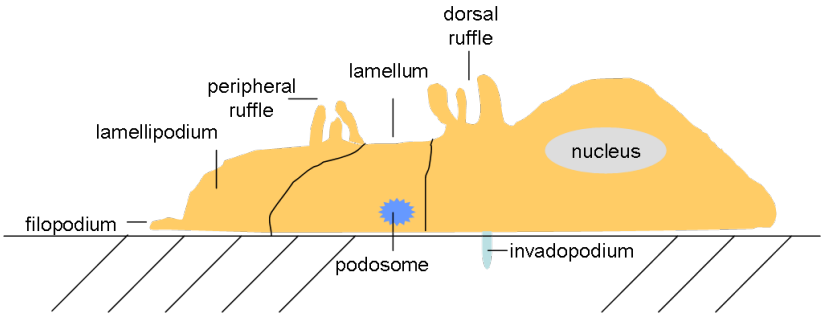

Figure 4: **Actin structures that characterize cell motility.**

1.2.2 Actin structures and migration mechanism

1.2.2.1 Filopodia and lamellipodia

Filopodia act mainly as mechanosensors, exploring the surrounding environment, and contain long, unbranched parallel actin bundles. Lamellipodia, the structures that generate the traction forward movement, are thin veil-like structures. They can be characterized by a ruffle, which is the result of a retrograde movement of a lamellipodium that did not adhere. The ruffle continues to fold over backward as it simultaneously retracts and eventually dissipates near the cell body (*Figure 5)* (Stossel, 1993).

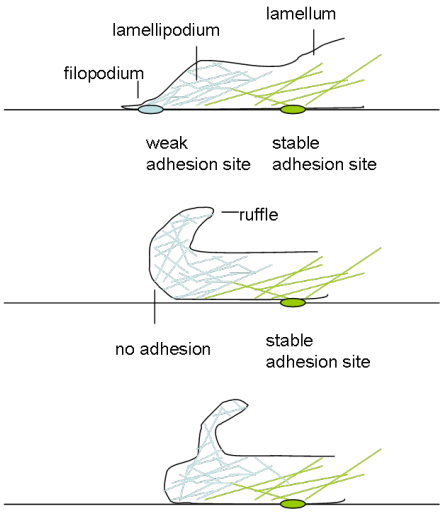

Figure 5: **Formation of a ruffle on the leading edge of a migrating cell.**

The polymerization of actin pushes the membrane forward, and eventually causes the cell to move. Mainly thanks to integrins, a new contact between the ventral stress fibres in the cell and the substrate is formed, the nascent adhesions that contain

actively polymerizing actin (Parsons et al., 2010). The nascent adhesion may mature by elongating and growing into focal complexes, and finally into larger structures that stably attach and transmit force to the extracellular matrix, the focal adhesions (FAs) (Oakes et al. 2012).

1.2.2.2 Focal adhesions

The FAs are multiprotein structures that form a link between the actin stress fibres in the cell and the extracellular matrix (ECM), providing force transmission between the inside and outside of the cell (Geiger et al., 2009). A FA can further mature into fibrillar adhesions, which are not seen in migrating cells, and are composed of large stress fibres, characterized by the presence of tensin (Pellegrin and Mellor, 2007).

The assembly of a FA is a highly regulated process, in which protein recruitment occurs in a sequential manner (Zaidel-Bar et al., 2004), and starts with integrin clustering. Integrins are the "anchor" of a cell to the ECM, and are able to trigger several transduction events such as tyrosine phosphorylation, pH elevation, synthesis of PIP_2 following Rac1 activation and activation of the MAPK cascade (Petit and Thiery, 2000). The integrin cytoplasmatic tails are able to bind various components of the focal adhesions, such as from tensin and the focal adhesion kinase (FAK) (Miyamoto et al., 1995).

FAK is the most important regulator of the integrin-associated focal adhesions, associating with Src and controlling downstream signal transduction pathways (McLean et al., 2007) (*Figure 6*). FAK is a non-receptor tyrosine kinase that binds to integrin clusters, mediates outside-inside signalling, and acts as an adaptor protein for the creation of the FA complex. The expression of FAK has been often linked in various epithelial cancers with the invasive potential of the tumors (McLean et al., 2005). FAK autophosphorylates in response to integrin clustering, creating a docking site for the SH2 domain of Src that activates FAK via phosphorylation (Schaller et al., 1994). Src is also responsible for the formation of podosomes, the so called "cellular feet" (Tarone et al., 1985).

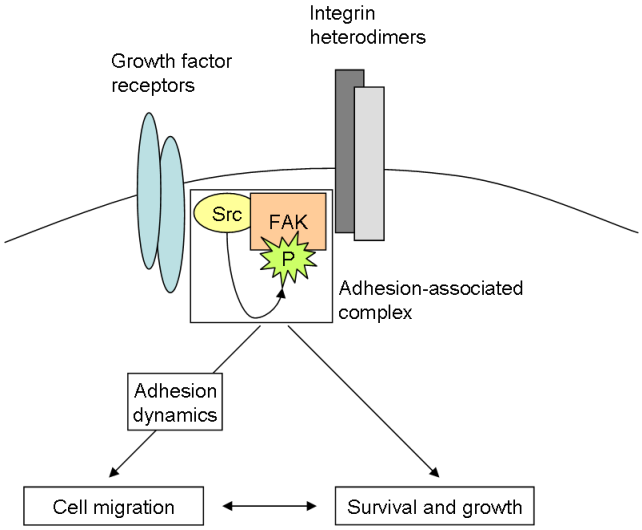

Figure 6: **FAK signalling.** FAK autophosphorylates Y397 upon integrin clustering, creating a binding site for SRC. The interaction of FAK with SRC causes a conformational change of the latter, which results in its activation and phosphorylation of two tyrosine residues on the kinase domain of FAK that activate it (adapted from McLean et al., 2005).

1.2.2.3 Podosomes and invadopodia

These ring-shaped adhesions share many components with the FAs, including talin, vinculin and paxillin, but the Wiskott Aldrich Syndrome protein (WASP) is unique to podosomes. The tyrosine kinase substrate with five SH3 domains (Tks5), another protein found in podosomes, is found also in the invadopodia, a structure related to podosomes that is described below. Another difference to the FAs is the presence of proteins that regulate the polymerization of actin (gelsolin, the Arp2/3 complex and fimbrin). Podosomes are observed in monocyte-derived cells such as osteolclasts and macrophages, and have a similar adhesive function as focal adhesions (Buccione et al., 2004), although podosomes also have a role in cell invasion. The secretion of matrix metalloproteinases (MMP) enables the cell to degrade the ECM and promotes diapedesis (Calle et al., 2006), migration (Rottiers et al., 2009) and tissue infiltration (Cougoule et al., 2010).

Invadopodia are closely related to podosomes, with which they share adhesive properties and the ability to degrade the ECM. Nomenclature of these two structures is still under debate, but it is generally accepted that invadopodia are found only in transformed and tumor cells (Murphy and Courtneige, 2011). Compared to podosomes, invadopodia are less frequent in the cell, and they also have a slower

turnover (Buccione et al., 2004). Upon outside-inside signalling from ECM-integrins or growth factor-receptor tyrosine kinase interactions (e.g. EGF, PDGF and TGFβ) there is activation of various signalling pathways, mainly involving Src and PKCμ (Bowden et al., 1999), and a subsequent recruitment and activation of protein components of the actin regulation machinery (*Figure 7)*.

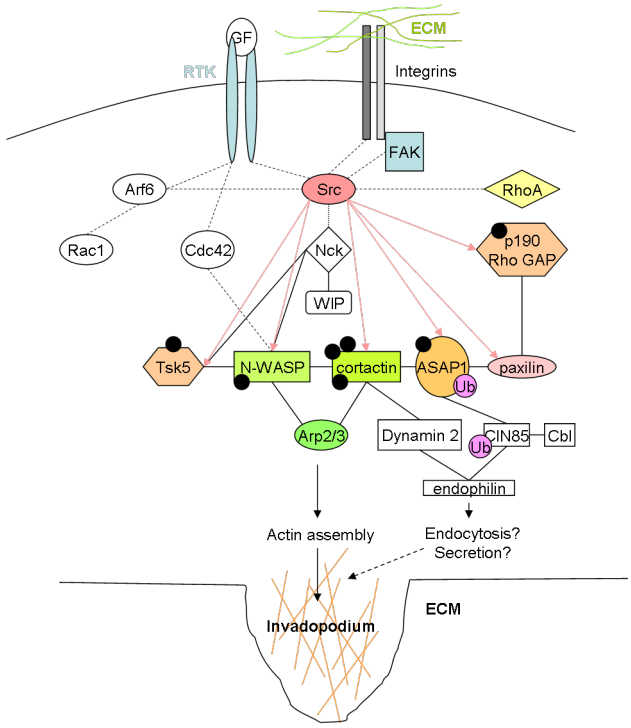

Figure 7: **The signalling network involved in the invadopodium formation.** Black dots: tyrosine phosphorylation; solid lines: direct protein-protein interaction; dotted lines: intermediates not known; Ub: monoubiquitination; dashed arrows: Src substrates. (Adapted from Stylli et al., 2008)

The most important components for the invadopodia are the proteins linked with actin polymerization (Arp2/3 complex, N-WASP and WASP interacting protein (WIP), cortactin), ASAP1 (Arf-GAP with SH3 domain, ANK repeat and PH domain-containing protein 1), the adaptor proteins paxillin and Tks5 as well as a disintegrin and metalloproteinases (ADAMs) and membrane type-1 matrix metalloproteinases (MT1-MMP) (Stylli et al., 2008).

1.2.2.4 Translocation of the cell body and retraction of the rear

To move forward the cell must translocate the body and retract the rear. The cell body rolls behind the lamellipodium due to a contraction of the actomyosin cytoskeleton, without any de novo polymerization of actin (Anderson et al., 1996). At the same time

myosin II decreases the tension at the leading edge, resulting in a retraction of the rear and a parallel extension of the front (Jay et al., 1995; Verkhovsky et al., 1999). The FAs at the rear disassemble and "slide" inwards towards the front, with multiple proteins moving along the stress fibres, whereas integrins stay on the membrane and must be exchanged (Palecek et al., 1998). The protease calpain also participates in the retraction mechanisms by promoting the proteolysis of adhesion proteins such as talin 1, and integrin β3 cytoplasmatic domain (Parsons et al., 2010).

FAK is again the main regulator of the disassembly process, as it can induce a decrease in local myosin contractility through downstream pathways that include ERK and myosin light chain kinase (MLCK) (Broussard et al., 2008).

1.2.3 Different forms of migration

The movement of cells can be single (amoeboid or mesenchymal) or collective (in cell sheets or cluster), depending on a variety of factors such as protease activity in the ECM, differences in cell-cell and cell-ECM adhesion, polarity of the cell and the rearrangement of the cytoskeleton (Yilmaz and Christofori 2010). The migration of cancer cells can occur with both forms, or as a combination, depending on the differentiation stage (Friedl and Wolf, 2003). *In vivo,* tumor cells also can interconvert between single or collective modes, as they are not mutually exclusive (Roussos et al., 2011).

Cells that migrate in a collective form maintain their cell-cell junctions, but the mechanisms that promote the motility are very similar to the single-cell migration. The leading cells, which may be the tumor cells themselves or stroma cells associated with the tumor, are responsible for localized proteolytic activity via secretion of MMPs (Friedl and Gilmour, 2009). Similar to single cell migration, collective cell migration is characterized by the formation of ruffles and pseudopodia, and the consequent attachment to the ECM via specific adhesion molecules. The main difference is that instead of retracting the rear, as happens to a single cell, the presence of cell-cell junctions creates pulling forces that make the mass move as a whole, while cells mostly keep their original conformation (Yilmaz and Christophori, 2010). A different form of collective migration is cell streaming, where single cells move by following one each other, but without keeping cell-cell contacts (Roussos et al., 2011).

1.2.4 The Ras superfamily of small GTPases

The remodelling of the membranes and of the actin cytoskeleton in the cell requires a tight regulation and coordination. The Ras superfamily of small GTPases, comprising more than 150 members, is a major actor in these events.

The ~150 members of the Ras superfamily of small GTPases can be divided into five families on the basis of their sequence as well as their functional similarities: Ras (the oncogene founding member), Rho, Rab, Ran and Arf (Wennerberg et al., 2005). There are also additional small GTPases, which are still considered as "unclassified", as they do not show any of the features of the five major classes. These monomeric GTPases work as molecular switches via the binding of GDP/GTP to specific motifs. The switch to GTP enables these proteins to bind to their specific effector targets.

Structurally, the N-terminus of these proteins is characterized by five conserved G box GDP/GTP-binding motif elements, the G motif, of about 20kDa. This domain is common not only among all the members of the Ras superfamily, but also to the Gα and other GTPases. The G motif includes the so-called "switch" domains I and II, which contain the residues responsible for the binding of the protein to GTP or GDP (*Figure 8)*.

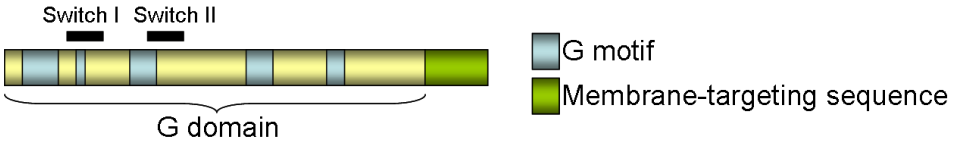

Figure 8: **Generic structure of a member of the Ras superfamily**

The switch between the two nucleotides is regulated by two classes of proteins: GEFs (guanine-nucleotide exchange factor) and GAPs (GTPase activating protein). The former ones promote the exchange of GDP to GTP, thereby activating the ras family proteins (Cherfils and Chardin, 1999). The GAPs are responsible for the hydrolysis of GTP to GDP because the Ras proteins have a very low intrinsic GTPase activity (Bernards and Settleman, 2004). These small GTPases can have posttranslational lipid modification, which enables their binding to the plasma membrane or facilitates subcellular localization (Wennerberg et al., 2005).

Among the Ras superfamily of small GTPases, the Arf proteins recently emerged as having a prominent role in regulating the actin cytoskeleton and the organization of focal complexes/adhesions (Turner et al., 2001). Therefore their activities and

regulation has become relevant for the understanding of both basic cell biology, as well as disease (D'Souza-Schorey and Chavrier, 2006)

1.2.4.1 The Arf family of GTP-binding proteins

The Arf (ADP rybosylation factor) proteins were first identified in 1984 as cofactors required for the cholera toxin-dependent ADP rybosylation of the Gs subunit regulating the adenylate cyclase (Kahn and Gilman, 1984). They are ubiquitously expressed in eukaryotic cells, where they have a major role in vesicle biogenesis, membrane trafficking and cytoskeletal organization (Pasqualato et al., 2002). One feature that makes these proteins unique is the N-terminal amphipathic helix, usually a myristoyl group (Colicelli, 2004). Another characteristic of the Arfs is the presence between switch I and II of an interswitch domain, that upon binding of GTP moves and displaces an amphipathic helix that becomes available for membrane insertion (Gillingham and Munro, 2007) *(Figure 9)*.

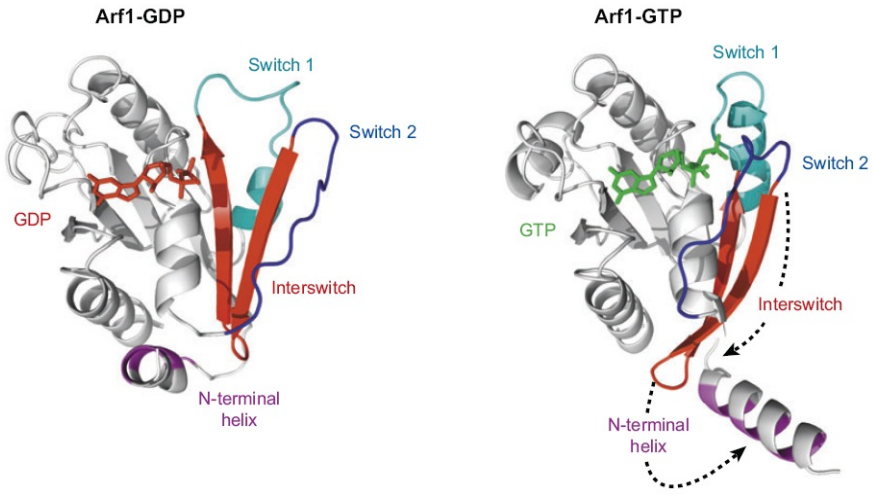

Figure 9: **Structure of Arf1**, showing the conformational changes that occur after switching from GDP to GTP: the interswitch moves away from the GTP binding site and the amphipathic helix is free to bind the lipid bilayer of the membrane.

The six known mammalian Arf proteins are divided into three classes on the basis of their structure: class I, which includes Arf1, Arf2 (not present in humans) and Arf3; class II, which includes Arf4 and Arf5; Arf6 is the only member of class III.

Arf1 and Arf6 are the most extensively studied and are involved in various cellular activities. Arf1 controls the formation of coat protein I (COPI)- coated vesicles of the Golgi – ER retrograde transport. It is also involved in the assembly of clathrin/adapter

protein 1 (AP1)–complex-associated vesicles at the trans-Golgi network and on immature secretory vesicles. Furthermore, Arf1 controls the formation of clathrin/adapter protein 3 (AP3)-containing endosomes (Wennerberg et al., 2005). Arf1 is also able to recruit the Golgi-localized γ-ear-containing Arf-binding proteins (GGAs) to the Golgi apparatus (D'Souza-Schroey & Chavrier, 2006).
Arf6, which is absent from plants, controls endocytosis as well as the organization of the actin cytoskeleton at the cell periphery (Donaldson et al., 2003).

1.2.4.2 The Arf GAP family

The hydrolysis of the GTP in the Arf proteins is catalyzed by a class of GAPs specific for the Arfs, namely the Arf GAPs. In humans there are at least 31 genes that encode an Arf GAP domain (East and Kahn, 2011). The resulting proteins are divided on the basis of their other domains into two major groups, Arf GAP1 and AZAP, each containing proteins that differ in their specificity *(Figure 10)* (Randazzo, Inoue and Bharti, 2007).

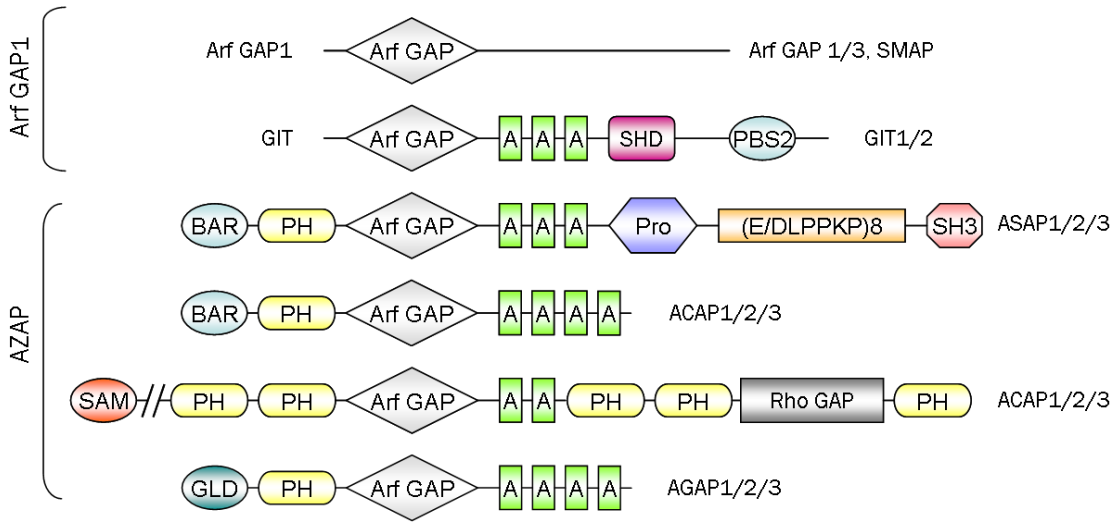

Figure 10: **Schematic representation of Arf GAPs proteins and their characterizing domains:** A (ankyrin repeats); SHD (Spa–homology domain); PBS2 (paxillin-binding site 2); BAR (Bin, amphiphysin and Rvs 161 and 167); PH (plekstrin homology); SAM (sterile α-motif); GLD (GTP-binding protein-like domain) (adapted from Randazzo and Hirsch, 2004)

The first group is the Arf GAP1 type, which has the Arf GAP domain at the immediate N-terminus. This family includes six members, further divided into Arf GAP1 and Gits (G protein-coupled receptor kinase interactors). The Arf GAP1 subtype includes Arf GAP1/3 and SMAP1/2 (stromal membrane associated protein).

The Git1 and Git2 proteins have additionally three ankyrin (ANK) repeat domains immediately C-terminal of the Arf GAP domain, an SHD (Spa-homology domain) and a unique C-terminus, characterized by a PBS2 (paxillin binding site 2).

The proteins belonging to the AZAP type (Arf GAP with ANK repeats and PH domains) have PH (plekstrin homology) domain immediately N-terminal and ANK repeats immediately C-terminal of the Arf GAP domain. The AZAP type is encoded by twelve genes, and the "Z" in the acronym corresponds in each of the four subtypes to the characterizing domain. For each subtype, three members have been identified.

The ASAP sub-family is comprised of three members (ASAP1/DEF1/DDEF1/centaurin b4/AMAP1, ASAP2/PAP/AMAP2 and ASAP3/UPLC/DDEFL1/ACAP4). ASAP1 and ASAP2 contain a SH3 (Src homology 3) domain at the C-terminus. These subtypes also possess a BAR (Bin, amphiphysin and Rvs 161 and 167) domain at the N-terminus, which, by binding to the membrane, is able to bend it and may thus be involved in the endocytosis process. The ASAPs are characterized by a proline-rich domain that enables the binding to SH3-bearing proteins. There are at least three splicing variants of both ASAP1 and ASAP2, which lack one or more of these proline rich domains. ASAP3 does not have the SH3 domain, but is nevertheless included in this group because of the similarity of its domain structure, as well as phylogenetic analysis. The other AZAPs described in the literature are listed in *Table 1*.

Name	Characteristics
ASAPs	▪ Proline rich domain ▪ ASAP1 and ASAP2 have SH3 and BAR domain
ACAPs	▪ Predicted coiled-coil domain in the N-terminus
AGAPs	▪ GLD (GTP-binding protein-like domain) in the N-terminus ▪ Split PH domain
ARAPs	▪ Rho GAP domain ▪ SAM (sterile α-motif)

Table 1: **The AZAP families and their characteristics**

Among these Arf GAPs, ASAP1 has emerged from work in our laboratory, as well as that of others, as being a protein that is involved in the promotion of motility and invasiveness in vitro, and that contributes to metastasis formation in vivo (Ehlers et al.,

2005; Onodera et al., 2005; Lin et al., 2008; Müller et al., 2010). This protein was the focus of my PhD studies.

1.3 ASAP1

1.3.1 Structure of ASAP1

As already mentioned, ASAP1 belongs to the Arf GAP family, type AZAP. ASAP1 contains a BAR and a PH domain, a zinc finger, three ankyrin repeats, a proline rich region that contains alternative splicing regions and SH3 binding motifs, eight repeats of the sequence E/DLPPKP, and a SH3 domain (*Figure 11*). Each domain contributes to the features of ASAP1 by enabling it to bind to various proteins and cellular structures, thereby defining its subcellular localization and its activity. ASAP1 is found in peripheral FAs, but moves to the cell edge during cell spreading (Randazzo et al., 2000). It localizes also to the cytoplasm in a perinuclear reticular network (Brown et al., 1998).

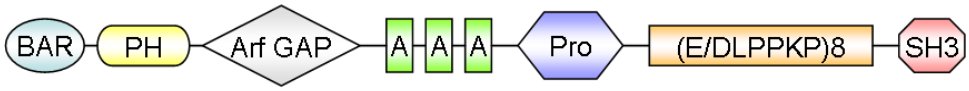

Figure 11: **Schematic picture showing the structure of ASAP1 and its domains**

Via the BAR domain ASAP1 is able to bind to acid phospholipids of the plasma membrane, and has therefore a role in membrane trafficking (Nie et al., 2006). The BAR domain seems to be also involved in the formation of podosomes (Bharti et al., 2007), one of the cytoskeletal structures in which ASAP1 is involved.

ASAP1 binds phosphatidyl-inositol-4,5-bisphosphate (PIP_2) through the PH domain, which is required for the Arf GAP activity of ASAP1, together with the Arf GAP domain (Che et al., 2005). The Arf GAP domain consists of ~140 residues, four of which are invariable cysteines that coordinate a zinc ion (Goldberg et al., 1999; Mandiyan et al., 1999). Together with the ankyrin repeats, these three domains form the so-called PH-Zn-finger-ANK (PZA) motif, which is conserved in plants, worms and flies, suggesting the importance of this module. These domains provide the Arf GAP activity of ASAP1, which is specific for Arf1 and Arf5, to a lesser extent to Arf6 (Brown et al., 1998).

The ankyrin repeats (one of the most common protein–protein interaction motifs), the proline-rich regions and the SH3 domain are all motifs that enable the binding of ASAP1 to a plethora of proteins, that regulate and mediate the variety of cellular processes that ASAP1 is involved in.

There are two splicing variants identified in humans, ASAP1a and ASAP1b, the latter of which misses part of the proline-rich region. In our laboratory we identified a third splicing variant, rASAP1c, which has an even shorter proline-rich region and lacks a sequence of 15 amino acids between the BAR and the PH domain. These variations however do not impair the binding of ASAP1 to its partner proteins, nor the Arf GAP activity (Müller et al., 2010).

1.3.2 Roles of ASAP1 in the cell

1.3.2.1 Regulation of the actin cytoskeleton

ASAP1 plays a role in the regulation of the actin cytoskeleton, in particular via its association with four cytoskeletal structures: focal adhesions, circular dorsal ruffles (CDRs), and invadopodia/podosomes (Randazzo et al., 2007). ASAP1 associates with these structures via binding to other proteins that are part of these structures.

The localization of ASAP1 is mainly in peripheral FAs (Randazzo et al., 2000) due to its interaction with Crk/CrkL (chicken tumor virus 10 regulator of kinase/Crk-like) via its proline-rich regions (Brown et al, 1998; Oda et al., 2003) and with FAK via the SH3 domain (Liu et al., 2002). The overexpression of ASAP1 causes a change in the localization of these two proteins to the cytosol, reducing their stable association in the focal adhesions (Liu et al., 2002). The same does not happen if a SH3 domain mutant or a form lacking the GAP activity is used, suggesting a role of ASAP1, and in particular of its GAP activity, in focal adhesion dynamics.

Circular dorsal ruffles form transiently upon stimulation of the cell with various agonists, for example PDGF (Buccione et al., 2004). Randazzo and co-workers demonstrated that ASAP1 co-localizes with these structures and regulates the actin cytoskeleton (Randazzo et al., 2000). In fact, overexpression of ASAP1 in fibroblasts caused a slowing down of cell spreading, as well as a decreased formation of dorsal ruffles upon stimulation with PDGF. This effect is dependent on the Arf GAP domain of ASAP1, as demonstrated by using a mutant form lacking this activity (Randazzo et al., 2000). Moreover, the localization of ASAP1 in the cell also contributes to the

regulation of cytoskeletal remodelling. For example, the mislocalization of ASAP1 to the mitochondria prevents efficient cell spreading on fibronectin. The same was observed when ASAP1 was silenced (Liu et al., 2005). A role for ASAP1 in the regulation of cell motility is also indicated by an increase in migration towards PDGF when ASAP1 is over expressed (Furman et al., 2002).

ASAP1 also binds to the ubiquitous adaptor protein CD2AP (CD2-associated protein) in membrane ruffles (Liu et al., 2005). CD2AP possesses three SH3 domains at its N-terminus, and binds to ASAP1 via the first two. Interestingly, CD2AP binds cortactin, another binding partner of ASAP1, in breast cancer cells stimulated by EGF, and co-localizes with ASAP1 in membrane ruffles (Lynch et al., 2003). Cortactin, a component of invadopodia/podosomes is also able to bind to ASAP1 via its SH3 domain (Onodera et al., 2005). This protein is encoded by the *EMS1* gene in the 11q13 amplicon, a region commonly amplified in 13% of primary breast cancers and 30% of head and neck squamous cell carcinomas of the head and neck (Schuuring et al., 1992; Fantl et al., 1993; Williams et al., 1993; Karlseder et al., 1994; Peters et al., 1995).

ASAP1 is also a component of podosomes, and its presence is necessary for the formation of these structures (Bharti et al., 2007). This role is not due to the Arf-GAP activity. Instead, phosphorylation of ASAP1 on Tyr 782 and the SH3 domain are necessary for podosome formation. The phosphorylation is mediated by Src, another binding partner of ASAP1 (Bharti et al., 2007).

Src is also a fundamental component of invadopodia, another cytoskeletal structure ASAP1 participates in (Bharti et al., 2007), and is one of the proteins required for invadopodia-mediated matrix degradation in a variety of tumor cell lines (Stylli et al., 2008). The BAR domain of ASAP1 also seems to play role in invadopodia formation, although it is still not clear how (Bharti et al., 2007). Interestingly, ASAP1 also binds via the BAR domain to GEFH1, a GEF for Rho A which inhibits the formation of podosomes (Shiba and Randazzo 2011). As the BAR domain inhibits the GAP activity of ASAP1 (Jian et al., 2009), it is plausible that the binding of GEFH1 results in a reduced binding to Arf, and thus to a reduction in podosome formation.

Pyk2 (Proline-rich tyrosine kinase 2), a non-receptor tyrosine kinase related to FAK, is also able to bind ASAP1 (Kruljac-Letunic et al., 2003), but unlike FAK, Pyk2 is localized in the cytoplasm and concentrated in perinuclear regions (Matsuya et al. 1998). It acts upstream of small G-proteins, linking transmembrane receptors to MAPK pathways. The binding of ASAP1 to Pyk2 is mediated by the SH3 domain of ASAP1 and the

proline-rich region of Pyk2. Upon binding, ASAP1 can be phosphorylated by Pyk2, and this results in a reduction of its GTPase activity (Kruljac-Letunic et al., 2003). The effect of this interaction in the regulation of the cytoskeleton is still unclear.

1.3.2.2 Vesicle trafficking and receptor internalization

Arf1, one of the substrates of ASAP1, is the main regulator of the trafficking of lipids and protein between the membrane-delimited organelles (Balch et al., 1984a; 1984b). By exchanging GDP with GTP, Arf1 binds to the membrane, and can recruit several coat proteins that bind to and concentrate cargo. Arf GAPs like ASAP1 are also recruited, and may bind both to coat proteins and to the cargo without hydrolysing the GTP on the Arf protein (Nie and Randazzo, 2006). Coat proteins are able to deform membranes and thus to promote the budding and eventually the fission of the vesicle (Bonifacino and Glick, 2004). The hydrolysis of GTP catalysed by the Arf GAP causes the dissociation of Arf from the membrane, leaving the newly formed vesicle free to fuse with acceptor membranes *(Figure 12)* (Nie and Randazzo, 2006a).

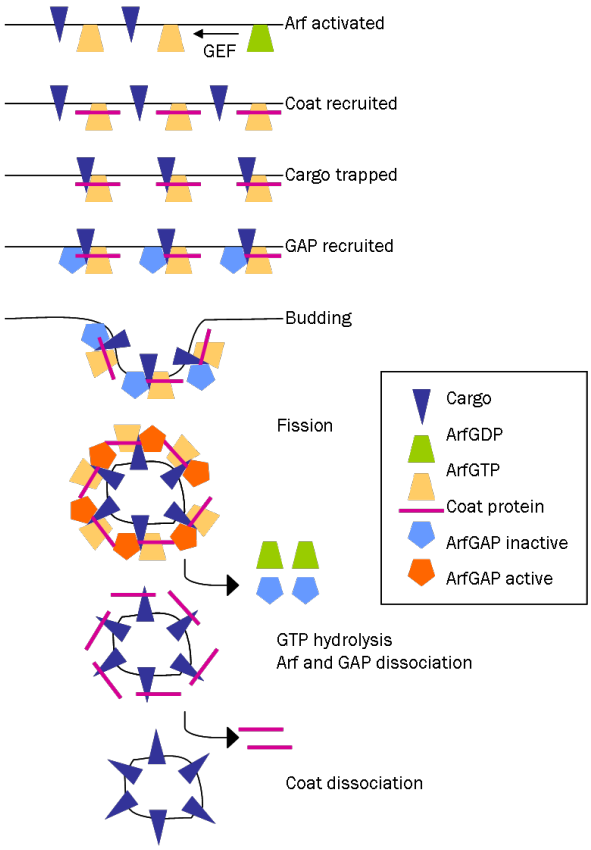

Figure 12: **Mechanism of vesicle fission mediated by Arf and Arf GAPs** (adapted from Nie and Randazzo, 2006)

In accordance with its role as an Arf GAP protein, there is quite a body of literature connecting ASAP1 with vesicle trafficking and receptor internalization. Interestingly, this feature is often connected with the regulation of the cytoskeleton, as exemplified by the interaction of CIN85 (Cbl-interacting protein of 85kDa) with ASAP1 in invadopodia (Nam et al., 2007).

Via its BAR domain ASAP1 is able to dimerize and subsequently bind to phosphoinositides in the plasma membrane via its PH domain. This interaction, together with binding to Arfs present on the membrane, causes bending of the membrane (*Figure 13)*. ASAP1 is thus able to tubulate membranes *in vivo*, and therefore may be able to generate vesicles (Nie and Randazzo, 2006). For example, depletion of ASAP1 led to an accumulation of transferrin and transferrin receptor to the cell edge, instead of the usual perinuclear localization, in a compartment containing Rab11 and FIP3 (Inoue et al., 2008). These proteins are typical recycling endosomes markers, and ASAP1 binds to FIP3 via its BAR domain (Inoue et al., 2008).

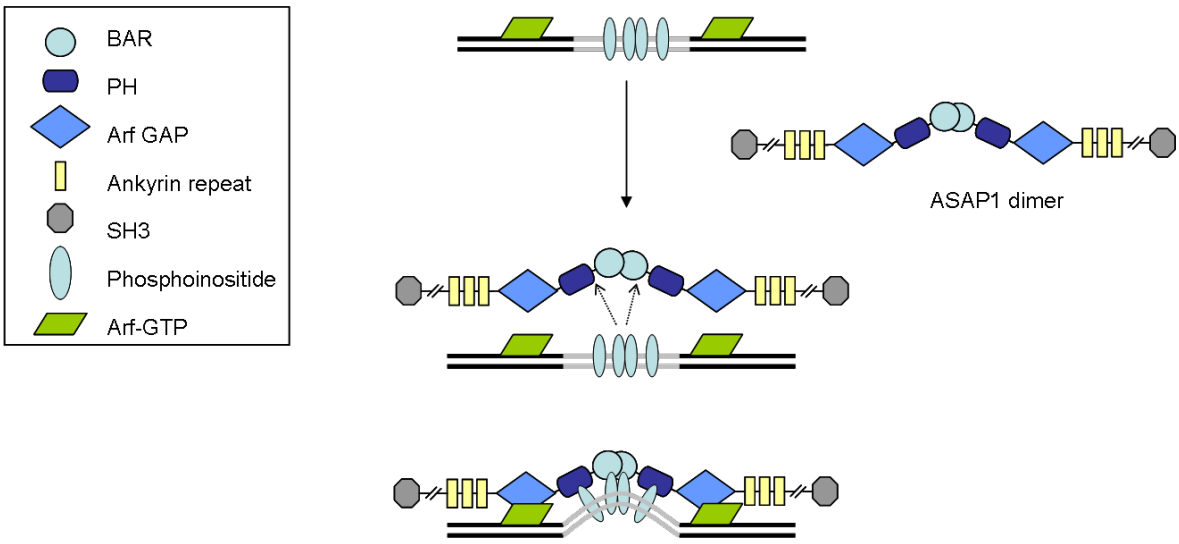

Figure 13: **Via specific domains, ASAP1 is able to dimerize and bind to the plasma membrane, bending it to facilitate receptor endocytosis** (adapted form Nie et al., 2006b)

1.3.3 ASAP1 and cancer

1.3.3.1 Roles of ASAP1 in tumor development and progression

ASAP1 has been first linked to cancer in our laboratory. It was found in an unbiased screen for genes associated with metastasis that we performed (Nestl et al., 2001). Later Onodera and colleagues showed that the protein levels of ASAP1 correlate with the invasiveness of different human breast cancer cells (Onodera et al., 2005). In their model, ASAP1 was able to bind both cortactin and paxillin via the SH3 domain, forming a trimeric complex that was detectable only in highly invasive cell lines. In the same year, a potential role for ASAP1 as an oncogene in uveal melanoma was suggested (Ehlers et al., 2005). This pathology is usually accompanied by an amplification of the 8q chromosome, where ASAP1 is located. Indeed, they showed that both mRNA levels and protein expression were significantly enhanced in high-grade melanomas. Furthermore, ectopic expression of ASAP1 in low-grade melanoma cells resulted in a significant increase in cell motility, a feature of high-grade metastasizing cells (Ehlers et al., 2005).

Overexpression of ASAP1 has been also linked to prostate cancer (Lin et al. 2008). A metastatic and a non-metastatic subline were derived from the same prostate cancer tissue and gene expression was compared. Both ASAP1 mRNA and protein were expressed at a significantly higher level in a metastatic tumor subline, compared to the non-metastatic one.

Following up on our observation that ASAP1 belongs to a group of genes whose expression is exclusive to or at least upregulated in metastatic mammary, pancreatic and prostate cells lines (Nestl et al., 2001), our laboratory found that ASAP1 expression correlated with tumor progression in a number of cancers, and that the expression of ASAP1 functionally regulates metastatic potential in rat tumor models (Müller et al., 2010). Moreover, the staining of several human tumor tissues (carcinomas of stomach, colon, gall bladder, breast, bladder and ovary, papillary carcinoma of the thyroid, and esophageal, head and neck squamous cell carcinomas) showed the presence of ASAP1, which was not present in the corresponding healthy tissues *(Figure 14)*. The analysis of tumor material obtained from patients with colon adenocarcinomas revealed that the expression of ASAP1 in the patients that developed metachronous metastases was significantly higher, again underlying the relevance of ASAP1 to tumor progression. In patients with colorectal adenocarcinomas

the expression of ASAP1 is correlated with a short metastasis-free survival, as well as with a poor overall survival (Müller et al., 2010).

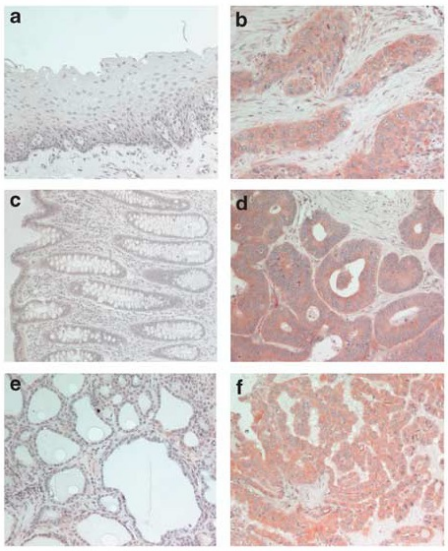

Figure 14: **Expression of ASAP1 in human tumors.** Normal esophageal, colorectal, and thyroid tissues (a, c, and e, respectively) and their corresponding tumors (b, d, and f, respectively) were immunostained using the 7B12 antibody and AEC (red color), followed by counterstaining with hematoxylin (blue color) (Müller et al., 2010)

1.3.3.2 Role of the proline-rich domain in ASAP1

As already mentioned, the proline rich region of ASAP1 is able to bind to several proteins involved in the control of cell motility, such as c-src and Crk (Brown et al., 1998). Our laboratory showed that a mutant form of ASAP1 containing a point mutation in this region (R811A) is unable to promote *in vitro* wound healing and migration in contrast to the wild type ASAP1 protein *(Figure 15)* (Müller et al., 2010).

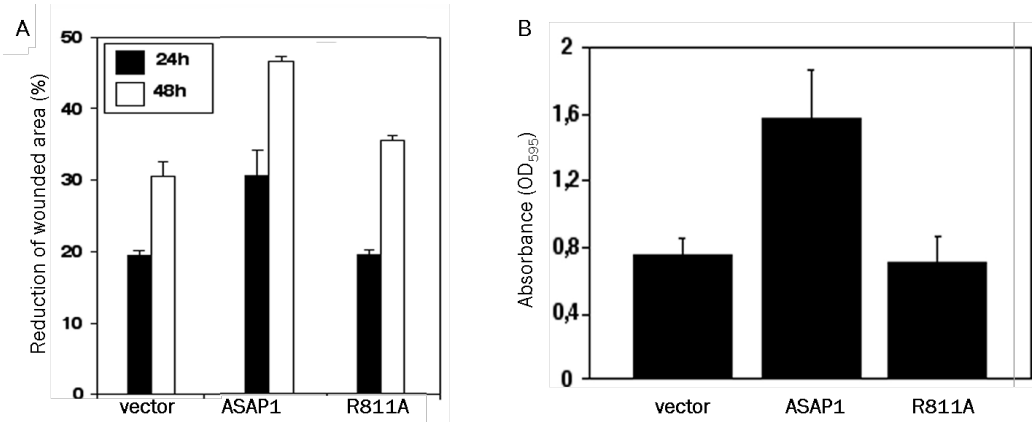

Figure 15: **Wound healing and migration assays.**1AS rat pancreatic cells transiently transfected with empty vector, wild type ASAP1 or the mutant R811A were used for **A.** wound healing assay and **B.** invasion assay (Müller et al., 2010)

Consistently, only animals bearing tumors derived from pancreatic cancer cells that were engineered to express the wild type form of ASAP1 were able to develop lung metastasis, whereas the animals bearing tumors derived from pancreatic cancer cells that expressed the mutated form behaved comparably to the control tumors and did not develop lung metastasis *(Figure 16)* (Müller et al., 2010).

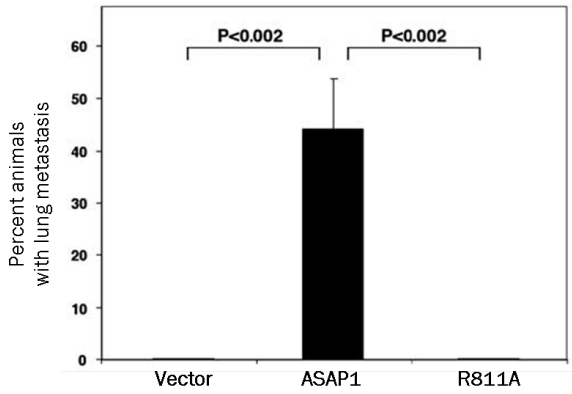

Figure 16: 1AS rat pancreatic cells stably transfected with the vectors indicated and injected in syngeneic animals. The graph shows the effect on the formation of lung metastasis (Müller et al., 2010)

These results strongly indicate that the interaction of ASAP1 with SH3 domain bearing proteins through its proline rich regions plays an important role in the promotion of motility and metastasis.

1.3.3.3 The EGFR-ASAP1 pathway in breast cancer

A variety of observations suggest that ASAP1 plays an important regulatory role in the recycling and signalling of EGFR, and by this means may contribute to the invasiveness of tumor cells. For example, Arf1 is involved not only in internal vesicle trafficking, but also has a prominent role in the internalization of receptors such as EFGR in breast cancer cells, thereby influencing the PI3K pathway and the subsequent motility and invasive properties of the cells (Boulay et al., 2008). Through modulating Arf1 activity, ASAP1 likely functions as a key regulator of EGFR signalling.

Other protein interaction partners of ASAP1 are also involved in EGFR regulation. For example, CIN85 is an adaptor protein that via its SH3 domains binds the ubiquitin ligase Cbl, and together they down-regulate EGF receptors (Haglund et al., 2002). ASAP1 is able to interact with CIN85 via its proline rich regions, participating in the regulation of receptor recycling. In fact, overexpression of ASAP1 led to an increase in

receptor recycling in CHO cells, which was specific for EGFR (Kowanetz et al., 2004). Increased internalization and recycling of the EGFR receptor has been shown to be particularly important in the promotion of cell motility and invasive potential. In cancer cells expressing mutant p53, the recycling of integrins and EGFR is enhanced, and this results in an increase in cell migration and invasion (Muller et al., 2009).

In addition, EGFR signals to ASAP1 to stimulate formation of invadopodia. Arf6 uses ASAP1 as an effector, is over expressed in highly invasive breast cancer cells, and plays an important role during invasion (Sabe et al., 2006). GEP100 is the specific GEF for Arf6, and its knock down inhibits the formation of invadopodia in MDA MB 231 cells. In these cells GEP100 binds the phosphorylated tyrosines of the activated EGF receptor via its PH domains and activates Arf6 (Morishige et al., 2007). The active Arf6 recruits ASAP1 to the plasma membrane, where they co-localize in invadopodia, as well as to cytoplasmatic large vesicles (Hashimoto et al., 2005). The binding of ASAP1 to Arf6 is stable and does not lead to immediate hydrolysis of GTP. The recruitment of ASAP1, together with other protein such as cortactin and paxillin, is the starting point for the formation of invadopodia (*Figure 17)*. Therefore the activation of EGFR stimulates the formation of invadopodia in a manner that is dependent on ASAP1.

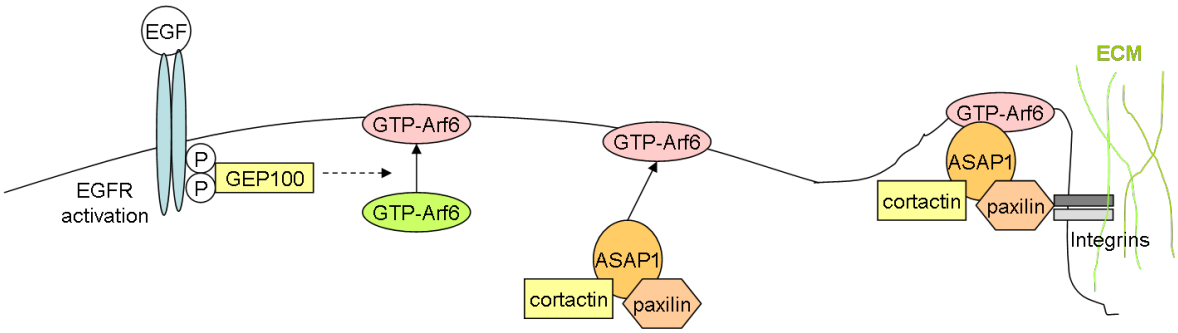

Figure 17: **The EGF-GEP100 pathway links ASAP1 with the formation of invadopodia.**

Another study links EGFR, integrins (β1 in particular) and ASAP1. Onodera et al. showed how the signalling of EGFR induces the activation of Arf6 and the subsequent recruitment of ASAP1 to the plasma membrane. This forms a complex with the protein kinase D1 (PKD1) and the β1 integrin to promote its recycling and thus increase the invasiveness of breast cancer cells (Onodera et al., 2012)

1.3.4 New interaction partners

ASAP1 is a multidomain protein, and is therefore able to bind to several partners. Its role in promoting motility and metastasis has already been shown (Onodera et al., 2005; Müller et al., 2010), but the mechanisms are still unclear. In particular it has still to be elucidated which of the many ASAP1-interacting proteins contribute to this activity. In collaboration with Prof. Zollo who works on h-prune and Nm23-H1, our lab obtained evidence from co-immunoprecipitation experiments that indicated a physical interaction between ASAP1 and both h-prune (Müller et al., 2010) and Nm23-H1 (*Figure 18)*, possibly suggesting the presence of a ternary complex able to regulate metastasis formation.

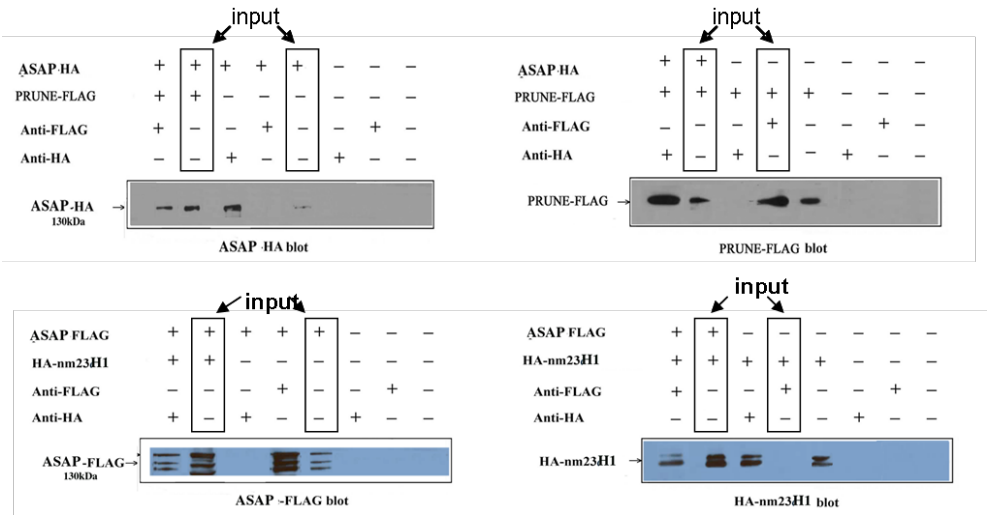

Figure 18: Western blot pictures showing the co-immunoprecipitation of ASAP1 with both h-prune (upper blots) and Nm23-H1 (lower blots) (Zollo lab, unpublished results; Müller et al., 2010).

1.3.4.1 h-prune

The human prune (h-prune) gene is the orthologue of the *Drosophila* prune gene involved in development of the eye color. In the case of a homozygous mutation in this gene, the eyes of *Drosophila* are purple-brownish instead of red. There is no effect on viability or fertility, but this mutation (both hemi- or homozygous), when present with a single copy mutation of the abnormal wing disc (*awd*) gene (*awd*$^{K\text{-}pn}$*, killer-of-prune*), is lethal (Timmons and Shearne, 1996). The *awd* gene is the *Drosophila* orthologue of the Nm23-H1 protein described below.

H-prune belongs to group II of the DHH (Asp-His-His) phosphoesterase superfamily, and possesses a PDE (phosphodiesterase) activity that is able to induce cell motility in breast cancer cells (D'Angelo et al., 2004). Recently, it has been shown that h-prune also possesses an exopolyphosphatase activity (PPase) (Tammenkoski et al. 2008), and that both of these activities could be potential therapeutic targets. For example, the treatment of MDA-MB-234 breast cancer cells with dipyridamol, a potent inhibitor of the h-prune PDE activity, was able to reduce cell motility (D'Angelo et al., 2004).
In addition to the DHH motif at the N-terminus, there is a less conserved DHHA2 domain that provides substrate-binding residues and therefore influences specificity. The C-terminal region includes a cortexillin homology domain with putative coiled-coil and proline rich regions. GSK-3β is able to bind to h-prune through this domain (residues 330-453), and together they regulate the disassembly of focal adhesions and thereby promote cell migration. H-prune has also been reported to bind to gelsolin, a molecule involved in cytoskeleton remodeling. Consistent with a role in promoting cell motility, the h-prune protein has been found to be expressed at higher levels in breast (D'Angelo et al., 2004), colorectal (Forus et al., 2001), and gastric carcinomas (Kobayashi et al., 2006), promoting both tumour invasiveness and metastasis formation. Amplification of h-prune copy number induces cell proliferation in an established breast cancer cell model (Reymond et al., 1999). The metastasis promoting activity of h-prune is further enhanced by the binding with Nm23-H1, as described below.

1.3.4.2 Nm23-H1

Nm23-H1 belongs to a family of nucleoside diphosphate kinases (NDPK) and is encoded by one of the ten Nm23 human genes (Marino et al., 2011). The members of group I (NME1-4) are ubiquitously expressed, and are found mainly in the cytoplasm, except for NME4, which is localized to the mitochondria (Tokarska-Schlattner et al., 2008). They are all hexameric and possess NDPK activity (Lacombe et al., 2000). In group II, the enzymatic activity has only been demonstrated for the product of NME6, which is also the only member of this group that is not expressed in ciliated structures (Tsuiki et al., 1999). The Nm23/NDPKs have several roles in proliferation, differentiation, development, cytoskeleton dynamic, endocytosis, apoptosis and cell signalling (wnt, p53, GTPases) (Boissan et al., 2009).

In 1988 Steeg and co-workers were able to show that the expression of NM23 was significantly higher in a low metastatic cell line compared to a high one, suggesting a role as a metastasis suppressor for the Nm23-H1 protein (Steeg et al., 1988). Nevertheless, the mechanism underlying this feature is still not completely understood. It is also known as NDPK-A (nucleotide diphosphate kinase-A), due to the enzymatic activity that it possesses (Biggs et al., 1990, Wallet et al., 1990), but this well-characterized activity has never been correlated with its metastasis suppressing effects (MacDonald et al., 1993). In addition to the NDPK activity, Nm23-H1 also possesses a histidine kinase activity, via the very same phosphohistidine (H118) that mediates the phosphorylation of nucleoside 5'-diphosphates to triphosphates. At least three substrates for this enzymatic activity have been identified: ATP-citrate lyase (Wagner et al., 1995), aldolase C (Wagner et al., 2000) and the kinase suppressor of Ras (KSR) (Hartsough et al., 2002) (*Figure 19)*. The physiological effects of the phosphorylation on the first two proteins are still unknown. KRS is a scaffold protein for the MAP kinase pathway, recruiting several proteins to the cell membrane. The phosphorylation of its serines 392 and 434 by Nm23-H1 causes a degradation of the KRS protein and a consequent decrease in pErk activity in tumor cells (Hartsough et al., 2002).

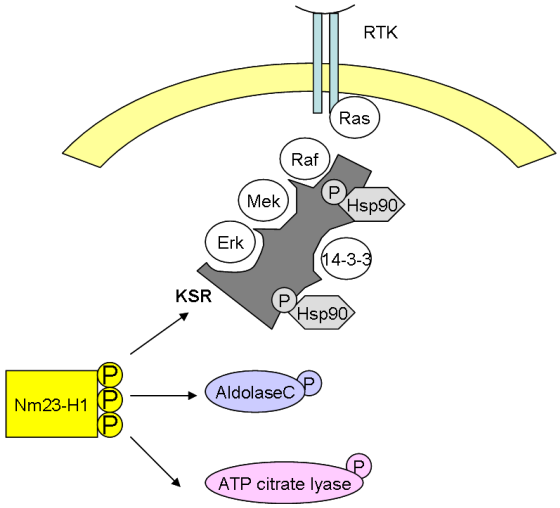

Figure 19: **The histidine kinase activity of Nm23-H1.** The autophosphorylation of Nm23-H1 activates its histidine kinase activity on three substrates, as shown in this picture: KSR, aldolase C and ATP citrate lyase (adapted from Steeg et al., 2008)

Recently it has been shown that Nm23-H1 also possesses a 3'-5' exonuclease activity, which is associated with proofreading processes during DNA repair and replication (Ma

et al., 2004). This activity seems to be required for the metastasis suppressor function of Nm23-H1, (Zhang et al., 2011), which is not surprising, considering that reduced or absent expression of 3'-5'-exonucleases has been associated with increased cancer progression (Jackson and Loeb, 1998).

A plethora of binding partners of Nm23-H1 have been reported, underlying the crucial role of this protein in many cellular processes (Marino et al., 2011). For example, Nm23-H1 binds to various GEFs such as Tiam1 (Otsuki et al., 2001), Lbc (Iwashita et al., 2004) and Dbl (Murakami et al., 2008a; 2008b) as well as to members of the Ras family of small GTPases: Arf6 (Palacios et al. 2002) and Rad (Tseng et al., 2001). Nm23-H1 is also able to bind to receptors (ER, RORα/RZR) and transcription factors (EBNA1-3C, Oct transcription factor complex and SET), thereby regulating some of the transcriptional complexes involved in metastasis formation (Curtis et al., 2007; Paravicini et al., 1996; Subramanian et al., 2001; Zheng et al., 2003; Fan et al., 2003). Finally, Nm23-H1 is also involved in cytoskeletal regulation through binding to vimentin, tubulin, Icap-1α and plakoglobin (Otero et al., 1997; Otero, 2000; Pinon et al. 1999; Lombardi et al., 1995; Fournier et al., 2002; Aktary et al., 2010).

1.3.4.3 h-prune and Nm23-H1 interaction in cancer

The interaction of the human Nm23-H1 with h-prune was first demonstrated in 1999 by Reymond et al. by using *in vitro* co-immunoprecipitations (Reymond et al., 1999). This binding was then confirmed and analyzed in further studies that also characterized the PDE activity of h-prune and its relevance in regulating cell motility (D'Angelo et al., 2004). There is a direct correlation between the interaction of h-prune with Nm23-H1 and the increase in the PDE activity of h-prune. Zollo and co-workers have shown that the overexpression of h-prune in cancer cells leads to an increase in motility, and thus in metastatic potential, via the binding of Nm23-H1. Indeed, h-prune is able to act as a negative regulator of the anti-metastatic activity of Nm23-H1 in two ways. On the one hand, high levels of h-prune in the cell sequester the free Nm23-H1, whose metastasis suppressing activity is therefore reduced. In parallel, the binding of Nm23-H1 to h-prune causes an increase in the PDE activity of h-prune, which leads to an overall increase in cellular motility (*Figure 20)*.

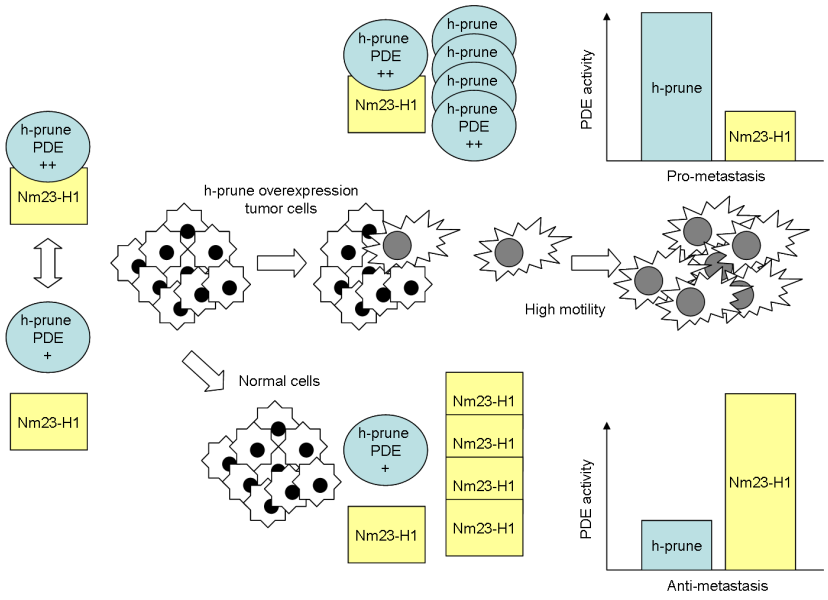

Figure 20: **Schematic representation of the interaction of h-prune and Nm23-H1 in tumor, and the effects of this binding.**

The region that interacts with h-prune is the carboxyl terminus of Nm23-H1, around S120, S122 and S125. The phosphorylation of these serines by casein kinase I (CKI) is essential for the binding of h-prune to Nm23-H1 (Garzia et al., 2008). Indeed, treatment with IC261, an inhibitor of CKI, is able to disrupt the complex, identifying a further potential therapeutic approach together with the PDE inhibitor dipyridamol (*Figure 21*).

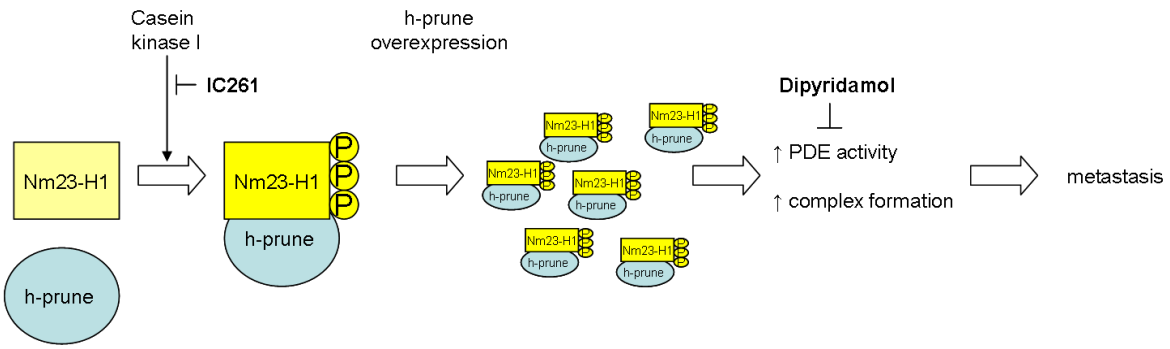

Figure 21: **The interaction between Nm23-H1 and h-prune and the subsequent metastasis promoting effects can be impaired by the use of a CKI inhibitor and dipyridamol.**

2. AIMS OF THE STUDY

ASAP1 is a multidomain adaptor protein that is involved in several physiological processes such as cytoskeletal re-organization (Randazzo et al., 2000) and vesicle trafficking (Nie et al., 2006). ASAP1 has also been shown to play a role in tumor development (Lin et al., 2008) and progression (Morishige et al., 2008; Müller et al., 2010). ASAP1 is able to bind to several SH3 bearing proteins via its proline rich regions that may mediate its activities, in particular the promotion of motility and invasiveness, and thus of metastasis formation. ASAP1 has been shown by the laboratory of Prof. Zollo to interact also with Nm23-H1 and h-prune, a protein duo involved in cell motility and invasion. The aim of my study was to investigate if and to which extent these binding partners of ASAP1 are able to affect its metastasis-promoting activities. For this purpose I chose two prominent features of ASAP1, namely its role in vesicle trafficking and growth factor internalization, as well as its ability to promote motility. The specific aims of my study were as follows:

- Establish an assay for measuring the internalization of EGF in the highly invasive model of the MDA MB 231 cells
- Investigate the possible effects of the two new binding partners of ASAP1, Nm23-H1 and h-prune, on the uptake of EGF and the motility promoted by ASAP1
- Identify additional SH3 domain-bearing proteins that bind to ASAP1, and then analyze the possible interference of Nm23-H1 and h-prune with this binding
- Evaluate the influence of SH3-domain ASAP1 binding partners on the motility-promoting activity of ASAP1.

3. MATERIALS AND METHODS

3.1 Instruments

Centrifuges	Thermo Fisher Scientific, Schwerte
Developer for X-ray films CAWOMAT 2000R	CAWO, Schrobenhausen
Diaphragm Pump	Vacuubrand, Wertheim
Electrophoresis Apparatus	PeqLab, Erlangen; BioRad, München
ELISA reader Multiskan Acscent	Thermo Fisher Scientific, Schwerte
FACS-can	BectonDickinson, Franklin Lakes USA
Fluorescence microscope Axio Imager D1	Carl Zeiss, Jena
FPLC system	GE Heathcare, München
Gel dryer MGD 5040	VWR International, UK
Incubator	Binder, Tuttlingen
Incubator HeraCell	Thermo Fisher Scientific, Schwerte
Microscope Axiovert 40 CFL	Carl Zeiss, Jena
NanoDrop	PeqLab, Erlangen
PCR-Cycler	Analytikjena, Jena
Shaker for bacteria Certomat IS	Sartorius, Göttingen
Sonicator Sonoplus	Bandelin, Berlin
Sterile hood Hera Safe	Thermo Fisher Scientific, Schwerte
Thermomixer 5436	Eppendorf, Hamburg
Ultracentrifuge Sorval RC6 plus	Thermo Fisher Scientific, Schwerte
UV-Transiluminator	INTAS, Göttingen
Vortex	VWR International, UK
Water bath	Memmert, Büchenbach

3.2.Chemicals, reagents and consumables

0.25% Trypsin-EDTA (1x), phenol red	Life Technologies, Darmstadt
AceGlow	PeqLab, Erlangen
Acetic acid	Roth, Karlsruhe
Acrylamide/N,N‘-Methylenbisacrylamide (37,5:1)	Roth, Karlsruhe
Agarose	Biozym, Wien, Austria
Ammonium peroxodisulfate (APS)	Roth, Karlsruhe
Ampicillin	Roth, Karlsruhe
BCA assay	Thermo Fisher Scientific, Schwerte

Bovine serum albumin (BSA)	PAA, Pasching, Austria
Bromophenol blue	Roth, Karlsruhe
Butanol	Roth, Karlsruhe
Chloroform	Roth, Karlsruhe
Coomassie Brilliant Blue R250	Roth, Karlsruhe
Deoxynucleoside-triphosphates (dNTPs)	Life Technologies, Darmstadt
Diethylpyrocarbonate (DEPC)	Roth, Karlsruhe
Dimethylsulfoxide (DMSO)	Sigma Aldrich, Steinheim
Dithiothreitol (DTT)	Fluka, Neu-Ulm
Dulbecco‘s modified Eagle Medium (DMEM)	Life Technologies, Darmstadt
ECL-Western blotting detection reagent	Thermo Fisher Scientific, Schwerte
Ethidium bromide	Roth, Karlsruhe
Ethylenediaminetetraacetic acid (EDTA)	Sigma Aldrich, Steinheim
Fetal Calf Serum (FCS)	Life Technologies, Darmstadt
Glycerol	Sigma Aldrich, Steinheim
Glycine	Roth, Karlsruhe
HEPES	Roth, Karlsruhe
Lipofectamine 2000	Life Technologies, Darmstadt
Lipofectamine LTX	Life Technologies, Darmstadt
Lithium chloride	Roth, Karlsruhe
Magnesium chloride	Roth, Karlsruhe
Methanol	Roth, Karlsruhe
N, N, N‘, N‘-Tetramethylethylendiamine (TEMED)	Roth, Karlsruhe
Oligonucleotides	Metabion
OptimMem	Life Technologies, Darmstadt
Paraformaldehyde	J.T. Baker, Deventer, The Netherlands
Penicillin/Streptomycin	Life Technologies, Darmstadt
Phenol	Roth, Karlsruhe
Phenylmethylsulfonyl fluoride (PMSF)	Roth, Karlsruhe
Phosphate buffer saline (PBS)	Life Technologies, Darmstadt
Plasmid Maxi Kit	Qiagen, München
Propanol	Roth, Karlsruhe
Protein G+ Agarose	Calbiochem, Darmstadt
Reagents for developer	AGFA, Bonn
Restriction enzymes and buffers	Fermentas, Thermo Fisher Scientific, Schwerte
SOC	Life Technologies, Darmstadt
sodium acetate	Roth, Karlsruhe
sodium chloride	Roth, Karlsruhe
sodium orthovanadate	Roth, Karlsruhe
sodium dodecylsulfate (SDS)	Roth, Karlsruhe
sodium hydroxide (NaOH)	Roth, Karlsruhe

Superscript II	Life Technologies, Darmstadt
T4-Ligase	Fermentas, Thermo Fisher Scientific, Schwerte
Taq-DNA-Polymerase and Buffer	Fermentas, Thermo Fisher Scientific, Schwerte
Tip-500-columns	Qiagen, München
TOPO-TA-Cloning Kit	Life Technologies, Darmstadt
Tris-HCl, Tris-Base	Sigma Aldrich, Steinheim
Triton X-100	Sigma Aldrich, Steinheim
Trizol	Life Technologies, Darmstadt
Tryptone	Roth, Karlsruhe
Tween 20	GE Heathcare, München
Yeast extract	Roth, Karlsruhe

3.2.1 Antibodies

3.2.1.1 Primary antibodies

Anti-ASAP1	mouse, monoclonal, self-production
Anti-FLAG-M2	mouse, monoclonal, Sigma
Anti-Nm23-H1	mouse, monoclonal, Abcam
Anti-HA	mouse, monoclonal, Covance
Anti-SLK	rabbit, polyclonal, Abcam
Anti-His	rabbit, polyclonal, MicroMol
Anti-β-actin	mouse, monoclonal, Sigma
Anti-cortactin	mouse, polyclonal, Millipore
Anti-GST (clone 2D5)	rat, self production
Anti-TNP	mouse, self prooduction

3.2.1.2 Secondary antibodies

All secondary antibodies were from DAKO, polyclonal, produced in goat

Anti mouse HRP

Anti rabbit HRP

Anti Rat HRP

3.2.2 Oligonucleotides

huHPRT (Hypoxanthine–Guanine Phosphoribosyltransferase) primers

forward: 5´- CCAAAGATGGTCAAGGTCGC- 3´

reverse: 5´- CTGCTGACAAAGATTCACTGG - 3´

huASAP primers

forward: 5´- GCCACCATGAGATCTTCAGCCTCCA- 3´

reverse: 5´- CTGCGTTTTGCTAGTCAGACAGGATATG- 3´

Cloning of human SLK

forward: 5´- CACCATGTCCTTCTTCAATTTCCG - 3´

reverse: 5´-TGA TCC GGT GGA ATG CAA GCT GGG AAT- 3´

3.2.3 Cells

3.2.3.1 Prokaryotic cells

One Shot® TOP10 Chemically Competent *E. coli* (Invitrogen)

XL1-Blue *E. coli*

3.2.3.2 Eukaryotic cells

NAME	SPECIFICATION	REFERENCE
MDA MB 231	Human breast adenocarcinoma	Brinkley et al., 1980
Hek293	Human embryonic kidney	Graham et al., 1977
7B12	Mouse hybridoma cells	Self production (Müller et al., 2010)
Primary mouse embryonic fibroblasts		Self purification

3.3 Cell culture methods

3.3.1 Eukaryotic cell maintenance

Except for primary mouse embryonic fibroblasts (MEFs), all mammalian cells used in this study were maintained at 37°C in an incubator in 5% CO_2 and 95% air humidity. The MEFS were kept for a maximum of 6 passages under the same conditions as the other cells, but with a constant 3% of O_2. Cells were grown in Petri dishes, multi well or flasks of varying size depending on the application. Both culture medium and trypsin were warmed to 37°C before applying them to the cells.

In general, the cells were grown until a confluency of 80-90% had been reached, detached by trypsinization and re-seeded at lower density. Briefly, culture medium was removed followed by one wash with PBS. A 0.25% trypsin solution was added and the cells were incubated at 37°C until they detached. Fresh medium was then added, the cells centrifuged and re-suspended to obtain the desired concentration and plated in a new dish.
All cell lines were routinely screened for mycoplasma infection using the VectorGem Myco Detection kit (Vector).

3.3.2 Freezing and thawing

Logarithmically growing cells were trypsinized, harvested by medium addition and centrifuged as described above. The supernatant was then removed and the cells re-suspended in normal culture medium containing 10% DMSO. The suspension was placed in appropriate 1.8 ml vials. Prepared cells were immediately placed in - 80°C and after some days moved to liquid nitrogen.
Cells were quickly thawed at 37°C, and warm medium was added to dilute the DMSO. They were then centrifuged, re-suspended in fresh medium and immediately plated.

3.4 DNA and RNA methods

3.4.1 Measurement of the concentration of nucleic acids

DNA or RNA concentration was measured by using 2 µl of the aqueous nucleotide solution and the Nanodrop spectrophotometer. The optical density (OD) of the nucleic acids was measured at 260 and 280 nm. A 260/280 OD ratio of ~1.8 indicates a relatively pure DNA and a ratio of ~2.0 is generally accepted as pure for RNA.
A 50 µg/ml solution of double stranded DNA or a 40 µg/ml solution of single stranded RNA has an absorbance of 1.0 at 260 nm. Therefore the concentration is calculated by the software ND-1000 (version 3.1.2) as follows:

$$\text{DNA concentration (µg/ml)} = (OD_{260}) \times (\text{dilution factor}) \times (50\ \mu g\ DNA/ml)/(1\ OD_{260}\ \text{unit})$$

$$\text{RNA concentration (µg/ml)} = (OD_{260}) \times (\text{dilution factor}) \times (40\ \mu g\ RNA/ml)/(1\ OD_{260}\ \text{unit})$$

3.4.2 Agarose gel electrophoresis

Dependent on the size of the fragments to be analysed, 0.8-1.5% agarose gels were used to separate DNA or RNA. The agarose was dissolved in 1X TAE buffer with the help of a microwave oven. When the solution was cool, a few μl of ethidium bromide were added before pouring the solution into the running chamber, already provided with a comb. As soon as the gel solidified, the comb was removed and the chamber was filled with sufficient amount of 1X TAE buffer to fill the wells and cover the gel. Finally, loading buffer was pipetted to an appropriate amount of DNA or RNA. The probes were loaded and a 60-80V current was applied to the gel, until they reached the desired separation. The bands were then visualized with UV light and a picture was taken.

50X TAE for agarose gel

Tris	2 M
Acetic Acid	2 M
EDTA pH8.0	50 mM

6X Loading buffer for agarose gel

Bromphenol blue	0.25% (w/v) FF
Xylene cyanol	0.25% (w/v)
Sucrose	40% (w/v)

3.4.3 Whole RNA Cell Extraction

Cells were grown to confluency on a 100 mm diameter Petri dish. They were washed twice with PBS before adding 6 ml Trizol. The cell lysate was collected in a fresh tube and incubated for five minutes at room temperature for complete disruption. After addition of 1.2 ml of chloroform, the tube was vigorously shaken for 15 seconds and then allowed to stand for two minutes in order to separate the organic from the inorganic phase. The solution was then centrifuged at 12000g, at 4°C for 15 minutes, so that the upper aqueous phase could be recovered and put in a fresh tube. To precipitate the nucleic acid, 750 μl isopropanol were added and the solution was incubated for 10 minutes at room temperature, followed by 10 minutes of

centrifugation at 12000g at 4°C. The supernatant was removed, and the RNA was washed with 75% ethanol by vortexing and centrifuging for five minutes at 7500g at 4°C. The ethanol was then removed and the RNA was air dried, before re-dissolving it with 80μl of water. Finally, the solution was heated to 57°C for 10 minutes.
The concentration of the RNA was measured and the purity was assessed by loading the probe on an agarose gel.

3.4.4 cDNA synthesis

For cDNA synthesis, Superscript II was used according to manufacturer's instructions, and the reaction was performed in the buffer provided (5X First Strand Buffer). Briefly, a 20 μl reaction was set up for each RNA sample, starting from the master mix:

10 mM dNTPs mix	1 μl
150 ng random primers	1 μl
2 μg total RNA	x μl
Sterile, distilled H_2O	up to 12 μl

This mix was heated at 65°C for 5 minutes, quick chilled and briefly centrifuged to recover the whole solution. Then 4 μl 5X First Strand Buffer and 2 μl 0.1M DTT was added, and the mix incubated at 25°C for 2 minutes. After this incubation time, 1 μl Superscript was finally added to the reaction mixture, and gently pipetted up and down to ensure proper mixing. The tube was put in the thermo cycler with the following conditions:

10 minutes 25°C
50 minutes 42°C
15 minutes 70°C

To check the integrity of the cDNA, a control PCR reaction with HPRT primers was performed using 25 μl of cDNA from the first-strand reaction. The PCR product was then loaded on an agarose gel.

5X First Strand Buffer

250 mM Tris-HCl (pH 8.3 at room temperature),
375 mM KCl,
15 mM $MgCl_2$

3.4.5 PCR

If not otherwise stated, DreamTaq (Fermentas) was used. The reaction mixture was combined while keeping all the reagents and the tubes on ice. For each reaction, a 50 μl master mix reaction was prepared, pipetting to the provided 10X buffer the following reagents:

dNTPs 10 mM	1 μl
Forward primer	0.2 μM
Reverse primer	0.2 μM
DNA or water	2 μl

Finally, 0.4 μl of the DreamTaq enzyme was added, nuclease-free water was pipetted up to the desired volume and the samples were put into the thermocycler for the reaction (*Table 2*). This started with a pre-run (step 1), followed by a short heating that allowed the DNA strands to separate from each other (Tm = melting temperature). In step three the temperature drops and the primers can thus anneal to the single strands (Ta = annealing temperature). The reaction is then heated up again in step four to reach the optimal temperature for the DNA polymerase, allowing the synthesis of the new strand by extension of the primer (Ts = synthesis temperature). This sequence is then repeated for several cycles, until a final elongation at 72°C (Te = elongation temperature) concludes the reaction (step 5).

Oligo/ reaction	Step 1		Step 2		Step 3		Step4		Step 5		Cycles no.
	Tm1	time	Tm2	time	Ta	time	Ts	time	Te	time	
huHPRT	95	2'	95	1´	61	30´´	72	2`	72	5'	30
huASAP1	95	2´	95	15´´	70	30´´	72	5`		5'	30
SLK cloning	98	30´´	98	10´´	64	30´´	72	2`		10'	30

Table 2: **Cycling conditions for the PCR reactions.** All the tempreatures indicated are in °C

3.4.6 Isolation of DNA fragments from agarose gels

The band of interest was cut out from the gel and weighed, and subsequently purified with the PeqGold Gel Extraction Kit from PeqLab according to the manufacturer's instructions. The purified fragment was eluted with 30 μl water and the concentration

was measured with a Nanodrop spectrophotometer. The purity of the fragment was also assessed by loading it again on an agarose gel.

3.4.7 Preparation of $CaCl_2$ competent E. coli cells

An E. coli culture at OD_{600} of 0.06 was added to 50 ml LB selective medium. When the bacteria reached the logarithmic phase of growth, cultures were centrifuged at 4,000 rpm for 10 minutes at 4°C. The pellet obtained was then washed twice in 20 ml 0.1 M $MgCl_2$. The clean pellet was resuspended in 2 ml 0.1 M $CaCl_2$, before being incubated on ice for at least 2 hours. Sterile glycerol (ratio 1:1) was added, the competent cells aliquoted and frozen in liquid nitrogen.

3.4.8 Isolation of plasmid DNA

One vial containing 100 µl of competent XL1-Blue bacteria was thawed on ice for 15 minutes. Then 20 ng of DNA was added and incubated with the bacteria for 30 minutes. The bacteria were then heat shocked at 42°C for 90 seconds and then immediately chilled on ice for three minutes. SOC medium was then added to a final volume of 1 ml and the vial was put on a shaker at 37°C for one hour. Bacteria were then streaked on a selective agar plate containing ampicillin and incubated over night at 37°C. On the following day, several colonies were picked and allowed to grow over night in 1.5 ml selective LB medium at 37°C under constant shaking. The cell suspension was then centrifuged at 17000g for one minute, and 200 µl TELT buffer containing lysozyme were added, followed by vortexing in order to completely lyse the bacterial cells. The suspension was heated for three minutes at 96°C and quickly chilled on ice for five minutes. In order to clear the lysate, it was centrifuged for eight minutes at 17000g at room temperature, and the pellet was carefully discarded. To precipitate the DNA, 150 µl isopropanol was pipetted to the solution and centrifuged at 17000g for five minutes. The supernatant was discarded, and the pellet was washed twice with 70% ethanol. Finally the pellet was air dried and re-dissolved in 50 µl ddH_2O. The concentration was assessed by Nanodrop measurement.

TELT buffer for plasmid mini preparation

Tris pH8	50 mM
EDTA	62.5 mM
Triton X-100 (TX-100)	0.4%
LiCl	2.5 M
Lysozyme	1 mg/ml

Luria Bertani (LB) medium for bacteria growth (g/l)

NaCl	5
Yeast Extract	5
Tryptone	10

3.4.9 Digestion of DNA with restriction enzymes

For restriction enzyme digestions, 1 μg of DNA was incubated with the appropriate buffer and 1 μl of enzyme(s) for one hour at 37°C. The reaction was then stopped by heat inactivation of the enzyme at 65°C for 20 minutes.

3.4.10 Large-scale plasmid preparation

Large-scale plasmid preparations were performed with the Quiagen Maxi kit following the manufacturer's instructions. Briefly, a single colony from a freshly streaked selective agar plate was picked and inoculated into 3 ml of LB medium containing ampicillin. The bacteria were grown for ~8 hours and then this starter culture was diluted into 200 ml of selective medium using a vessel with a volume of at least four times greater than that of the medium. Again the bacteria were allowed to grow under constant shaking (~300 rpm) over night. The next day the cells were centrifuged and either stored at -20°C or immediately processed for plasmid isolation following the manufacturer's protocol.

3.4.11 RNA interference

The corresponding company controls were used for each siRNA. The ratio nmol siRNA:μl Lipofectamine™ 2000 was always 0.1:5. For all oligonucleotides, the transfection was performed as follows. Cells were seeded to reach a confluence of ~50% on the transfection day. Both the oligonucleotides and the Lipofectamine™ 2000 were separately diluted in OptiMem according to the Lipofectamine™ 2000

protocol. In case of a co-transfection, the RNA amount was divided equally between the two sequences, in order to maintain a constant total amount of RNA.

Briefly, the diluted Lipofectamine™ 2000 was incubated for five minutes at room temperature, and subsequently combined with the diluted oligonucleotides. The mixture was incubated for 20 minutes at room temperature, and finally added drop wise to the cells. These were maintained in medium containing FCS, but without antibiotics. The knock down was most efficient after 72 hours for all three siRNAs.

The following silencing sequences and protocols have been used:

Gene	Name/company	Sequence 5´- 3´
ASAP1	Stealth RNAi™/ Invitrogen	GACCAGAUCUCUGUCUCGGAGUUCA
SLK	Stealth RNAi™/ Invitrogen	UGUCCUUCUUCAAUUUCCGUAAGAU
Nm23-H1	*Silencer*® Validated siRNA/Ambion	GGAACACUACGUUGACCUGtt

3.4.12 DNA plasmid transfection

For the transfection of plasmid DNA, Lipofectamine 2000 or Lipofectamine LTX were used, depending on the cell type and the application. The cells were plated to reach a density of ~90% on the day of transfection. For both cases, manufacturer's instructions were followed for the preparation of the transfection mixture, and the cells were always kept in an antibiotic-free medium. Both DNA and Lipofectamine 2000 were diluted in OptiMem. The ratios of DNA:Lipofectamine used were:

- Lipofectamine LTX 1:3
- Lipofectamine 2000 1:2.5

In case of a co-transfection, the DNA amount was divided equally between the two plasmids, in order to maintain a constant total amount of DNA. The DNA solution was added drop wise to the cells. After 48 hours the transfection efficiency reached its maximum, and the cells were ready for subsequent analysis or experiments.

3.4.13 Cloning of human Ste20-Like Kinase

The cloning of human Ste20-like kinase was performed with the pcDNA™3.1*/*V5-*His TOPO*® TA kit (Life Science, Darmstadt). This kit allows the insertion of the expression sequence of the gene in frame with a polyhistidine tag, thus the resulting protein will

be a fusion protein. Total RNA from 293T cells was isolated, and cDNA was synthesized as previously described. Specific primers were designed and used to amplify the SLK sequence of the cDNA. For the PCR reaction, the proofreading polymerase Phusion (NEB) was used. A master mix was prepared by combining the provided 5X buffer with 1 µl each of 10 mM dNTPs, forward primer, reverse primer and the polymerase. Either 2 µl of cDNA or of water as a control were added, and finally nuclease-free water was added up to 50 µl for each reaction. The cycling conditions were as shown in *Table 2*. The PCR product was then loaded onto an agarose gel, and the band was excised and purified as previously described.

For the cloning, the following reaction was set up:

PCR product	4ul
Salt solution (1.2 M NaCl; 0.06 M $MgCl_2$)	1ul
TOPO vector	1ul
H_2O	up to 6ul

The mixture was incubated for 15 minutes at room temperature, before adding 2µl of the mixture to 50 µl of Top10 cells, previously thawed on ice. The bacteria were kept on ice for 15 minutes and then heat shocked for 30 seconds at 42°C. Then 250 µl SOC medium were added to the cells, which were kept at 37°C for one hour with shaking. Finally, 200 µl of bacteria suspension was plated on pre-warmed, selective LB-agar plates. The next day, several colonies were picked and inoculated with 1.5 ml selective LB and allowed to grow over night. The cloning was checked with a mini preparation of DNA and the resulting plasmid digested with an appropriate enzyme (XhoI) at 37°C for 90 minutes. The digestion with this enzyme of the plasmid containing the correct insert would result in two unique fragments of distinct molecular weight (8.5 kDa + 0.7 kDa). The fragments were loaded onto an agarose gel, and the colonies that contained the correct plasmid were inoculated for a maxi DNA preparation as previously described. This was checked again by digestion with the XhoI enzyme (*Figure 22*), before proceeding with the sequencing carried out by Eurofins MWG, Ebersberg.

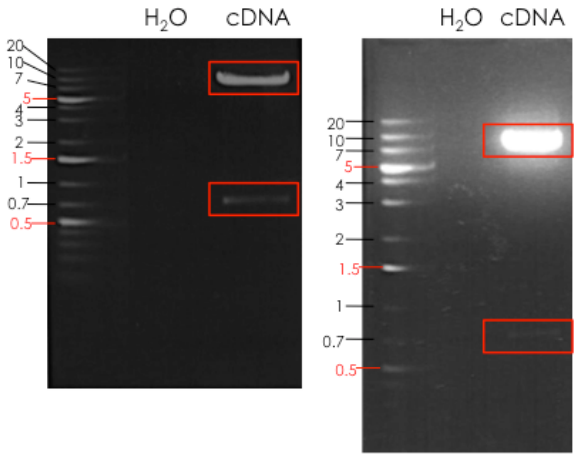

Figure 22: Control digestion of the His-SLK expression plasmid. The gel was photographed twice during the run (the picture on the right is a longer run) to better visualize the two fragments of 8.5 kDa and 0.7 kDa, respectively, that result form the digestion with XhoI of the His-SLk expressing plasmid.

3.5 Protein methods

3.5.1 Preparation of protein samples for SDS-PAGE

Protein samples were prepared as follows, unless otherwise indicated:
Cells were kept on ice and washed twice with cold PBS. Approximately 100 µl cold lysis buffer/10^6 cells were added and the cells were detached from the plate by scraping. The lysate was collected in a fresh tube and sheared five times through a 27G needle, before centrifuging it for 15 minutes at 4°C at 12000g. The cleared lysate was then either stored at -20°C or immediately used for subsequent analysis.

Lysis buffer

Tris pH 7.5	50 mM
NaCl	150 mM
EDTA	5 mM
TX-100	1%
PMSF	1 mM
Protease inhibitor cocktail (Roche)	1x dilution

3.5.2 Protein concentration determination

The protein concentration of cell lysates was assessed with a commercially available bicinchoninic acid assay, using known concentrations of bovine serum albumin for the calibration curve. A 1:5 dilution of the lysate was used for the colorimetric reaction that was performed in a flat bottom 96 well plate. The color development is proportional to

the amount of protein present in the solution, and was measured at 595nm with an ELISA reader. The concentration was then calculated with the Ascent software, according to the calibration curve.

3.5.3 SDS-polyacrylamide gel electrophoresis (PAGE)

SDS-PAGE gels were prepared as follows. The percentage of acrylamide for the resolving gel was selected according to the size of the proteins to be separated. The components of the solution were carefully mixed, avoiding the formation of air bubbles. APS and TEMED were added only at the end, as they start the polymerization reaction. The resolving gel solution was poured first, and the surface was immediately covered with a thin layer of water-saturated butanol. When the gel was polymerized, the butanol was removed and the gel was briefly washed with water. The comb was then put into place and the stacking gel solution was carefully poured and allowed to polymerize. When ready, the comb was carefully removed and the resulting wells delicately washed with running buffer. The gel was then taken out of the casting stand and inserted into a clamping frame together with another gel or with the provided buffer dam to create a leak-proof seal. The electrode assembly was inserted into the tank filled with running buffer and the protein samples were loaded.
These were prepared by adding 4X loading buffer and boiling them at 95°C for five minutes. The samples were briefly spun down and loaded onto the SDS-PAGE gel. Gels were run with constant Amperes and 60V until the protein front reached the resolving gel, then a voltage of 80V was applied. The gels were run until the blue dye reached the lower edge of the resolving gel. They were then removed from the apparatus and soaked in transfer buffer for equilibration.

Buffers and solutions

4X Loading Buffer

Tris-HCl pH 6.8	0.1 M
SDS	8%
Glycerol	40%
Bromophenol Blue	0.02%
DTT	0.1 M

Solutions for acrylamide gel preparation:

	Resolving Gel	Stacking Gel
Tris pH8.8	0.375 M	-
Tris pH6.8	-	0.125 M
acrylamide	8-12%	3%
Water	up to volume	
SDS	0.01%	
APS 10%	0.01%	
TEMED	0.001%	

1x Running buffer

Glycine	25 mM
Tris	192 mM
SDS	0.1%

3.5.4 Coomassie stain

When needed, SDS-PAGE gels were soaked in the staining solution and allowed to stain overnight under shaking at room temperature. The day after, the gel was de-stained by doing several one-hour washes with the de-staining solution until clear. Finally, the gel was put on a filter paper in the Gel Dryer for three hours at 60°C.

Staining solution

Coomassie brilliant blue	2%
Methanol	40%
Glacial acetic acid	5%
Water up to volume	

De-staining solution

Methanol	40%
Glacial acetic acid	5%
Water up to volume	

3.5.5 Western Blot

SDS-PAGE gels were soaked in transfer buffer before assembly of the blot. An appropriate size of PVDF membrane was cut and prepared for the blotting, which was carried out according to manufacturer's instructions. Briefly, the membrane was soaked for a few seconds in methanol until translucent, and then wetted in water for 2 minutes. Finally, it was soaked in the transfer buffer for equilibration for at least 5 minutes.

The stack for the blotting was prepared as follows, starting from the cathode side: one sponge pad, two layers of filter paper, the gel, the membrane, two filter paper sheets and another sponge pad. Attention was paid not to allow air bubbles to form between the layers. The gel was electro-blotted onto the membrane with continuous stirring of the transfer buffer either for 2 hours at 100V, or overnight at 30V.

At the end of the blotting, the gel was discarded and membrane was briefly rinsed with washing buffer and air dried, before being incubated with blocking buffer for one hour at room temperature. The incubation with the primary antibody, diluted in the blocking buffer, was performed either at room temperature for two hours or over night at 4°C. The appropriate secondary antibody was incubated with the membrane for one hour, following a five-minute wash with washing buffer. Finally, the membrane was rinsed three times before proceeding to the chemiluminescent reaction. For this process the ECL detection reagent was prepared according to manufacturer's instruction and pipetted onto the membrane. After one minute incubation the membrane was exposed to several X-ray films for between 5 seconds and up to 30 minutes, depending on the strength of the signal. In case of a weak or even absent signal the membrane was shortly rinsed and the procedure was repeated with another detection reagent, AceGlow, which ensured a higher sensibility.

If proteins of the same or similar molecular weight were to be visualized onto the same membrane, this was subjected to a stripping procedure. The membrane was soaked into a stripping solution at 42°C for 30 minutes, and then washed three times for ten minutes with the washing buffer. The membrane was then incubated again with the blocking buffer for one hour

Buffers and Solutions

1x Transfer buffer

Glycine	25 mM
Tris	192 mM
SDS	0.1%
Methanol	15%-20% according to protein size

Tris-buffered saline (TBS) 10X

Tris HCl, pH 7.4	500 mM
NaCl	1.5 M

Washing buffer

TBS	1X
Tween	0.05%

Blocking buffer

Bovine serum albumin	1%
TBS	1X
Tween	0.05%

Stripping solution

SDS	2%
β-mercaptoethanol	**0.7%**
Tris-HCl pH 6.8	62.5 µM

3.5.6 Co-immunoprecipitation

293T cells were transfected with a Flag-tagged ASAP1 expression plasmid alone or in combination with Nm23-H1 or h-prune as described in 3.5.13. After 48 hours post transfection cells were kept on ice and washed twice with cold PBS. Approximately 100 µl cold lysis buffer/10^6 cells was added and the cells were detached from the plate by scraping. The lysate was collected in a fresh tube and sonified twice for 30 seconds, with a five minute break in between. In order to get rid of the cellular debris, the lysate was then centrifuged twice for 15 minutes at 4°C at 12000g. The cleared lysate was then either stored at -20°C or immediately used for subsequent analysis.

Aliquots (400 μg) of cleared cell lysate were combined with 50 μl of protein G+ agarose resin and were incubated with rotation for two hours at 4°C. The lysate was then centrifuged for five minutes at 12000g at 4°C, then the supernatant was recovered and put in a fresh tube. The procedure was repeated a second time, in order to get rid of the non-specific binding to the resin. Flag M2 antibody (6 μg), the corresponding isotype antibody control, or no antibody were added to the cleared lysate, and incubated again with rotation for two hours at 4°C. Finally, 50 μl of protein G+ agarose resin were pipetted to each probe and the co-immunoprecipitation occurred over night, always under rotation, at 4°C. On the following day the beads were washed with the washing buffer by centrifuging them three times at 17000g for three minutes. An appropriate amount of 4X loading buffer was added and the beads were boiled at 95°C for five minutes. The suspension was quickly centrifuged and the supernatant loaded onto an SDS-PAGE gel.

Co-immunoprecipitation lysis buffer:

HEPES pH7.4	25 mM
NaCl	150 mM
$MgCl_2$	10 mM
Lubrol	1%
Na_3VO_4	10 mM
PMSF	1 mM
Protease inhibitor cocktail (Roche)	1x dilution

Washing buffer:

HEPES pH7.4	25 mM
NaCl	150 mM
$MgCl_2$	10 mM

3.6 SH3 Domain Array

The array used for this assay was purchased at Panomics/Affymetrix, (Santa Clara, USA), and is composed of two identical PVDF membranes on which specific SH3 recombinant proteins have been spotted. These proteins consist of the purified recombinant conserved binding site of the individual SH3 domain proteins, and are different among the four arrays available. We used the *SH3™ Domain Array I*, which contains the protein visualized in *Figure 23*. If the membrane is incubated with a cell

lysate containing Flag-tagged transfected ASAP1, this will selectively bind to its SH3 interaction partners. By subsequent incubation of the membrane with the anti-Flag antibody, the interaction and its strength will be visible as a spot in correspondence to the putative SH3 binding protein.

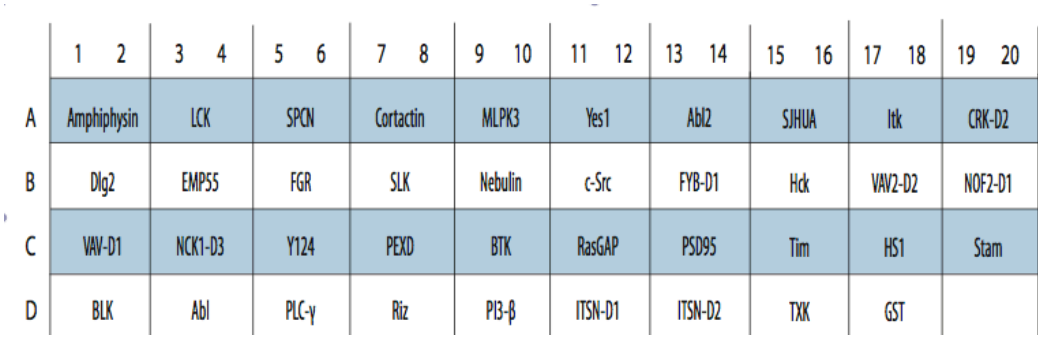

	1 2	3 4	5 6	7 8	9 10	11 12	13 14	15 16	17 18	19 20
A	Amphiphysin	LCK	SPCN	Cortactin	MLPK3	Yes1	Abl2	SJHUA	Itk	CRK-D2
B	Dlg2	EMP55	FGR	SLK	Nebulin	c-Src	FYB-D1	Hck	VAV2-D2	NOF2-D1
C	VAV-D1	NCK1-D3	Y124	PEXD	BTK	RasGAP	PSD95	Tim	HS1	Stam
D	BLK	Abl	PLC-γ	Riz	PI3-β	ITSN-D1	ITSN-D2	TXK	GST	

Figure 23: **Schematic diagram of the SH3 domain array I.** All recombinant proteins are spotted in double.

On day one, 293T cells were seeded in 15 cm diameter Petri dishes. The day after, the confluent cells were transfected with the indicated plasmids as described in 3.5.13 After 48h, the dishes were put on ice, then the cells were briefly rinsed and harvested with 5 mM EDTA-PBS. They were then counted, and lysed in the Resuspension Buffer containing proteinase inhibitors (approximately 1 ml buffer/10^6 cells). The lysate was sonified twice and finally centrifuged. The protein content was assessed, and the lysate was diluted with Resuspension Buffer to a final concentration of 1 mg/ml, then frozen. The transfection was checked by means of Western Blot.

For the assay, the lysates were thawed on ice and the SH3 domain array membranes containing the recombinant proteins was prepared following the manufacturer's instructions. Each membrane was then incubated for 90 minutes with the lysate to enable the possible binding of ASAP1 with the SH3 domain-bearing proteins. This step was followed by three washes of ten minutes with the washing buffer. The membrane was incubated overnight with the ASAP1 antibody diluted in the washing buffer.

On the following day, the membrane was washed three times for ten minutes, and then incubated with the appropriate secondary antibody for 30 minutes, followed by three ten-minute washes. For the detection, equal amounts of Detection Buffer A and B were combined and gently pipetted onto the membrane. The array was then exposed on X-ray films for various times.

Buffers provided by the kit:

1X Resuspension Buffer
1X Blocking Buffer
10X Washing Buffer
Detection Buffer A
Detection Buffer B

3.7 Recombinant Cortactin Dot Blot

PVDF membrane was cut to a ca. 10 cm x 3 cm rectangle, pre-wetted with 100% methanol and washed twice with the Western blot washing buffer. It was then allowed to semi-dry. Recombinant cortactin identical to the one used for the SH3 array was provided by Panomics as a 1 μg/μl solution. For each dot, 1 μl of a 1:10 dilution was spotted onto the membrane and allowed to absorb. The membrane was then incubated for one hour shaking at room temperature in washing buffer containing 1% BSA. The lysate-binding assay then followed the same protocol as for the SH3 domain array assay described above (Section 7). As a negative control, the membrane was incubated with the secondary antibody only. Incubation with an anti-GST antibody that binds to the recombinant cortactin spotted on the membrane served as a positive control.

3.8 Production of the 7B12 anti-ASAP Antibody

The 7B12 antibody-producing hybridoma cells were previously established in the lab by immunizing Balb/C-mice with a recombinant ASAP1 protein (Müller et al., 2010). Hybridoma cells were grown in 150 mm diameter plates with 50 ml medium until they died. The conditioned medium was then collected and stored at -20°C. A total amount of two litres of conditioned medium was collected. To remove cellular debris, the medium was centrifuged for 10 minutes at 4°C at 4000 rpm. Solid ammonium sulphate was added with slow stirring to obtain a final concentration of 50% (313 g/l). This solution was left gently stirring over night at 4°C, and finally centrifuged for 10 minutes at 4°C at 4000 rpm. The supernatant was discarded and the resulting pellet was re-suspended in 20 ml/l buffer A. This solution was dialysed for 24 hours against buffer A, changing the dialysis buffer three times. The dialyzed solution was

centrifuged for 10 minutes at 10000 rpm and Protein G+ agarose beads were added to the supernatant to a final amount of 3 ml 50% slurry/l medium. This suspension was then incubated for two hours with rotation at 4°C, and finally centrifuged at 3000 rpm to remove unbound protein. The beads were washed four times with buffer A and transferred into a BioRad poly-prep 1.5 ml column until the gel was packed and the excess fluid was drained off.

The elution of the antibodies was carried out using 100 mM glycine pH 2.5 (5x0.5 ml fractions neutralized with 50 µl 1M Tris pH 9.6) followed by 100 mM $NaHCO_3$ pH 10.8 (4x0.4 ml fractions neutralized with 87 µl 100 mM $Na_3C_6H_5O_7$ pH 5.0).

The concentration of each fraction was measured with the Nanodrop spectrophotometer. A microliter of sample was pipetted onto the optical surface of the instrument, and by closing the apparatus a sample column is formed. Using the spectral measurement at 280nm the instrument provides via its software the quantification of the sample. The formula applied was as follows:

$$1.35\ A_{280}\ \text{units of antibody} = 1\ \text{mg/ml}$$

The most concentrated fractions were pooled together and dialyzed against PBS over night. The antibody concentration was measured again, and the antibody was finally checked via SDS-PAGE and Coomassie stain. The aliquots were stored at -20°C.

Buffer A

$NaHPO_4$ pH7.0	20 mM
NaCl	150 mM

Buffer B

Glycine pH2.5	100 mM
Tris pH9.6	1 M
$NaHCO_3$ pH10.8	100 mM
$Na_3C_6H_5O_7$ pH5.0	100 mM

3.9 Fast protein liquid chromatography (FPLC)

For the FPLC studies, a Superose™ 10/300 GL Column (GE) was used, which is 30 cm long and has a diameter of 1 cm. The column was prepared following the manufacturer's instructions.

Technical details of the separation strategy:

Loaded volume	200 μl
Flow rate	0.5 ml/second
Gradient	no
Fraction size	250 μl
Start collecting fractions	10 ml
Stop collecting fraction	25 ml

For the separation, MDA MB 231 cells were harvested with 5 mM EDTA in PBS and counted. Approximately 75 μl lysis buffer/10^7 cells were used. The lysate was sheared five times through a 27G needle and centrifuged at 12000 g for 15 minutes. The protein content was assessed, and the separation performed only if the protein concentration was at least 10 μg/μl, in order to load at least 2mg total protein onto the column. The sample was always re-centrifuged before applying to the column in order to avoid air bubbles.

Fractions were collected in clean tubes and immediately put on ice. To 60 μl of each fraction, 20 μl of 4X loading buffer (see 3.5.3) were added. Samples were heated to 95°C for five minutes and loaded onto an appropriately-sized SDS-PAGE gel. On each gel, 40 μg of non-fractionated lysate were also loaded as a control.

Equilibration Buffer

Tris HCl pH 7.5	50 mM
KCl	100 mM

Elution Buffer

HEPES pH7.0	25 mM
NaCl	125 mM
$NaVO_4$	10 mM
Lubrol	1%
PMSF	1 mM
Protease inhibitors cocktail (Roche)	1x dilution

3.10 Isolation of Primary Mouse Embryonic Fibroblasts (MEFs)

The mice used for the isolation and purification of embryonic fibroblasts were ASAP1 knock out (RRS873), purchased from BayGenomics. The animals were kept in the ITG -

Institute for Toxicology and Genetics, part of the KIT - Karlsruhe Institute of Technology - animal facility under full specific pathogens free (SPF) conditions. The mice were bred onto a FVB background and kindly genotyped by Gitta Flaig, CBTM. The local authorities approved all studies performed with laboratory animals.

Pregnant female mice at F5 were sacrificed on embryonic day 13.5 by cervical dislocation. In a sterile hood the abdomen was swabbed with 70% ethanol and opened to expose the uterine horns. These were immediately excised and placed on a clean, PBS-filled Petri dish that was kept on ice during the whole isolation procedure. Each embryo was dissected from the placenta and was put on a clean Petri dish, avoiding contamination with maternal tissues. The yolk sack was removed and kept for subsequent genotyping. Head, heart, liver and spleen were removed from the embryo, and the remaining tissue was cut into smaller pieces. These were placed in cold PBS, washed once and allowed to settle on ice. The PBS was then removed, and 2 ml of ice cold 0.25% trypsin-EDTA was added. The digestion of the tissues occurred over night on ice. The following day, the trypsin was carefully removed and the tissue was incubated at 37°C for 20 minutes. After this time, 5 ml of warm media was used to gently pipette the lysed tissue up and down, in order to obtain a single-cell suspension. This suspension was finally plated in a T175 flask, together with 30 ml medium. On the following day, the medium was aspirated to remove cell debris and non-fibroblast cells. The MEFs were allowed to grow until they reached confluence and were then frozen in several aliquots in FCS + 10% DMSO.

3.11 FACS sorting

Due to the low transfection efficiency of the MEFs these cells had to be FACS sorted by co-transfecting the plasmid of interest with a GFP-expression construct. Freshly thawed, passage one MEFS were plated in 6 cm diameter dishes. On the next day they were re-seeded into 10 cm diameter plates, to be ~70% confluent on the day of transfection (day 3). For the co-transfection, 21 μl Lipofectamine LTX were mixed with 7 μg of DNA (3.5 μg for each plasmid) diluted in 5.6 ml OptiMem. The solution was vortexed for few seconds and incubated for 30 minutes. Meanwhile the cells were washed and the medium replaced with antibiotic-free medium. Finally, the transfection mixture was added drop wise to the cells, and the plate was gently rocked to evenly

distribute the solution. On the next day, cells were re-plated in 15 cm diameter plates, and the antibiotic solution containing penicillin and streptomycin was again added to the medium. After 48 hours of transfection the cells were trypsinized, washed once with PBS, re-suspended in 200 μl cold PBS containing 2% FCS, and kept on ice for the whole sorting procedure (~2 hours), which was kindly carried out by Melanie Grassl (CBTM – Mannheim). At the end the GFP-positive sorted cells were centrifuged, re-suspended in warm medium and plated in 48-well plates.

3.12 Motility Assay

3.12.1 Motility assay with MDA MB 231 cells

Aliquots of 0.15 x 10^6 cells were seeded in 35 mm diameter dishes and transfected as described above. Four hours post-transfection, cells were trypsinized, harvested and re-plated 1:10 in the same dishes. The remaining cells were used for the motility assay and seeded a 6-well plate, which were previously prepared by putting three sterile silicon inserts into each plate *(Figure 24)*. These were obtained by removing the silicon grid of an 8-well Lab-Tek™ Chamber Slide™ and by cutting it to the appropriate size. After soaking them in ethanol for few minutes, the inserts were air dried and sterilized with UV light for one hour before every assay.

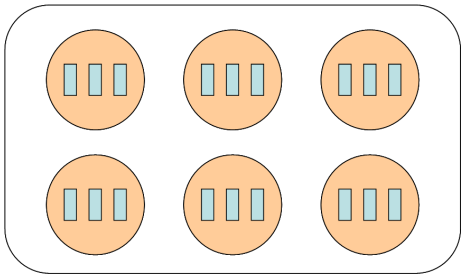

Figure 24: The 6-well plates used for the motility assays were prepared by adhering three silicon inserts to the bottom of the well prior to seeding the cells.

After 48 hours of transfection the assay was started. The cells in the 35 mm dishes were lysed in order to assess the transfection efficiency using western blotting. In parallel, the silicon inserts in the 6-well plates were carefully removed and the cells were washed twice with PBS. Pictures were taken immediately (t=0) and at later time points (24h, 32h and 48h). At t=24 the medium was changed. At the end of the assay, the cells in the 6-well plates were also lysed to check transfection efficiency at this time point. For each monolayer wound, five pictures were taken and in each picture the distance between the edges of the cell

monolayer was measured at four different points *(Figure 25).* The distance between the cell fronts was analysed with ImageJ software.

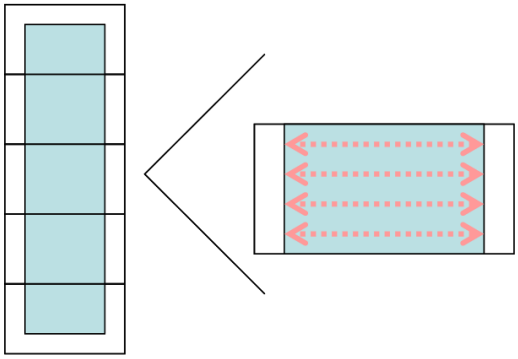

Figure 25: This figure depicts how the motility assays were analyzed. On the left it is shown how the five pictures were taken for each insert. The right figure represents one of these pictures and the dotted lines correspond to the measurements taken, namely four for each picture.

3.12.2 Motility assay with MEFs

For each experiment, three wild-type and three ASAP1 knock out MEFs were used. 0.05 x 10^6 cells per well were seeded in a 12-well plate. The plates were prepared with three silicon inserts per well as described above, but the inserts were shorter in order to fit into the well. On the following day, the inserts were carefully removed and the wells washed twice with PBS. Pictures were taken at t=0, 8 and 24 hours. To analyze the whole insert, it was divided in two pictures, each of which was measured at four points *(Figure 26).* The distance between the cells fronts was analysed with ImageJ software.

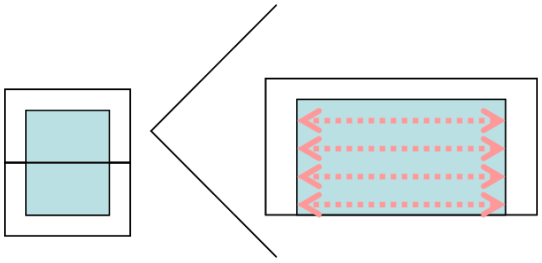

Figure 26: To analyze the motility of the MEFs the silicon inserts used were shorter and thus just two pictures were needed to take the whole area. For each picture the distance of the cells was measured at four different points of the cell front.

3.13 EGF recycling assay

One day prior to transfection, 1.4 x 10^6 MDA MB 231 cells were seeded onto four 10 cm diameter Petri dishes in antibiotic-free medium. Cells were transfected either with 600 pmol of ASAP1-specific siRNA or with the appropriate control using Lipofectamine 2000. The siRNA and the transfection reagent were diluted in OptiMem and prepared according to manufacturer's protocol.

For concomitant Nm23-H1 knock down, the medium was changed after 4 hours and the cells were transfected with Nm23-H1 specific siRNA, or with the appropriate scrambled control. For concomitant Nm23-H1 or h-prune over expression, the following day cells were transfected after a medium change with the corresponding plasmids, or with empty vector as a control. In all cases, the day after the second transfection the cells were trypsinized. The cells were split 1:10 into one 35 mm Petri dish and subsequently used to control transfection efficiency. The remaining cells were plated onto one 15 cm Petri dish, and used for the EGFR recycling assay 72 hours after ASAP1 siRNA transfection.

For the EGFR recycling assay, the cells were starved with serum-free medium for two hours at 37°C. They were then harvested with 5 mM EDTA-PBS, re-suspended in 3.6 ml serum-free medium and stored on ice. For each assay condition (no EGF control, no internalization and 30 minutes internalization) four cell aliquots of 300µl each were used for technical replicates. The "no EGF" control samples were pipetted into clean tubes and kept on ice. The remaining cells were incubated with fluorescent EGF (Alexa Fluor® 488 EGF complex, Life Technologies, Darmstadt) at a final concentration of 1 µg/ml for five minutes on ice. The cells were then centrifuged at 4°C and washed once with cold serum free medium. The "no internalization" sample was immediately stripped with Stripping buffer for five minutes. The other cells received pre-warmed, serum free medium, and were kept in the incubator for 30 minutes, before being stripped with Stripping buffer. The "no EGF" control cells were also stripped, and all samples were finally fixed with 37% buffered formalin. The cells were then subjected to FACS analysis and the fluorescence levels were assessed.

Stripping buffer (in H_2O)	
NaCl	0.5 M
Acetic acid	0.2 M

3.14 Cell staining

To visualize the cells that received the fluorescent EGF, after the FACS sort additional steps were done. The excess cells not used for the FACS were spotted onto clean slides (Superfrost plus, Thermo Fisher Scientific, Schwerte) and allowed to adhere by air-drying. The cells were then shortly rinsed with PBS and incubated for 30 minutes

with a 2 µg/ml solution of tetramethylrhodamine wheat germ agglutinin conjugate (Life Technologies, Darmstadt), that specifically stains the membrane of the cells. Following this steps the cells were counterstained with 0.5 µg/ml DAPI (4',6-diamidino-2-phenylindole) (Life Technologies, Darmstadt) for 10 minutes, before mounting a coverslip with an aqueous mounting medium (Fluoromount G - Southern Biotech).

3.15 Statistical analysis

For all experiments, statistical significance was calculated using a two-tailed student t-test. A p value of less than 0.05 was considered significant. In all the graphs where a statistical analysis is showed, the following symbols were used:

* = $p \leq 0.05$

** = $p \leq 0.01$

*** = $p \leq 0.001$

4. RESULTS

4.1 Role of ASAP1 in EGFR uptake and recycling

4.1.1 Establishment of a FACS-based EGF internalization assay

ASAP1 is able to bind and bend the plasma membrane via its BAR domain, thereby regulating the vesicle trafficking involved in receptor internalization and endosome recycling. Importantly, ASAP1 has been shown to induce tubular structures *in vivo* that contain the epidermal growth factor receptor (EGFR), and is thought to play a role in the internalization of this receptor (Nie et al., 2006). Overexpression of ASAP1 increases the recycling of EGFR in CHO cells (Kowanetz et al., 2004). ASAP1 has also been implicated in regulating the signalling of EGFR (see Introduction). The signalling pathways of the EGFR are known to promote growth and motility *in vitro* (Boulay et al., 2008), as well as metastasis formation *in vivo.* I therefore hypothesized that internalization and recycling of the EGF-EGFR complex by ASAP1 might contribute to the metastasis-promoting activity of ASAP1. To determine if this is the case, I established a quantitative assay to measure the amount of internalized EGF-receptor complex in highly metastatic human breast cancer MDA MB 231 cells, and investigated the influence of ASAP1 and its binding partners on this activity.

The assay I designed took advantage of the uptake of fluorescein-coupled EGF as a measure of the internalization activity of ASAP1 (Nie et al., 2006). To date, uptake in the published literature has only been assessed in a non-quantitative manner using microscopy. I therefore set out to develop an assay that used FACS measurement to quantify EGF uptake as a measure of EGFR recycling (*Figure 27)*. In this assay, serum-starved cells are harvested with PBS-EDTA to avoid cleavage of surface receptors, and cooled on ice to stop receptor internalization. The cells are then incubated with fluorescein-labelled EGF. Unbound EGF is subsequently washed away. The cells are then immediately processed, or incubated at 37°C for 30 minutes to allow internalization to occur. An acid stripping step before the fixation of the cells and subsequent FACS analysis allows cell surface-bound EGF to be removed, leaving fluorescent signal only from internalized EGF. The detailed protocol is outlined in "Materials and Methods".

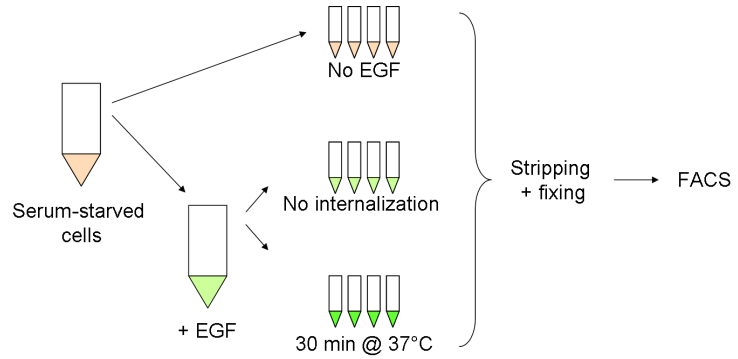

Figure 27: **Flow chart depicting the steps of the assay**. The serum-starved MDA MB 231 were gently collected with PBS-EDTA, put on ice and incubated or not ("no EGF") with the fluorescent EGF. Each treatment consisted of four technical replicates. The treated cells were then either immediately processed ("no internalization"), or let internalize the growth factor for 30 minutes at 37°C, before being processed for the FACS analysis.

4.1.1.2 Time of EGF internalization

First I performed several experiments to identify the optimal time for maximal internalization at 37°C of the fluorescein-labelled EGF. For this purpose I incubated MDA MB 231 cells with or without EGF for five minutes on ice, then immediately fixed them ("no internalization"), or allowed them to internalize the EGF for five or 30 minutes at 37°C. The FACS analysis revealed that maintaining the cells at 37°C for a longer time (30 minutes) increased the fluorescence of the cells that received EGF, but not of the control ones *(Figure 28)*. These and other results demonstrate the kinetics of the uptake of the growth factor, confirm the specificity of the fluorescence signal in the FACS analysis, and show that 30 minutes represents the optimal time at 37°C for EGF uptake following loading of the cells on ice.

4.1.1.3 Optimization of the stripping procedure

To further develop the EGF uptake assay, I implemented and optimized the stripping procedure as described in Lua and Low (Lua and Low, 2005) to be sure that I would only analyse receptor-bound and internalized EGF. Specifically, before fixing the EGF-treated MDA MB 231 cells for the FACS analysis, I treated them with an acidic stripping buffer. I tested its efficiency using FACS analysis, and cross-verified this analysis by visualization with a fluorescence microscope. The serum-starved cells were kept in suspension on ice and were given the EGF for five minutes, before incubating

them at 37 °C for five, ten or 30 minutes. After this time, the cells were “stripped” and fixed, or only fixed for the FACS analysis.

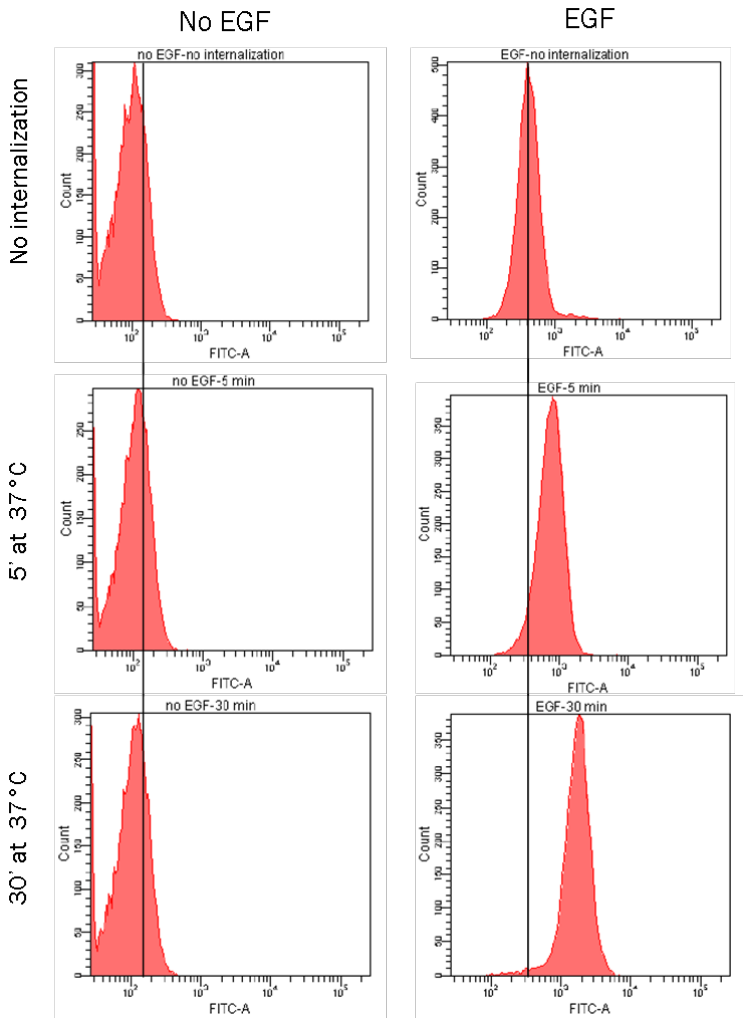

Figure 28: MDA MB 231 cells were treated or not treated with the fluorescent EGF as indicated, then either immediately processed (“no internalization”) or put at 37°C for five or 30 minutes. The peaks indicate the mean fluorescent intensity of the cells, which clearly increases with the time in the treated cells, but not in the untreated ones, showing the specificity of the signal.

The analysis showed that immediately after EGF incubation, around 50% of the fluorescent signal is removed by the stripping treatment, and thus represents unspecifically bound growth factor (*Figure 29A)*. The efficiency of the stripping was not 100%, perhaps suggesting that even on ice, receptor internalization still occurs to some extent. After 30 minutes at 37 °C, almost all EGF was internalized, as virtually no difference in fluorescence intensity between stripped and the non-stripped cells was observed (*Figure 29A)*.

The interpretation of the FACS analysis was confirmed using fluorescence microscopy *(Figure 29B and C)*. The accumulation of internalized EGF-EGFR complex in intracellular vesicles is clearly visible at the 30 minute time-point.

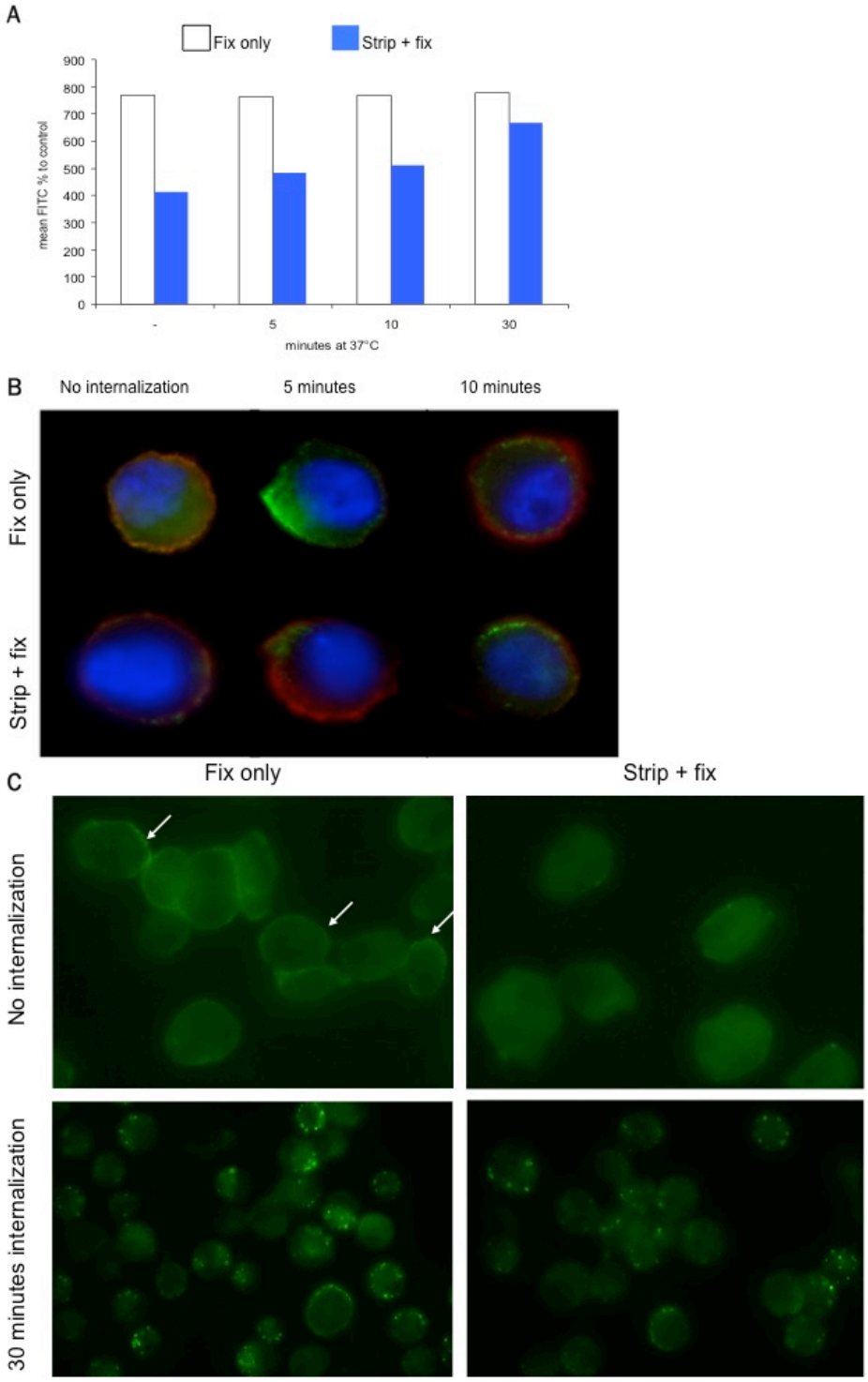

Figure 29. **Effect of the stripping treatment on the fluorescence signal in cells incubated with fluorescein-labelled EGF**. MDA MB 231 cells were incubated for five minutes with the fluorescein-

coupled EGF, washed, then allowed to internalize the receptor at 37°C for the times indicated. They were then immediately fixed, or stripped and fixed before analysing them by either FACS analysis (A) or microscopy (B and C). **A.** The mean fluorescence intensity as measured by FACS analysis is plotted against the time the EGF-treated cells were incubated at 37°C. **B.** Fluorescence microscopy images of representative cells incubated for up to 10 minutes at 37°C after treatment with fluorescein-labelled EGF on ice (no internalization). Cells were fixed either with or without stripping as indicated. A clear accumulation of EGF (green) is visible on the membrane (red) of the non-stripped cells compared to the stripped ones. **C.** Fluorescence microscopy images of cells incubated for 30 minutes at 37°C after treatment with fluorescein-labelled EGF on ice (no internalization). Cells were fixed either with or without stripping as indicated. The arrows indicate the efficiency of the stripping in the "no internalization" cells.

4.1.1.4 EGF incubation time

Another parameter that needed to be optimized was the incubation time of the EGF with the cells on ice prior to the internalization at 37°C. For this purpose, I kept the cells in suspension with the fluorescent EGF on ice for five, 30 and 60 minutes. Then I washed them and either processed them immediately (stripping and fixation), or allowed them to internalize the receptor at 37°C for five or 30 minutes, always followed by stripping and fixation. The binding of the EGF to the cells was very fast: the fluorescence signal did not show any difference whether the cells were incubated with the EGF for five, 30 or 60 minutes *(Figure 30)*.

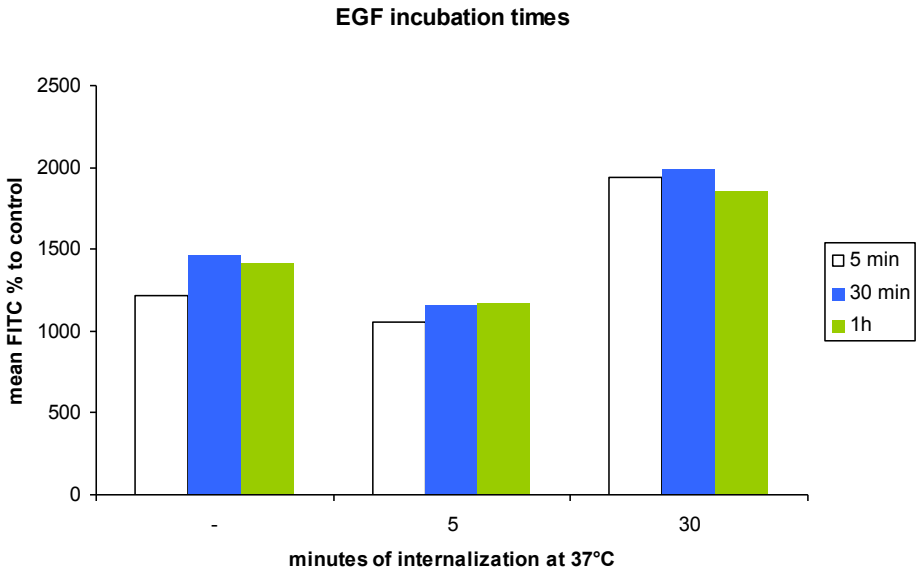

Figure 30: The graph shows the mean fluorescence intensity of the cells that were incubated with the EGF for five (white), 30 (blue) or 60 (green) minutes on ice. Each sample was allowed to internalize it at 37°C for five or 30 minutes, or not at all. The fluorescence intensity was measured via FACS.

This experiment suggested that incubating the cells on ice with EGF for longer times only slightly affects the final fluorescence intensity, whereas the duration of the internalization at 37°C is the main determinant of the increase in EGF signal intensity. Therefore for further experiments I chose to keep the cells for five minutes on ice before washing the unbound EGF away and proceeding with the internalization.

4.1.1.5 EGF concentration

Finally I needed to optimize the concentration of EGF to be given to the cells. For this experiment I incubated the cells for five minutes on ice with three different concentrations of EGF, before leaving them for five minutes at 37°C for the internalization. Although maximal signal was already obtained with 0,5 μg/ml fluorescein-labelled EGF, I decided to use a concentration of 1 μg/ml to ensure reliable saturation of the cell-surface EGFR *(Figure 31)*.

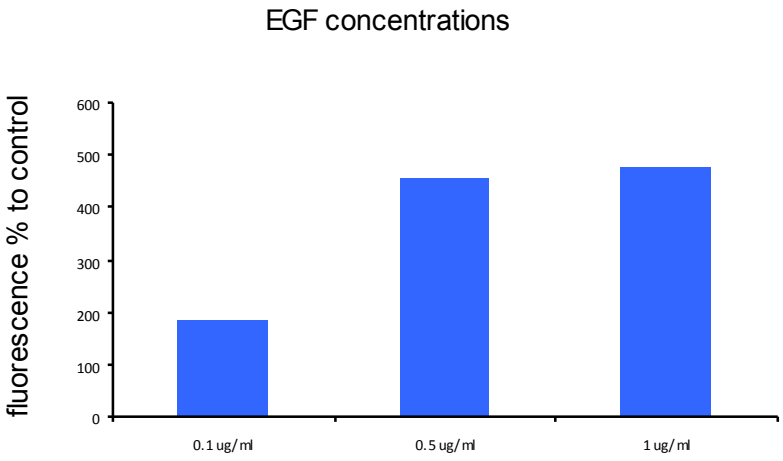

Figure 31: To identify the optimal concentration of EGF the cells were all treated equally (five minutes of incubation on ice followed by five minutes internalization at 37°C), but were given different EGF final concentrations, as indicated. This graph indicates that the fluorescence intensity is proportional to the EGF concentration.

4.1.2 ASAP1 knock down increases EGF fluorescent signal

Having established an assay for the measurement of the internalization of fluorescent EGF into the MDA MB 231 cells, I wanted to confirm a role for ASAP1 in EGF uptake. For this purpose I treated the cells with a specific siRNA for ASAP1, as well as with the appropriate scrambled siRNA control, and performed the internalization assay. The

knock down of ASAP1 resulted in a statistically significant increase in the fluorescence intensity compared to the control, even in the cells that were kept on ice during treatment *(Figure 32A)*. To confirm these results, I cross-verified the increased fluorescence signal using fluorescent microscopy to visualise the same cells used for the FACS analysis. The intensity of the fluorescence was consistent with the data from the FACS analysis, confirming the results obtained (data not shown).

A

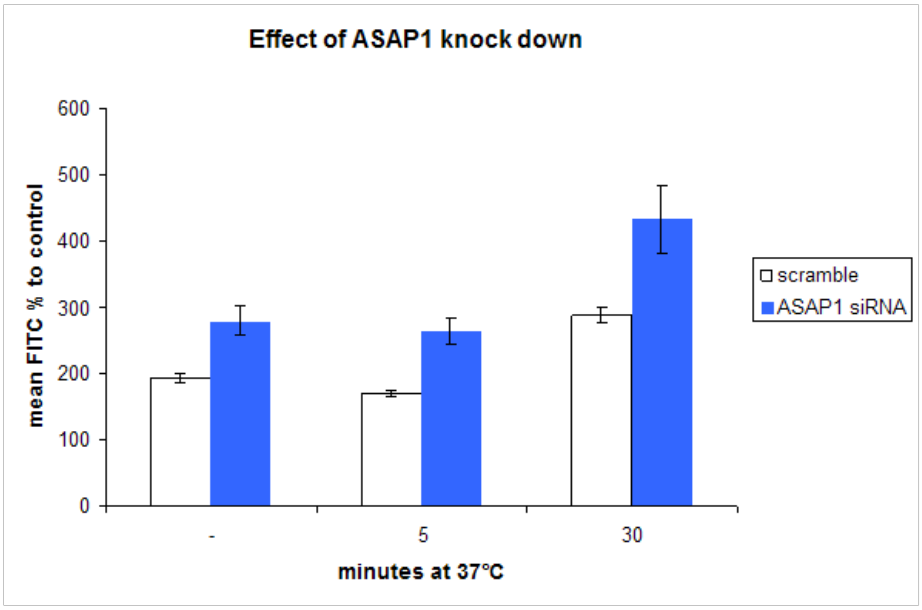

B

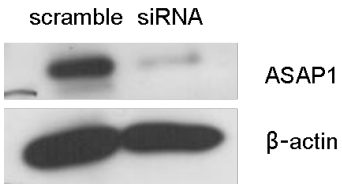

Figure 32: **Effect of ASAP1 knock down on the internalization of fluorescent EGF measured via FACS**. **A**. The graph shows the result of a representative experiment. The silencing of ASAP1 clearly increases the fluorescence intensity compared to the control. **B**. The efficiency of the knock down was assessed by means of Western Blot.

4.1.3 Nm23-H1 knockdown rescues the effect of ASAP1 silencing on EGF internalization

To determine whether Nm23-H1 expression influences ASAP1-mediated internalization of fluorescein-labelled EGF, I silenced Nm23-H1 expression alone or in combination with the knock down of ASAP1. The cells that had a reduced amount of ASAP1 showed an increase in the fluorescence intensity as in previous experiments *(Figure 33A).* However, this effect was reverted back to the basal level when the silencing of Nm23-

H1 and ASAP1 were combined. Importantly, the knock down of Nm23-H1 alone did not show any effect on the internalization of the receptor. Thus knockdown of Nm23-H1 may compensate for the silencing of ASAP1.

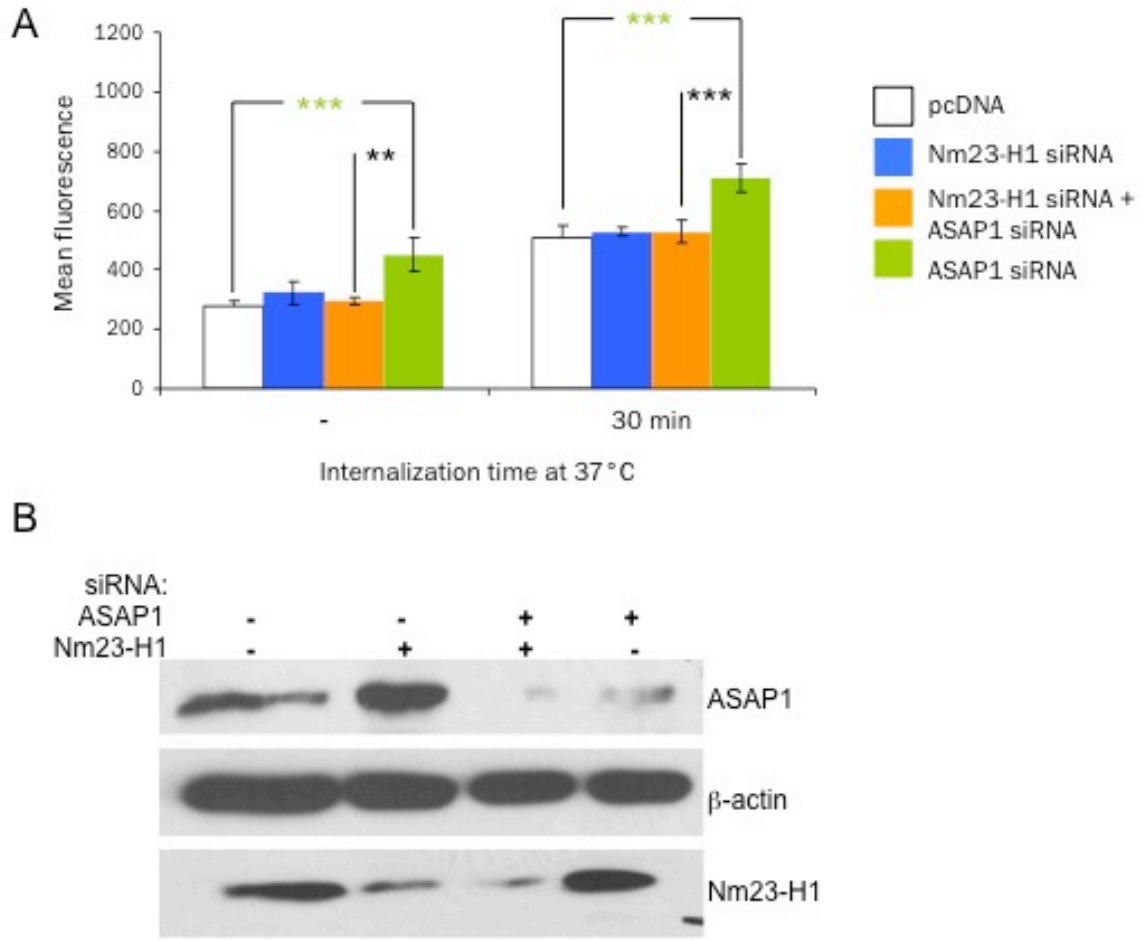

Figure 33: **Effect of the knock down of ASAP1 and/or Nm23-H1 on the internalization of fluorescent EGF measured via FACS. A.** The graph shows the result of a representative experiment. The fluorescence intensity of the cells treated with the ASAP1 knock down is clearly increased compared to the control ones (white) (significance indicated by green asterisks). No effect on the fluorescence intensity is observable with the knock down of Nm23-H1 (blue bars), nor with the combination of Nm23-H1 and ASAP1 silencing (orange bars). The black asterisks indicate the significance of the difference between the ASAP1 knock down alone compared to the double silencing. **B.** The efficiency of both knockdowns was assessed by means of Western Blot.

4.1.4 Nm23-H1 overexpression shows a similar effect as ASAP1 knockdown in EGF uptake assays

As knockdown of Nm23-H1 abrogated the increased fluorescence intensity observed in the EGF internalization assays after knockdown of ASAP1, I next investigated the effect of the overexpression of Nm23-H1 on this process. For this purpose I transfected the MDA MB 231 cells with an expression construct for Nm23-H1, with or without the silencing for ASAP1. Similar to the previous experiments, the knockdown of ASAP1 resulted in an increase of the fluorescence intensity compared to the control *(Figure 34)*. The overexpression of Nm23-H1 alone also led to a significant increase in the fluorescence intensity relative to the pcDNA-transfected control cells. However, the increased fluorescence in these cells was never as pronounced as that obtained with the knockdown of ASAP1. Furthermore, concomitant overexpression of Nm23-H1 in ASAP1 knockdown cells only increased the fluorescence intensity to the levels obtained with overexpression of Nm23-H1 alone, which was significantly lower than the increased fluorescence observed after knockdown of ASAP1 alone. These data suggest that ASAP1 and Nm23-H1 may act independently to regulate the internalization of EFG.

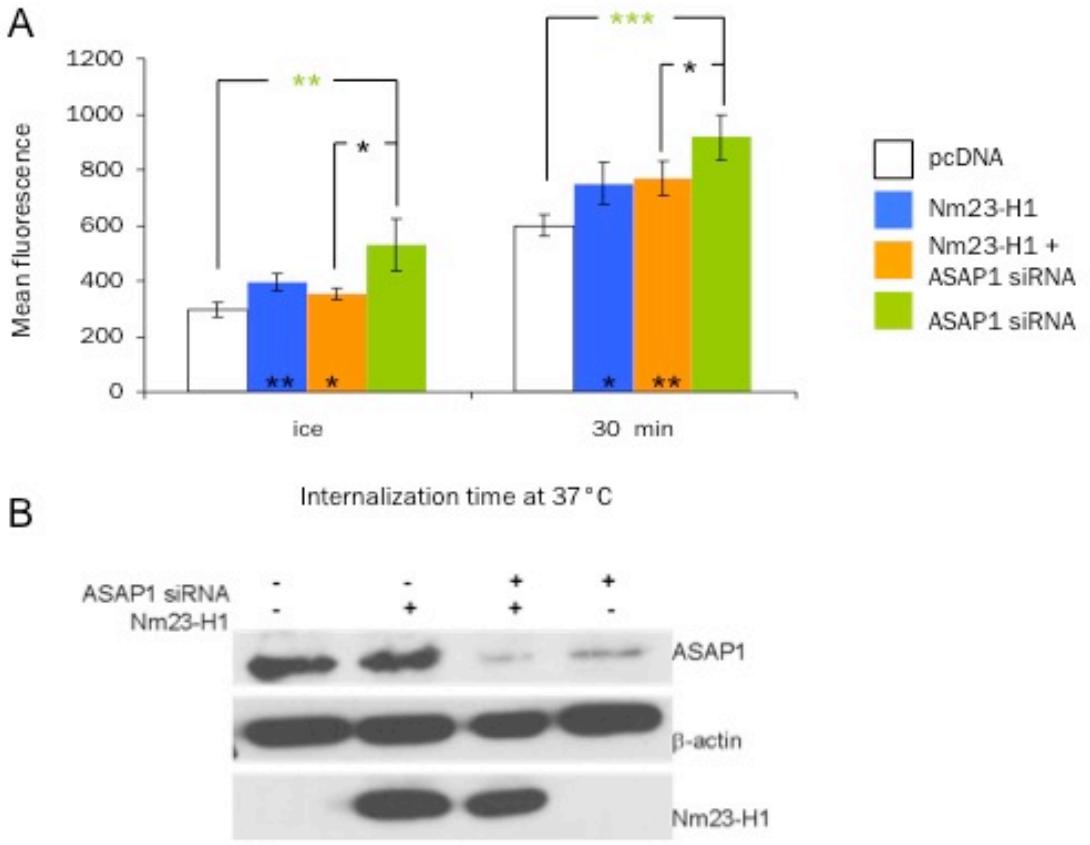

Figure 34: **Effect of the overexpression of Nm23-H1 and/or the silencing of ASAP1 on the internalization of fluorescent EGF measured via FACS**. **A.** The graph shows the result of a representative experiment. The asterisks in the bars represent the significance versus the control (white). The fluorescence intensity of the cells treated with the ASAP1 knockdown is clearly increased compared to the control cells (significance indicated by green asterisks). A significant increase in fluorescence is observable with the overexpression of Nm23-H1 (blue), also when combined with the silencing of ASAP1 (orange). The black asterisks indicate the significance of the difference between the ASAP1 knock down alone compared to the silencing combined with the overexpression of Nm23-H1. **B.** The efficiency of knock down and overexpression was assessed by means of Western Blot

4.1.5 Overexpression of h-prune does not influence ASAP1-mediated uptake of EGF

Next I investigated whether h-prune modulates the uptake of EGF mediated by ASAP1, similar to that observed with Nm23-H1. ASAP1-silenced MDA MB 231 cells were transiently transfected with an expression plasmid for h-prune, or with the empty vector as a control. All samples were analysed for the uptake of fluorescent EGF as before. The results clearly indicate that the overexpression of h-prune does not affect

the ability of ASAP1 knockdown to promote the internalization of the EGF-receptor complex *(Figure 35)*.

Therefore, although h-prune is able to bind to ASAP1, it does not appear to affect the role of ASAP1 in EGF internalization.

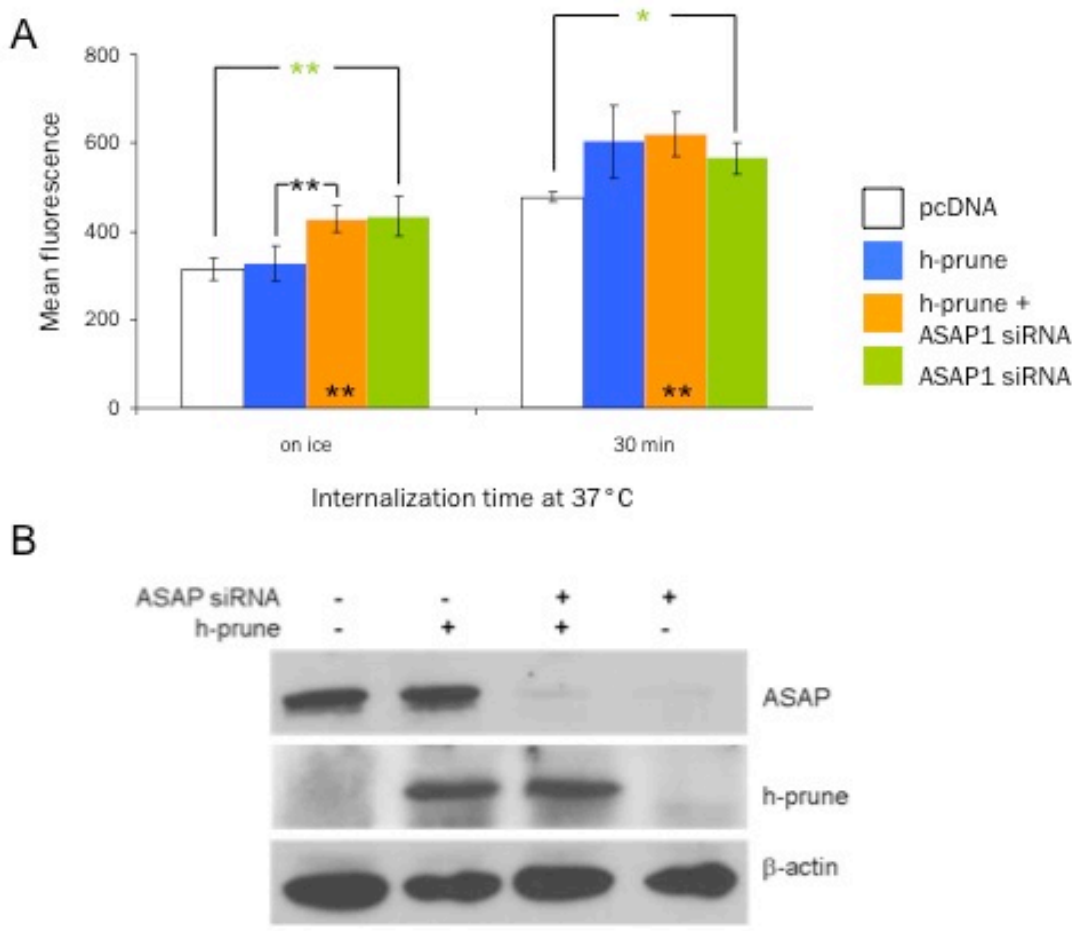

Figure 35: **Effect of the overexpression of h-prune and/or the silencing of ASAP1 on the internalization of fluorescent EGF measured via FACS. A.** The graph shows the result of a representative experiment. The asterisks within the bars represent the significance versus the control cells. The fluorescence intensity of the cells treated with the ASAP1 knock down is significantly increased compared to the control ones (indicated by green asterisks). This increase in fluorescence intensity is not impaired when combined with the overexpression of h-prune (orange). The black asterisks indicate the significant difference between the ASAP1 knock down alone compared to the silencing combined with the overexpression of h-prune.

B. The efficiency of knock down and overexpression was assessed by means of Western Blot

4.2 Influence of Nm23-H1 and h-prune on ASAP1-mediated motility

4.2.1 Effect of ectopic expression of Nm23-H1 and h-prune on ASAP1-dependent motility

ASAP1 is able to promote motility, most probably via the interaction with other proteins through its proline-rich SH3 binding domain (Müller et al., 2010). Both h-prune and Nm23-H1 are themselves known to regulate the motility of tumor cells. As h-prune and Nm23-H1 are binding partners of ASAP1, I set out to investigate whether these proteins interact to influence the ability of ASAP1 to promote invasiveness.

To evaluate whether Nm23-H1 or h-prune influence ASAP1-mediated motility, I performed monolayer wound healing assays using MDA MB 231 cells, which have a high endogenous expression of ASAP1. The cells were transfected with a siRNA specific for ASAP1 alone or together with either Nm23-H1 or h-prune expression plasmids. As controls, the cells were transfected with scrambled siRNA and the empty vector.

The analysis of the assays confirmed the role of ASAP1 in promoting cell motility. Cells transfected with the siRNA for ASAP1 had a reduced ability to close the wound in the monolayer, whereas the control cells moved more rapidly

Nm23-H1 overexpression had no influence on monolayer wound closure relative to the control cells, and furthermore had no effect on the reduced wound closure observed in ASAP1 knockdown cells *(Figure 36)*.

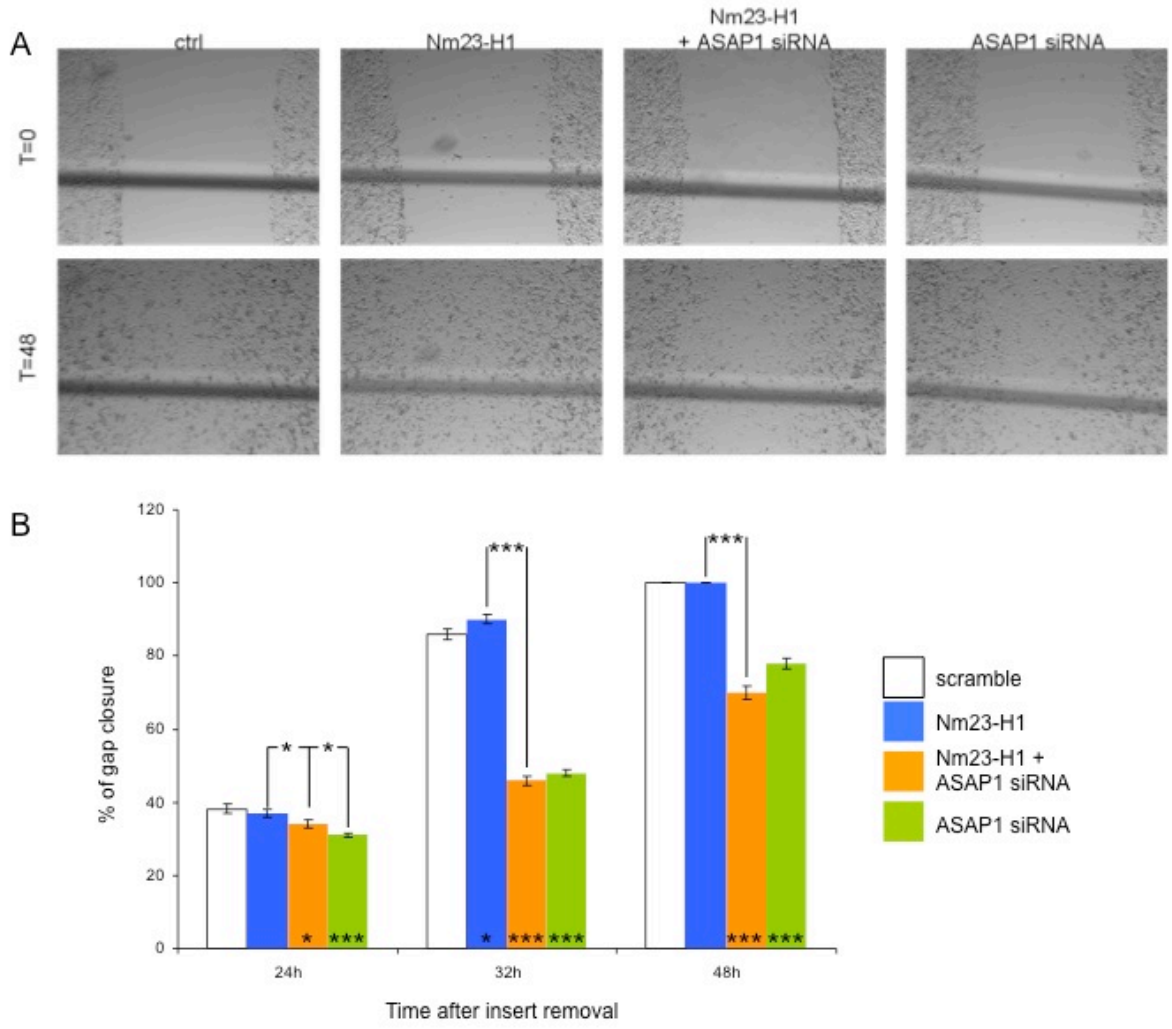

Figure 36: **Effect of the overexpression of Nm23-H1 on ASAP1-mediated motility.** MDA MB 231 cells were transfected with an expression plasmid for Nm23-H1 alone, or in combination with a siRNA against ASAP1. Controls included scrambled siRNA and empty vector-transfected cells, as well as cells with the ASAP1 knockdown alone. **A.** Representative pictures of the monolayer wounds are shown from the beginning (t=0) and the end (t=48 hours) of the assay. **B.** The graph shows the analysis of a representative motility experiment, indicating the percentage of wound closure at 24, 32 and 48 hours after insert removal. The asterisks in the bars represent the significance versus the control cells, the ones above them the significance between the indicated samples. The overexpression of Nm23-H1 (blue bars) did not influence the motility of the cells. The knock down of ASAP1 (green bars) significantly reduced the motility of the cells already at 24 hours, even in the presence of Nm23-H1 overexpression (orange bars). Error bars are standard error (n=60).

On the other hand, h-prune overexpression by itself slightly but significantly reduced monolayer wound closure, but again had no observable effect on the enhanced reduction in wound closure observed in ASAP1 knockdown cells *(Figure 37).*

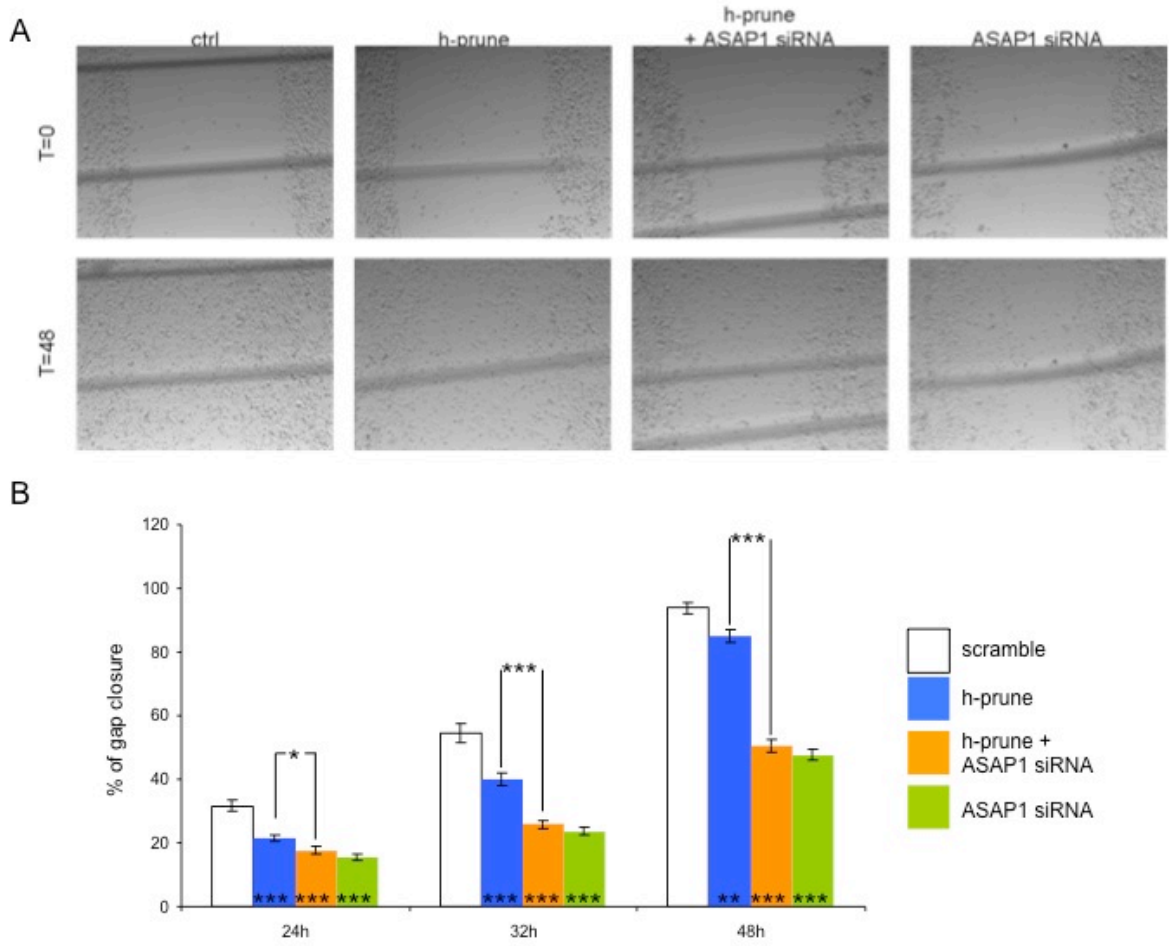

Figure 37: **Effect of the over expression and h-prune on ASAP1-mediated motility.** MDA MB 231 cells were transfected with an expression plasmid for h-prune alone, or in combination with a siRNA against ASAP1. Controls included scrambled siRNA and empty vector-transfected cells, as well as cells with the ASAP1 knockdown alone. **A.** Representative pictures of the monolayer wounds are shown from the beginning (t=0) and the end (t=48 hours) of the assay. **B.** The graph shows the analysis of a representative motility experiment, indicating the percentage of wound closure at 24, 32 and 48 hours after insert removal. The asterisks in the bars represent the significance versus the control cells, the ones above them the significance between the indicated samples. The overexpression of h-prune slightly but significantly reduced the motility of the cells. The knock down of ASAP1 (green) significantly reduced the motility of the cells already at 24 hours, even in the presence of h-prune overexpression (orange). Error bars are standard error (n=60).

Both the knock down of ASAP1 and the over expression of Nm23-H1 and h-prune were efficient throughout the duration of the assay, as shown in the Western Blot *(Figure 38)*, confirming the reliability of the experiment.

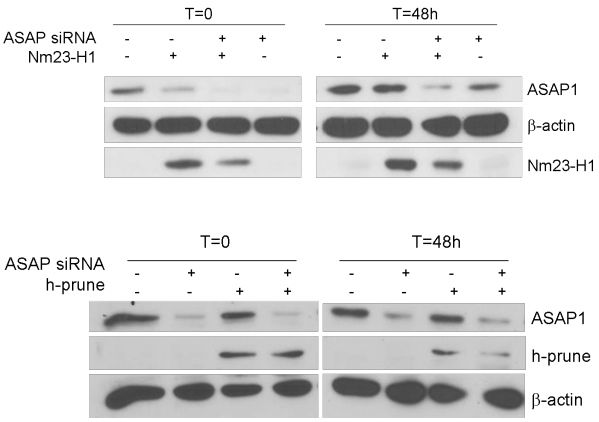

Figure 38: **Western blots showing the efficiency of the transfections.** Lysates were prepared at the beginning of the assay (t=0) and at the end (t=48), to verify the persistence of both the knock down of ASAP1 and the overexpression of Nm23-H1 (upper figure) and of h-prune (lower figure).

4.2.2 Nm23-H1 and ASAP1 silencing both reduce the motility of MDA-MB-231 cells

To further explore the possibility that the interaction of Nm23-H1 with ASAP1 might be necessary for ASAP1 to exert its motility promoting activity, I silenced both proteins either together or individually. As before, the silencing of ASAP1 decreased the motility of the cells. Silencing of Nm23-H1 also significantly reduced cell motility in these assays to the same extent as ASAP1 silencing. However, the decreased cell motility observed after the silencing of ASAP1 was not influenced by the additional silencing of Nm23-H1 *(Figure 39*). Western blot analysis confirmed that knockdown of the proteins was efficient (*Figure 40*).

Due to the lack of a suitable antibody against human h-prune, it was not possible to establish silencing of this protein.

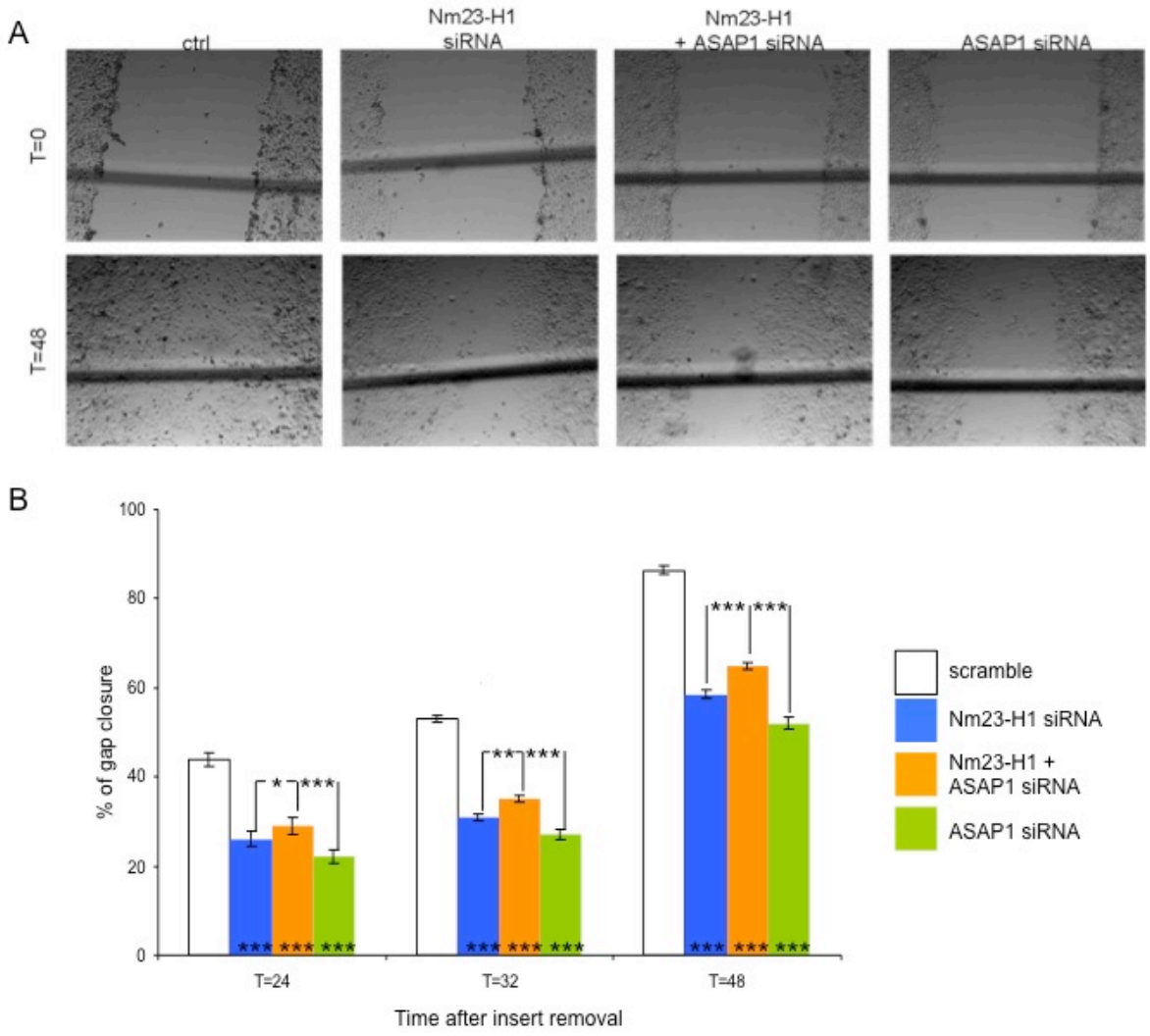

Figure 39: **Effect of Nm23-H1 siRNA on ASAP1 mediated motility.** MDA MB 231 cells were transfected with siRNA against either ASAP1 or Nm23-H1, or a combination of the two. Controls comprised scrambled siRNA-transfected cells. **A.** Representative pictures of monolayer wounds taken at the beginning of the assay (t=0) and at the end (t=48 hours). **B.** Graph showing the analysis of a representative motility experiment. The asterisks within the bars represent the significance versus the control cells, the ones above them the significance between the indicated samples. Error bars are standard error (n=60). The silencing of ASAP1 (green bars) and Nm23-H1 (blue bars) both reduce the motility of the cells, however the combination of the two does not result in a synergistic effect (orange bars).

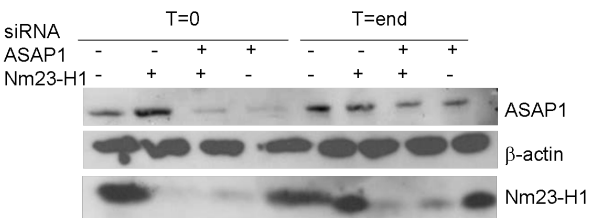

Figure 40: Western blot showing the efficiency of the transfections. Lysates were prepared at the beginning of the assay (t=0) and at the end (t=48), to verify the persistence of both the knock down of ASAP1 and Nm23-H1

4.3 The SH3 binding domain of ASAP1

4.3.1 Screening of SH3 domain arrays and identification of ASAP1 SH3 domain partners

ASAP1 is able to bind to several proteins, such as c-Src and Crk, via its proline-rich SH3 binding domain that interacts with the SH3 domain in these proteins. A point mutation in the proline-rich domain (R811A) is sufficient to impair the binding of ASAP1 to these proteins (Brown et al., 1998). In previous work, we have shown that ASAP1-mediated cell motility is required for its SH3-binding domain, because the R811A mutation led to a significant reduction in the ability of ASAP1 to promote cell motility and adhesiveness *in vitro*, and attenuated its metastasis-promoting activity *in vivo*, compared to the wild type protein (Müller et al. 2010). This strongly suggests that the SH3 binding domain is critical for the metastasis promoting function of ASAP1.

To gain further insight into how ASAP1 regulates cell motility and metastasis, I set out to identify additional potential binding partners of ASAP1 that interact with its proline rich region, and then to determine if these partners are able to influence the motility-promoting activity of ASAP1. I also wanted to determine whether h-prune and Nm23-H1 affect the ability of ASAP1 to bind to these SH3 domain proteins. For this purpose, I used a commercially available SH3 domain array containing 38 recombinant proteins, all of which bear an SH3 domain (see “Materials and Methods” for protocol details).

The array was incubated with lysates of 293T cells transiently transfected with Flag-tagged ASAP1, and probed with the specific anti-tag antibody. Signals were obtained for already-known interaction partners of ASAP1, such as cortactin and c-Src, which acted as positive controls and confirmed the reliability of the assay *(Figure 41).* In addition, the presence of several other positive signals identified new potential candidates that may bind ASAP1 via the SH3 binding domain and possibly affect the activity of ASAP1.

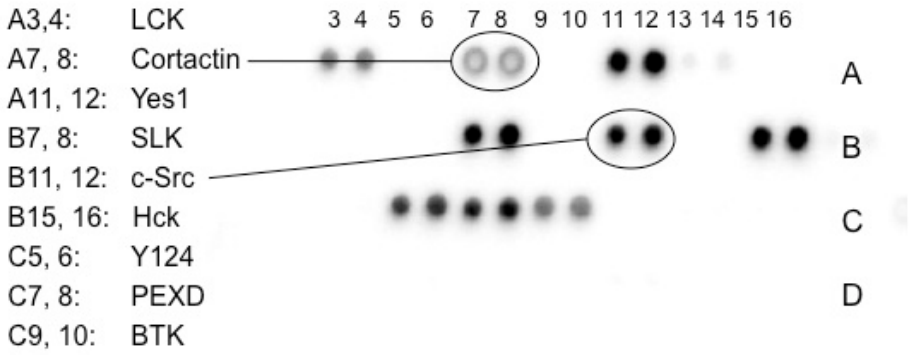

Figure 41: The SH3 domain array. The spots correspond to the interaction of ASAP1 with the indicated proteins, confirming already known interaction partners of ASAP1, highlighted by a circle. New putative binding partners emerged from this assay.

4.3.2 Nm23-H1 and h-prune do not interfere with the binding of ASAP1 to SH3 domain-bearing proteins

I next investigated whether h-prune and Nm23-H1 influence the interaction of ASAP1 with SH3 domain-containing partners. For this purpose, I repeated the SH3 domain array experiment using lysates of cells that had been co-transfected with ASAP1 and either an empty vector, or expression constructs for h-prune or Nm23-H1. After having assessed the efficiency of transfection via Western Blot, I incubated the lysates with the SH3 domain array and performed the assay. The only difference in signal intensity between the ASAP1-transfected cells, and the ASAP1-transfected cells that were co-transfected with Nm23-H1 or h-prune was a reduction in the signal intensity for cortactin with the h-prune transfected sample, possibly suggesting a reduced interaction of ASAP1 with cortactin under these conditions *(Figure 42A).* To verify this observation, I created a custom dot blot array using the same recombinant cortactin protein used in the SH3 domain assay *(Figure 42B).* This second experiment revealed that neither the overexpression of h-prune, nor of Nm23-H1 were able to affect the strong binding of ASAP1 to cortactin. This suggests that Nm23-H1 and h-prune do not affect the ability of ASAP1 to interact with protein partners via its SH3 binding domain.

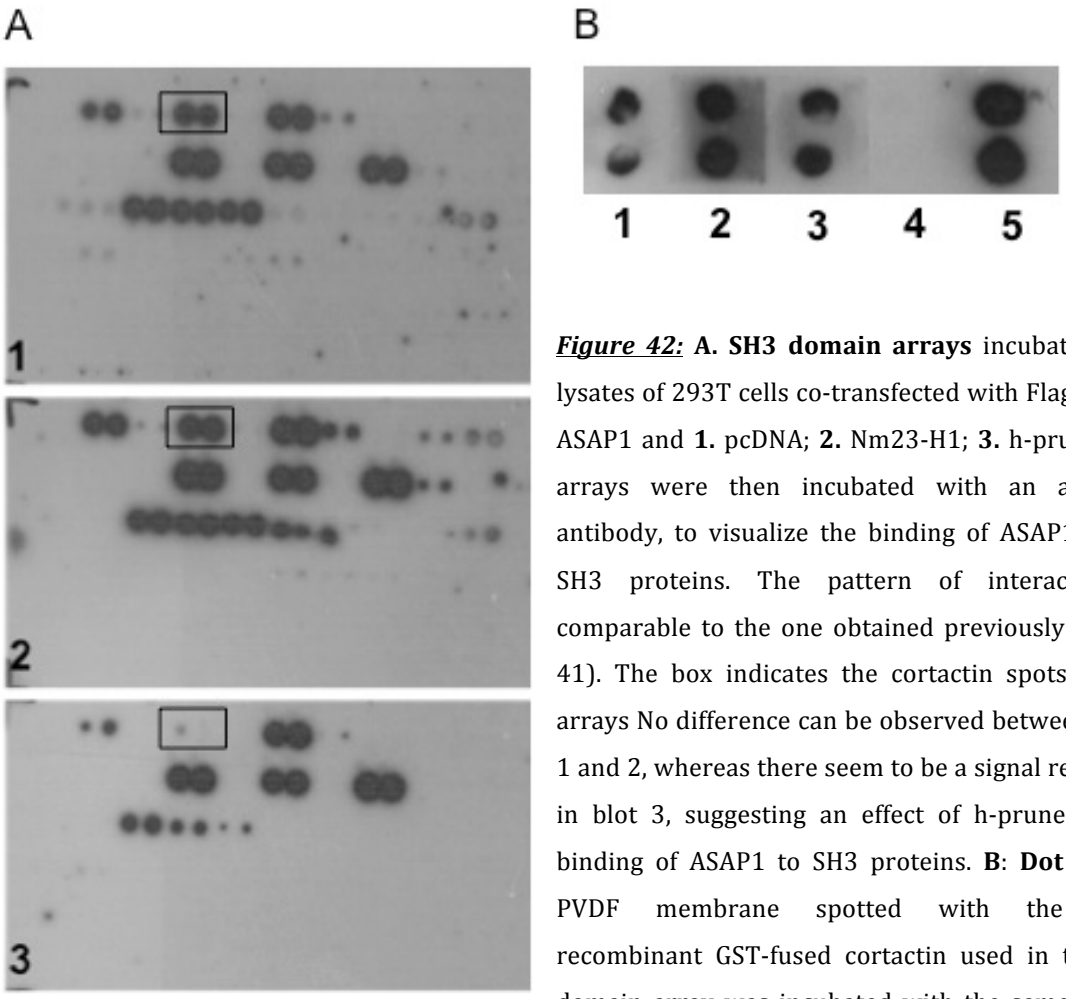

Figure 42: **A. SH3 domain arrays** incubated with lysates of 293T cells co-transfected with Flag-tagged ASAP1 and **1.** pcDNA; **2.** Nm23-H1; **3.** h-prune. The arrays were then incubated with an anti-Flag antibody, to visualize the binding of ASAP1 to the SH3 proteins. The pattern of interaction is comparable to the one obtained previously (Figure 41). The box indicates the cortactin spots on the arrays No difference can be observed between array 1 and 2, whereas there seem to be a signal reduction in blot 3, suggesting an effect of h-prune on the binding of ASAP1 to SH3 proteins. **B**: **Dot plot.** A PVDF membrane spotted with the same recombinant GST-fused cortactin used in the SH3 domain array was incubated with the same lysates and antibodies as in Figure 42A. Membrane **4** was incubated with the secondary antibody only (negative control) and membrane **5** with an anti-GST antibody, to confirm the presence of the spotted cortactin (positive control). The spots are identical, confirming that neither the presence of Nm23-H1 nor of h-prune can affect the binding of ASAP1 to the SH3 protein cortactin.

4.3.3 SLK is a novel binding partner of ASAP1

Among the putative novel binding partners that emerged from the screening of the SH3 domain array, one was of particular interest for us, namely the Ste20-like kinase (SLK). This protein has been shown to play a role in motility (Wagner et al., 2008), and like ASAP1 localizes to membrane ruffles in migrating fibroblasts (Wagner et al., 2002). Interestingly, SLK has also been shown to play a role in ErbB2-driven breast cancer motility (Roovers et al., 2009). I therefore set out to try and confirm the interaction between these to proteins by means of co-immunoprecipitation, as a first

step towards investigating whether SLK might contribute to ASAP1-mediated cell motility.

To this end I transfected a Flag-tagged form of ASAP1 into 293T cells that have a low expression of endogenous ASAP1. An anti-flag tag antibody was then used to immunoprecipitate the ASAP1 from lysates of the cells. The precipitates were resolved by SDS-PAGE, then probed with anti-SLK antibodies to determine whether ASAP1 and SLK interact. The immunoprecipitation confirmed the interaction of ASAP1 with the endogenous SLK protein, suggesting that SLK is a new interaction partner of ASAP1 that might cooperate with ASAP1 to regulate motility and invasion *(Figure 43)*.

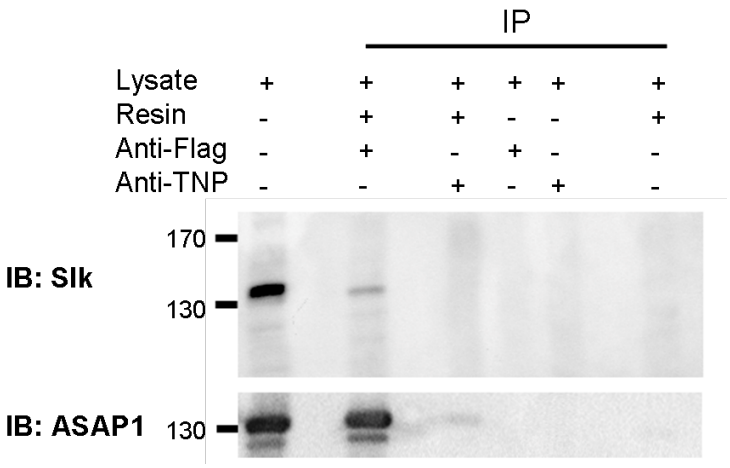

Figure 43: **SLK co-immunoprecipitation.** 293T cells were transfected with Flag-tagged ASAP1 and the tag was used to precipitate this protein with a G protein-coupled resin. The SLK antibody was then used to verify the presence of this protein in the immunocomplex (upper blot). The first lane on the left corresponds to the whole lysate and serves as a control for the presence of both proteins. As controls (lanes 3-6), following conditions were applied: isotype control with resin, no resin, isotype control without resin, no antibody. The blot was then stripped and incubated with an anti ASAP1 antibody, to verify the efficiency of the immunoprecipitation. The presence of the band in the second lane confirms the interaction between ASAP1 and SLK.

4.3.4 Overexpression of h-prune and Nm23-H1 does not affect the binding of ASAP1 to SLK

The results obtained with the SH3 domain arrays already suggested that neither h-prune nor Nm23-H1 affect the binding of ASAP1 to SH3 domain-bearing interaction partners. To confirm this finding, I repeated the co-immunoprecipitation of SLK in 293T cells co-transfected with Flag-tagged ASAP1 and either Nm23-H1 or h-prune

expression constructs, or with empty vector as a control. The blot shows that neither h-prune nor Nm23-H1 were able to affect the binding of ASAP1 to SLK *(Figure 44A)*, again suggesting that h-prune and Nm23-H1 interact with domains on ASAP1 other than the proline-rich SH3 binding domain, and also do not interfere with the ability of ASAP1 to bind to SH3 domain-bearing proteins via its SH3 binding domain.

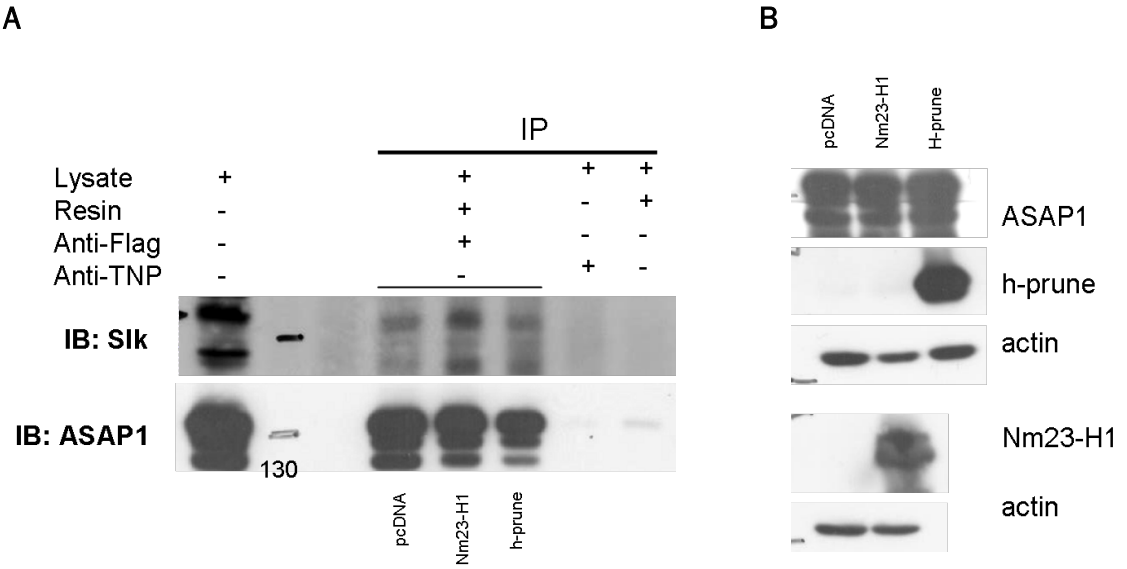

Figure 44: **Co-immunoprecipitation of SLK** in cells transfected either with Nm23-H1, h-prune or the appropriate control. **A.** The left lane shows the two proteins in the normal lysate. This blot was incubated first with the SLK antibody, to show the presence of this protein in the immunocomplex (upper blot), and then stripped and re-incubated with an anti ASAP1 antibody, to verify the efficiency of the immunoprecipitation. (lower blot). Neither the overexpression of h-prune nor of Nm23-H1 affects the ability of ASAP1 to bind to SLK. **B.** The transfection of the plasmids was checked via Western blot

4.3.5 Cloning of human Ste20 Like Kinase

Due to the known role of SLK in promoting motility, and having shown its interaction with ASAP1, I wanted to verify whether these two proteins act synergistically to promote the motility in MDA MB 231 cells. First I needed to clone the human SLK gene into an appropriate expression vector. For this purpose I used the pcDNA™3.1/V5-*His TOPO*® TA kit (Life Science, Darmstadt) and proceeded as described in "Materials and Methods". After having successfully cloned the gene, I verified the correctness of the plasmid by control digestion and sequencing of the plasmid. I also checked the ability

of the expression plasmid to drive the expression of SLK in 293T cells using Western blot analysis *(Figure 45)*.

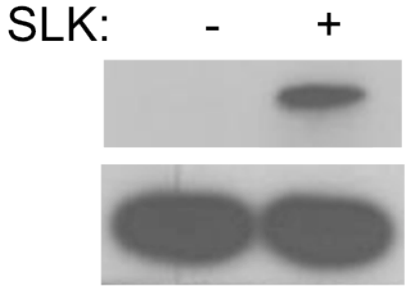

Figure 45: Blot showing the expression of the His-tagged SLK in the transfected 231T cells (right lane) compared to control cells. The upper part of the blot was incubated with the specific anti His antibody, while the lower part was incubated with an anti actin antibody as a loading control. This result confirmed the correctness of the expression plasmid.

4.3.6 SLK regulates cell motility independently of ASAP1 in MDA MB 231 cells

As ASAP1 and SLK interact and both proteins are involved in motility regulation, I wanted to investigate whether SLK cooperates with ASAP1 to promote motility, or whether these two proteins act independently. For this purpose I performed monolayer wound healing assays using MDA MB 231 cells transfected with ASAP1 siRNA alone, or in combination with either SLK siRNA or the expression plasmid for SLK.

As expected, knock down of either protein was able to significantly reduce the motility of the cells, although not to the same extent: ASAP1 silencing was more efficient. The combination of the two knockdowns did not show any additional effect on monolayer wound closure over and above that exerted by ASAP1 silencing *(Figure 46)*. Overexpression of SLK increased the closure rate of the monolayer wound as expected. Importantly, reduced wound closure upon the knockdown of ASAP1 was partially rescued by ectopic expression of SLK *(Figure 47)*, suggesting that SLK regulates cell motility independently of its interaction with ASAP1.

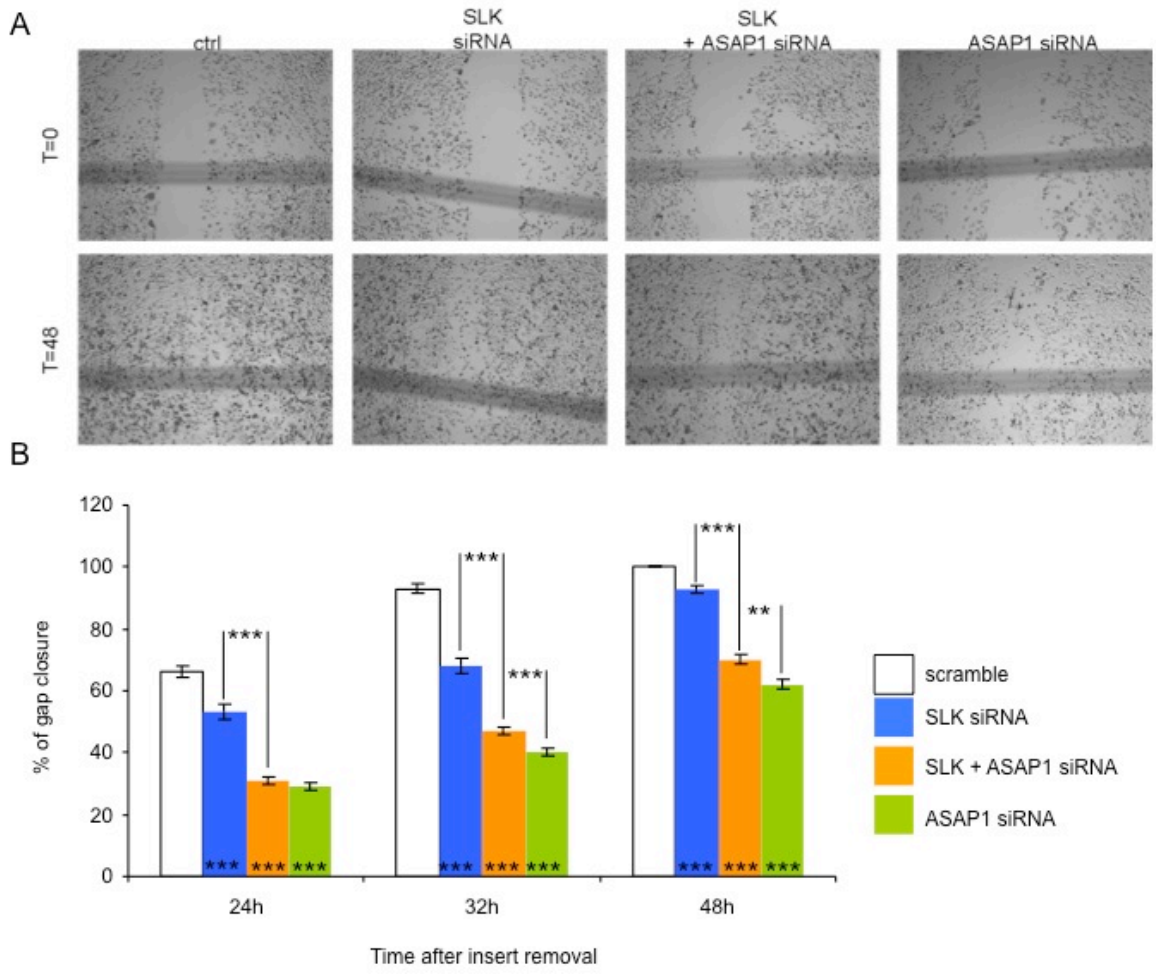

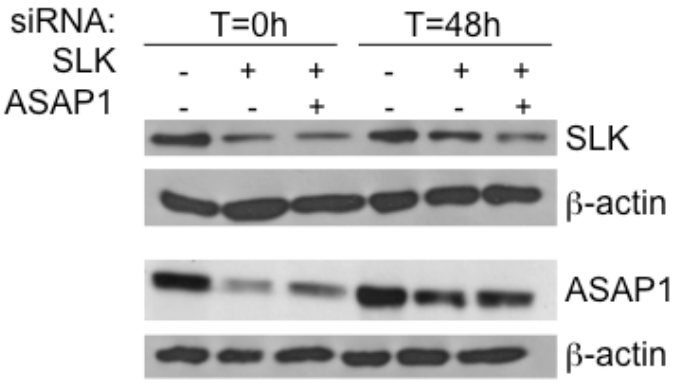

Figure 46: **Effect of the knock down of SLK combined with ASAP1 knock down on cell motility. A.** Representative pictures of monolayer wounds taken at the beginning of the assay (t=0) and at the end (t=48). **B.** Graph showing the analysis of a representative motility experiment. The gap closure was measured at 24, 32 and 48 hours after insert removal. The width of the two cell fronts at the beginning of the assay was considered as 100%. The asterisks within the bars represent the significance versus the control. The other asterisks represent the significance of the difference between SLK knock down cells (blue bars) compared to the double-knock out cells (orange bars), and of the double knock out cells to cells transfected with the ASAP1 siRNA alone (green bars). Error bars are standard error (n=60). Both ASAP1 and SLK knock down were able to reduce the motility, although to a different extent.

C. Western blot showing the efficiency of the knock down at the beginning of the assay (t=0) and at the end (t=48).

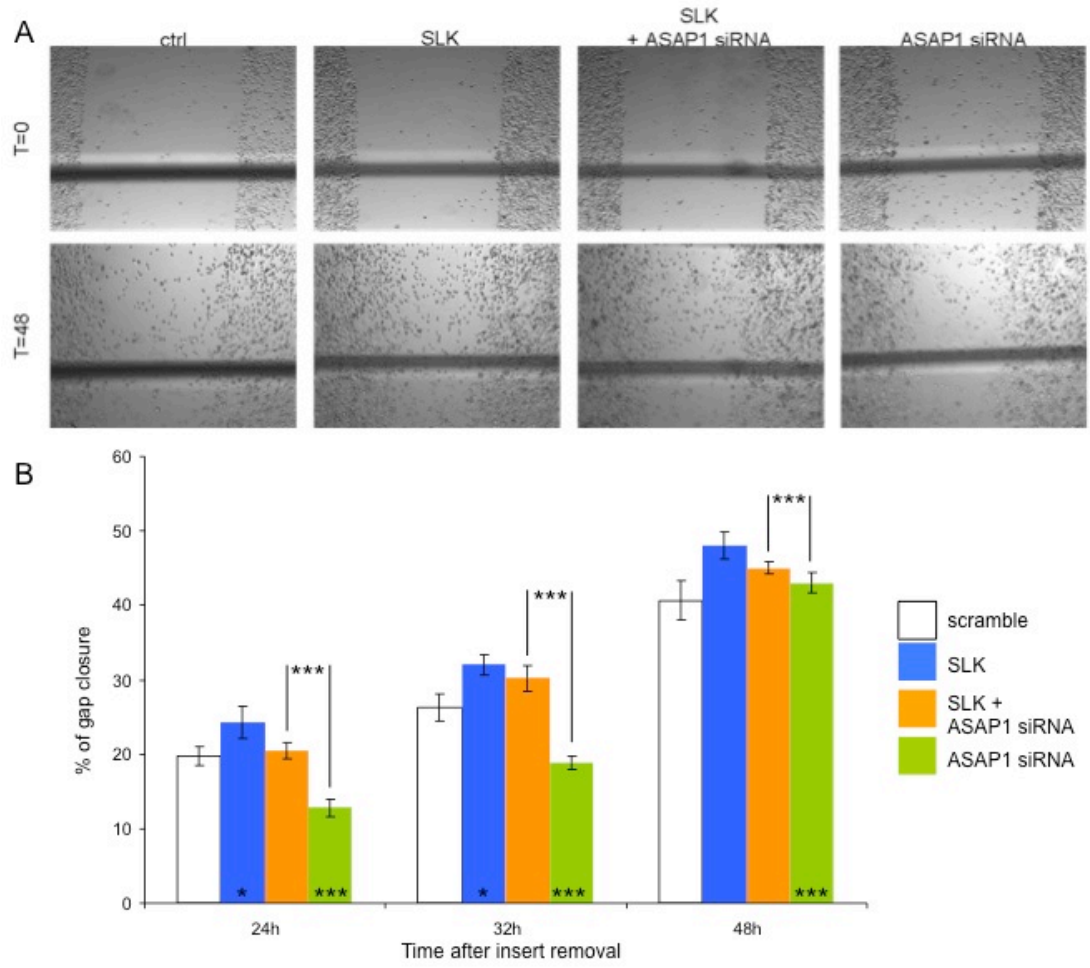

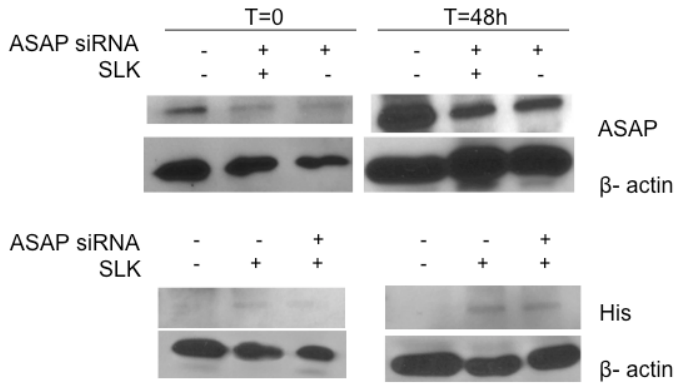

Figure 47: **Effect of the overexpression of SLK combined with ASAP1 knock down on cell motility. A.** Example pictures of the wound taken at the beginning of the assay (t=0) and at the end (t=48). **B.** Graph showing the analysis of a representative motility experiment. The asterisks within the bars represent the significance versus the control cells. The other asterisks represent the significance of the difference between ASAP1 knock down cells overexpressing SLK (orange bars) compared to ASAP1 knock down cells only (green bars). Error bars are standard error (n=60). The knock down of ASAP1 significantly reduced the motility of the cells, whereas the overexpression of SLK results in an increase of the cell motility. This effect is almost unchanged by the simultaneous knock down of ASAP1.

C. Western blot showing the efficiency of the transfections at the beginning of the assay (t=0) and at the end (t=48).

Taken together, these results indicate that although ASAP1 and SLK interact with each other, and are both able to affect the motility of the cells, they are likely to do so via independent mechanisms.

4.3.7 ASAP1 knock out mouse embryonic fibroblasts have impaired motility

The effects of ASAP1 binding partners on ASAP1-dependent motility have been all analyzed in the context of "loss of function" experiments using the silencing of the ASAP1 gene in the MDA MB 231. These cells have already a very high level of expression of ASAP1, making them unsuitable for performing "gain of function" analysis. For this purpose I took advantage of the ASAP1 knockout mice available in the laboratory, and prepared primary cultures of MEFs from wild type and knock out embryos. I reasoned that the knock out cells would enable me to analyze the effects of a "gain of function", namely what happens when ASAP1 is ectopically expressed on a knockout background.

I first analyzed the basal motility activity of the MEFs in the presence or absence of ASAP1. I performed the wound healing assays with three lines each per genotype. The assays clearly showed that the fibroblasts derived from the ASAP1 knockout mice had a statistically significant reduced motility compared to the wild type MEFs *(Figure 48 and Figure 49)*. This was not line dependent, and was reproducible over three experiments.

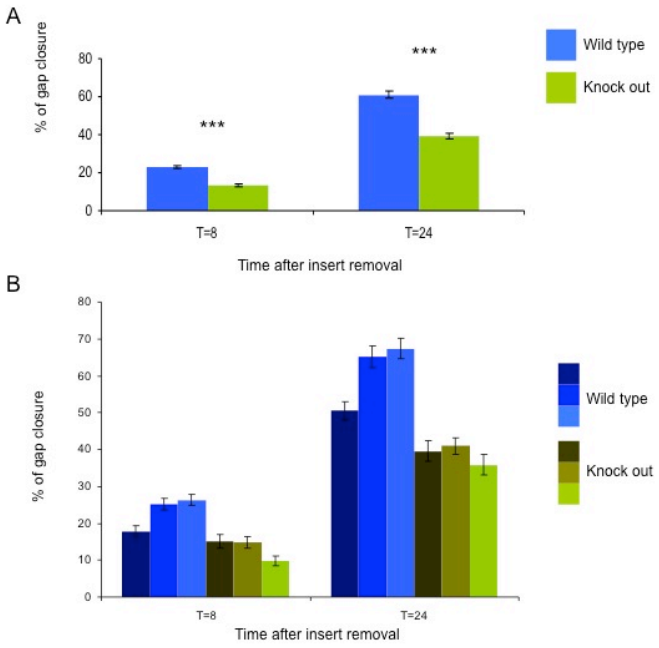

Figure 48: Representative experiment showing the difference in motility in wild type versus ASAP1 knock outs MEFs. Error bar is standard error (n=24 in A, n=72 in B). **A**. Mean of three different cell lines **B**. Results of the pooled individual cell lines.

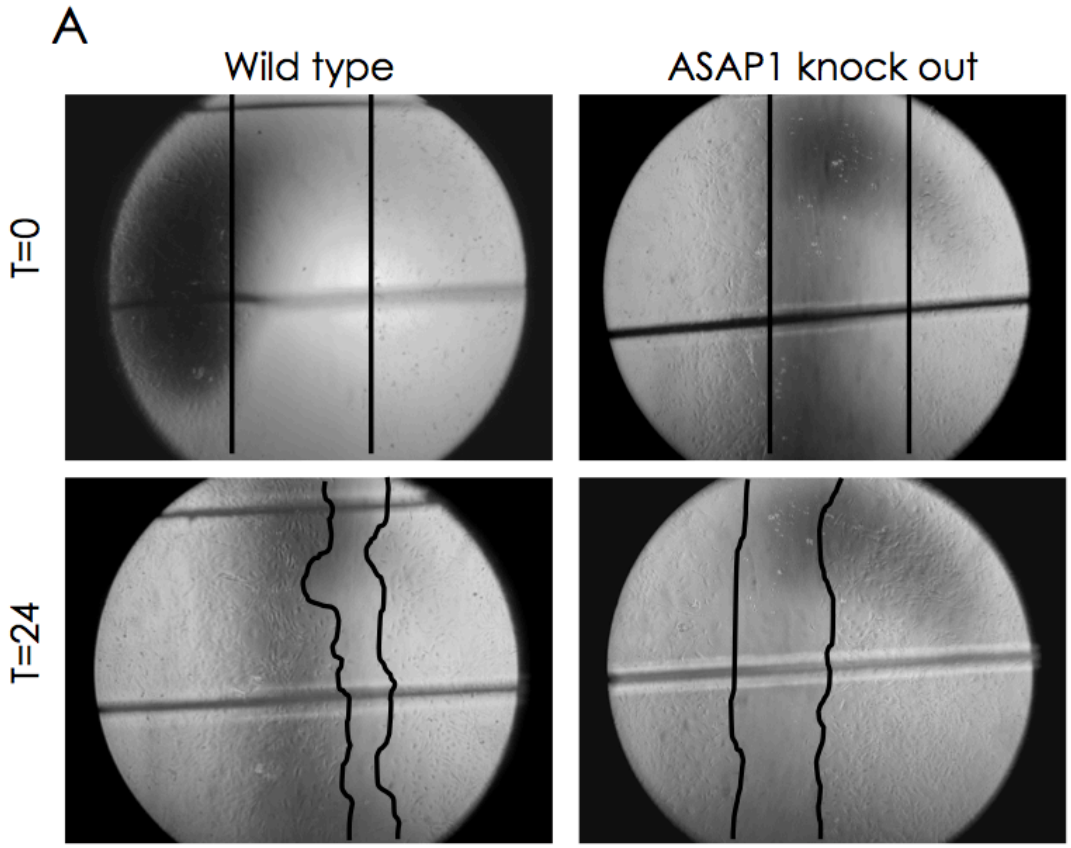

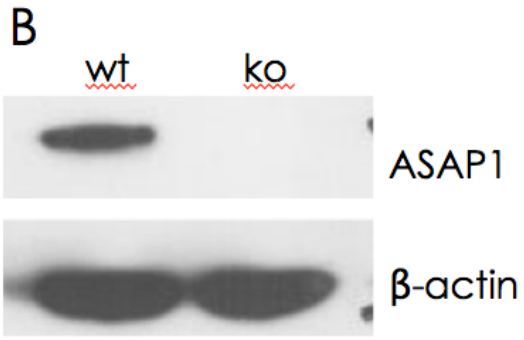

Figure 49: **A.** MEFs from ASAP1 knockout mice have impaired motility. Representative pictures showing the difference between the ability to close the gap of the wild type MEFs (left) versus the knockout cells (right) 24 hours after removing the insert. **B.** Western blot showing the missing expression of the ASAP1 gene in the knockout MEFs

4.3.8 SLK overexpression does not influence ASAP1-mediated motility in MEFs

MEFs lacking the ASAP1 gene have a reduced ability to close monolayer wounds. In MDA MB 231 breast tumor cells, overexpression of SLK partially rescues the reduction in motility caused by knockdown of ASAP1 *(Figures 46 and 47)*, suggesting that the two proteins regulate cellular motility independently. To verify this notion I transfected the ASAP1 knock out and wild type MEFs with the expression plasmid for SLK.

Additionally, I performed motility experiments with the ASAP1 knockout cells transfected with the ASAP1 expression plasmid and the mutant R14, which lacks one proline in the SH3 binding domain that is critical for ASAP1-mediated motility.

Due to the low transfection efficiency of the primary MEFs, in order to perform the assay I first had to FACS sort MEFs that were co-transfected with the plasmid of interest and a GFP-expression plasmid *(Figure 50).*

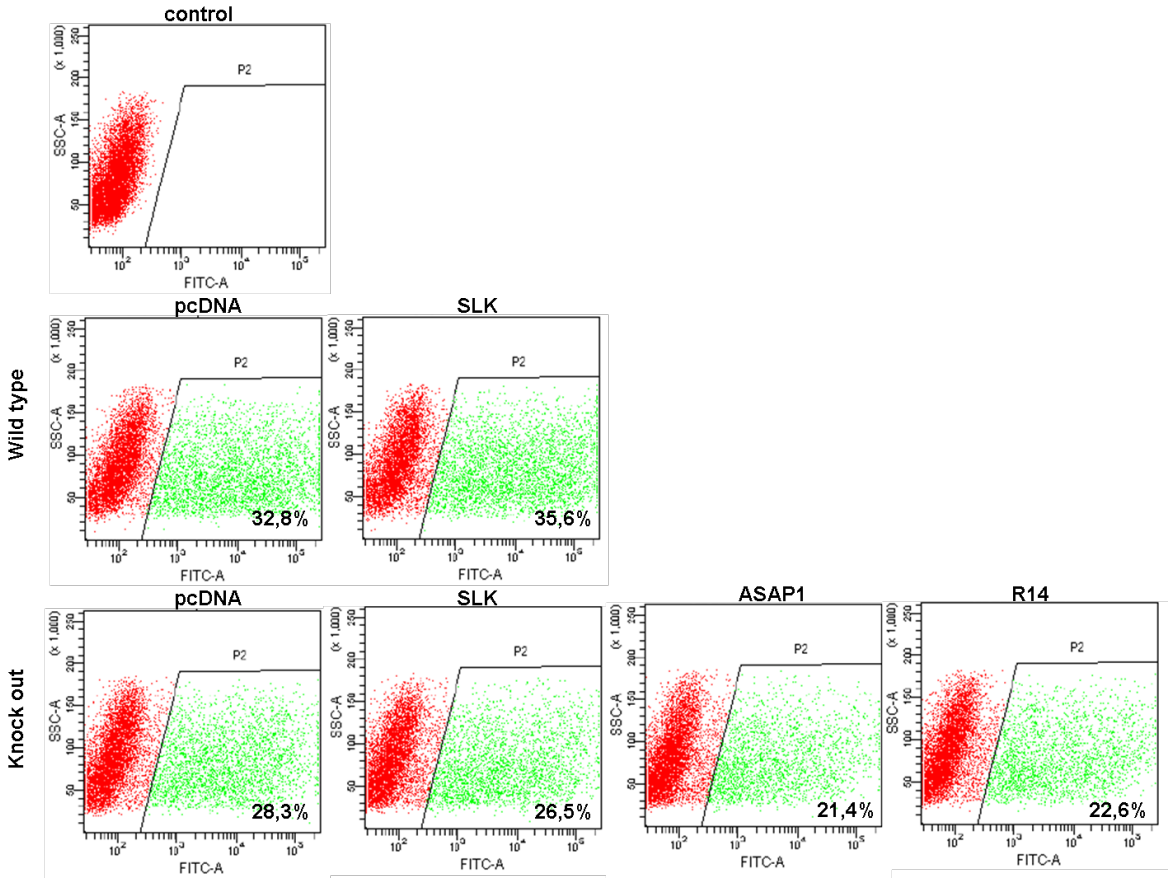

Figure 50: **FACS sort of co-transfected MEFs.** Wild-type and ASAP1 knock out MEFs were co-transfected with a GFP-expressing plasmid and either an empty vector as a control (pcDNA), or plasmids expressing the protein of interest (SLK, ASAP1 or R14). The control plot shows the absence of fluorescence in cells not transfected with the GFP-expressing plasmid. The population in green in the other plots represents the cells that have been successfully co-transfected (efficiency shown bottom right of the plot).

In both the wild type and knockout MEFs, the overexpression of SLK induced an increase in motility to a similar extent *(Figure 51).* This indicates that the motility promoting ability of SLK is independent of the presence of ASAP1. Furthermore, transfection of ASAP1 into the knockout MEFs caused a complete recovery in motility

back to the wild type levels. As expected, this did not happen when the cells were transfected with the R14 mutant *(Figure 51).*

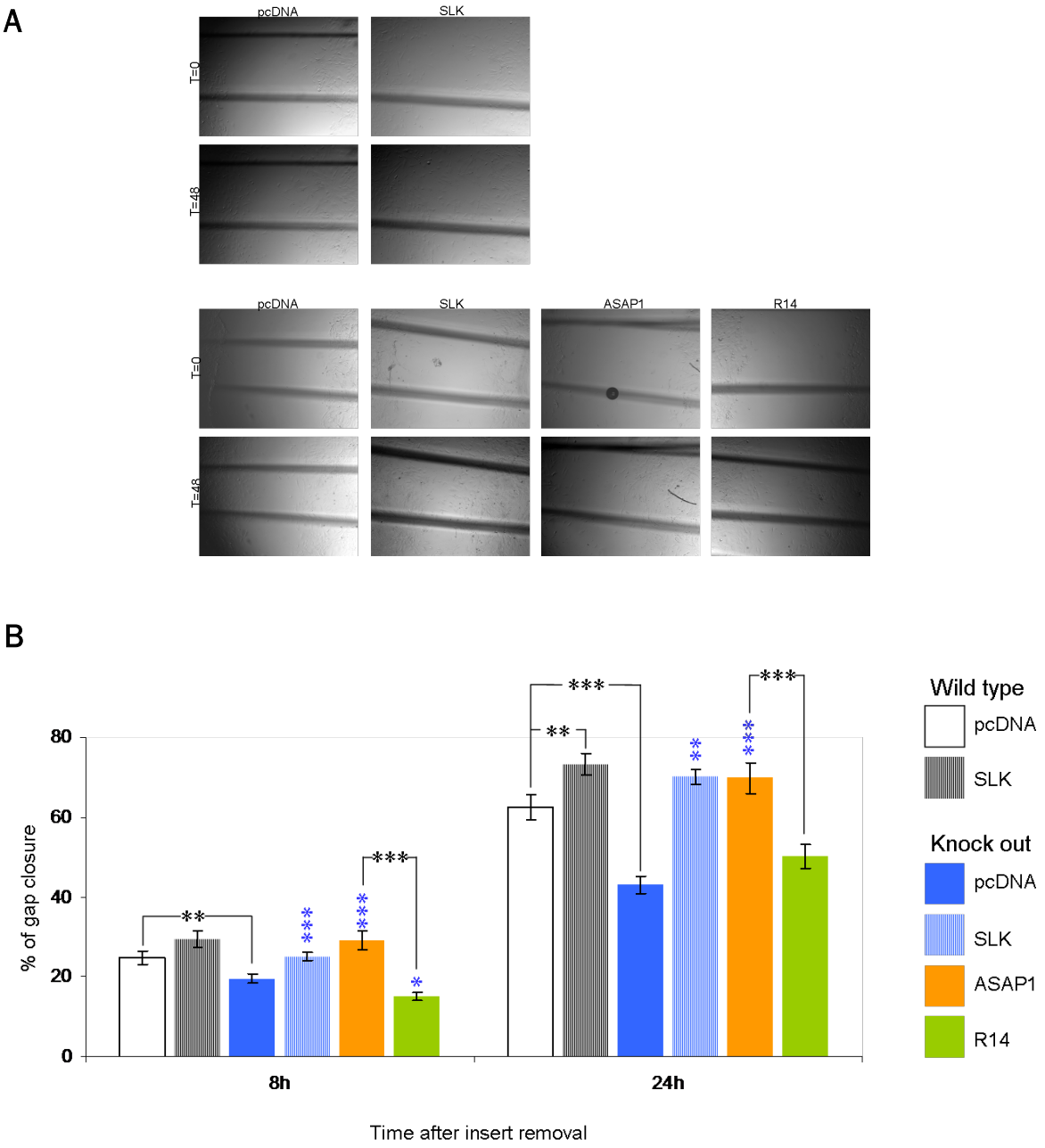

Figure 51: **A.** Representative pictures showing the effect on the motility of wild type and ASAP1 knock out MEFs of the transfection of various plasmids. **B.** Graph showing the analysis of one representative motility assay. Both wild type and ASAP1-knock out MEFs were transfected with SLK or with the appropriate control, and their wound closure measured. The ASAP1-knock out MEFs were additionally transfected with ASAP1 and R14 expression plasmids. Error bars are standard error (n=3). Blue asterisks represent the significance versus the knockout control cells.

Again, these experiments underscore the importance of the SH3 binding domain of ASAP1 in promoting the motility of the cells, but rule out the possibility that SLK is involved in this mechanism, confirming the results obtained with the MDA MB 231 cells.

4.4 ASAP1 as a multidomain protein

4.4.1 Establishment of a Fast Protein Liquid Chromatography System for analysis of ASAP1-containing protein complexes

ASAP1 is a multi domain adaptor protein that binds to a wide variety of other proteins through its different domains. Both Nm23-H1 and h-prune, which in tumor cells form a complex, have been shown via co-immunoprecipitation to interact with ASAP1. However, my results indicate that these two proteins do not influence the activities of ASAP1 that I analyzed, namely the regulation of receptor internalization and the promotion of motility. This raised the question of whether the binding of these two proteins to ASAP1 is relevant *in vivo*. Therefore I set out to investigate the presence of Nm23-H1 and h-prune in ASAP1-containing protein complexes extracted from cells. To this end I used a Fast Protein Liquid Chromatography (FPLC) system to perform size exclusion chromatography using a gel filtration column.

I first established a calibration curve of the column with specific molecular weight markers. Blue dextran (molecular weight approx. 2,000,000Da) was used to determine the void volume (V_o) of the column. This is column-specific, and is the volume of effluent required for the elution of a large completely excluded molecule. Then six proteins with known molecular weights were run through the column, and their elution volume (V_e) assessed (*Table 3*). The V_e corresponds to the peak of elution of the given protein. Plotting the logarithms of the known molecular weights of protein standards versus their respective V_e/V_o values produced a linear calibration curve *(Figure 52).* With the help of the calibration curve, I was able to calculate the corresponding approximate molecular weight for each fraction, and therefore to determine the size of the ASAP1-containing complexes.

	MW, kDa	Ve	Ve/Vo	Fraction no.
carbonic anhydrase	29	20.5	2.12	42
albumin	66	19.1	1.97	36
alcohol dehydrogenase	150	18.2	1.88	33
ß-amylase	200	17.7	1.83	31
apoferritin	443	16.5	1.71	26
thyroglobulin	669	15.2	1.57	21
blue dextran	2000	9.7		

Table 3: **Molecular weights and elution volumes of the protein standards used for the calibration curve.** Ve is the volume of elution that corresponds to the peak of the given protein. Vo is the void volume of the column. The ratio between these two values is used to create a calibration curve *(Figure 52)*.

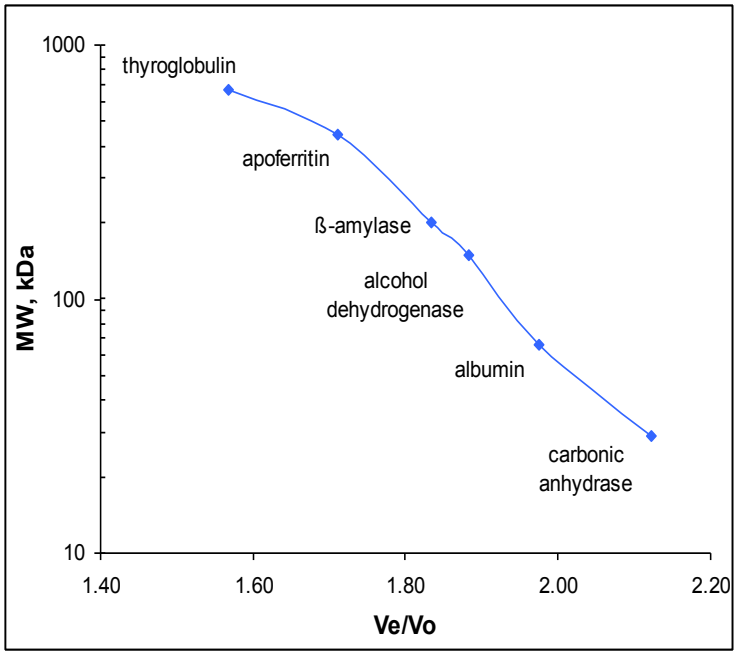

Figure 52: **The calibration curve for the column.** The V_e/V_o values for each protein standard, which depend on their elution volume V_e, were plotted against their known molecular weights in a logarithmic graph. The resulting curve was used to determine the unknown molecular weight of a protein or of a protein complexes eluting from the column by interpolation of their V_e.

The efficiency of the separation depends on the fraction size and number. To be sure that these two parameters were optimized in my system, I loaded a cell lysate onto the column, performed a separation, and loaded the collected fractions onto SDS-PAGE gels, which I stained to visualize the proteins. The gels obtained showed a good

separation pattern with clearly visible, discrete bands, indicating that the parameters used for the separation were suitable *(Figure 53).*

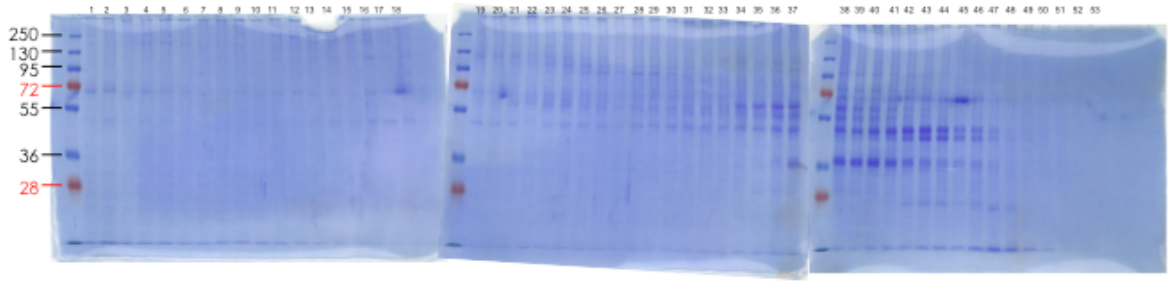

Figure 53: **Separation of cell lysate proteins.** Fractions collected after separation of the MDA MB 231 lysate were loaded onto SDS-PAGE gels and stained with Coomassie. The discrete bands visible and the absence of a "smear" show how the separation strategy chosen allows to elute distinct fractions corresponding to molecular weights from 250 kDa (upper band of the molecular weight marker) to 28 kDa (lower, red band of the molecular weight marker).

4.4.2 Endogenous ASAP1 protein complexes do not co-elute with h-prune and Nm23-H1 in size exclusion FPLC

To analyse ASAP1-containing protein complexes, I transfected MDA MB 231 cells with expression plasmids of tagged Nm23-H1 or h-prune, and prepared cell lysates that were applied to the column and separated as described in "Materials and Methods". The fractions were collected, and a set of SDS-PAGE gels for each protein of interest (ASAP1, h-prune and Nm23-H1) was run and Western blotted. The incubation of the membranes with the specific anti-tag antibodies showed that h-prune and Nm23-H1 indeed co-elute in similarly sized high molecular weight complexes larger than their own individual molecular weight, consistent with their reported interaction *(Figure 26).* Nevertheless, I was unable to detect a signal for these proteins in fractions in which endogenous ASAP1 eluted. According to the molecular weight of the mature protein (130 kDa), ASAP1 in monomeric form was expected to elute around fraction no. 33 *(see Table 3)*, but it was already detectable in fraction 13, which corresponds approximately to 700 kDa. This indicates that ASAP1 is indeed part of a high molecular weight protein complex, and that the gel filtration did not disrupt these interactions. However, h-prune and Nm23-H1 did not co-elute with these high molecular weight ASAP1-containing complexes, thus suggesting that they may not interact substantially with ASAP1 *in vivo*. Nevertheless, the results clearly demonstrate that ASAP1

monomers interact with other proteins as part of a protein complex. The bands staining with ASAP1 antibodies found in the elution fractions of Nm23-H1 and h-prune visible in blot C are much smaller that the normal size of the ASAP1 protein (*Figure 54*) might correspond for example to unglycosylated precursors of ASAP1, ASAP1 degradation products, or proteins bound non-specificially by the ASAP1 antibodies.

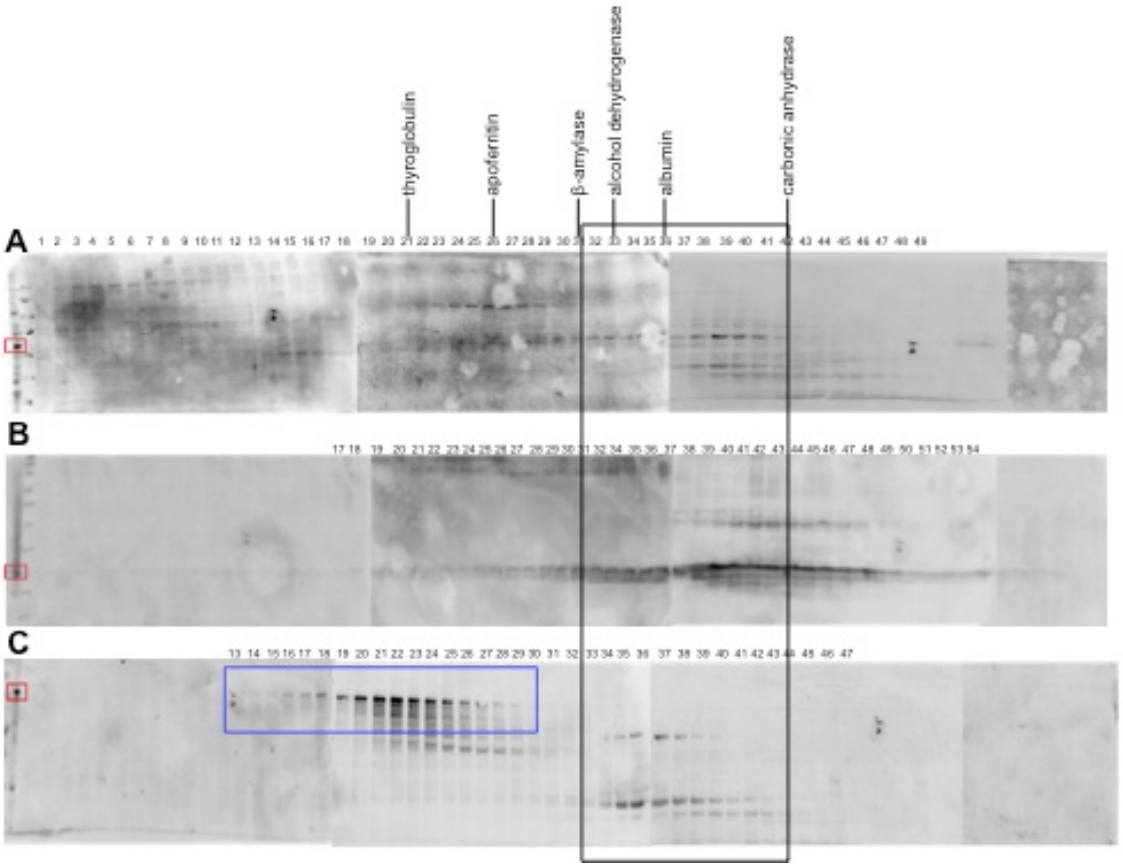

Figure 54: **Blots showing the separation of lysates of MDA MD 231 cells.** Blot A and B show the lysate eluate of cells transfected with tagged h-prune (**A**) and Nm23-H1 (**B**), respectively, and incubated with the corresponding antibody (anti-flag for blot A, anti-Nm23-H1 for blot B). The red boxes in the left lane indicate the monomeric protein bands visible in total lysate, as a control. As highlighted by the black box, the bands of the two proteins appear at the same fraction number, consistent with their interaction. Blot **C** corresponds to the fractions obtained from the non-transfected cell lysate, incubated with the anti-ASAP1 antibody. ASAP1 protein elutes mainly as a high molecular weight protein complex (blue box), indicative of its interaction with other binding partners. Note, however, that neither Nm23-H1 nor h-prune protein is present in the corresponding blots at this molecular weight. The bands in blot C that are visible in correspondence of the black box might be unglycosylated precursors of ASAP1.

5. DISCUSSION

5.1 Summary of main findings

During my PhD project I analysed the effect of different, newly-discovered ASAP1 interacting proteins on the ability of ASAP1 to promote EGF receptor internalization and cell motility. Nm23-H1 and h-prune, two proteins involved in the control of motility and metastasis, have been shown by the laboratory of Prof. Zollo to co-immunoprecipitate with ASAP1. However, in the highly metastatic breast cell line MDA MB 231, no substantial evidence to support a role for Nm23-H1 or h-prune in regulating the activity of ASAP1 was obtained. Furthermore, although size exclusion chromatography confirmed that most ASAP1 protein in MDA MB 231 cells is part of high molecular weight protein complexes, Nm23-H1 and h-Prune are not major components of these complexes.

ASAP1 is able to bind to several proteins via its SH3 domain, and previous results already suggest that this domain is responsible for the motility-promoting activity of ASAP1. Using an array of purified recombinant SH3 domain-containing proteins I was able to discover SLK as a new binding partner of ASAP1, and confirmed their interaction using co-immunoprecipitation. Nevertheless, other results I obtained indicate that SLK and ASAP1 regulate and promote motility independently of each other. This was confirmed in MDA MB 231 cancer cells, and in ASAP1-knock out and wild type MEFs. The experiments with the MEFs also further substantiate the importance of the SH3 binding domain of ASAP1 in its motility-promoting activity. Together these data cast further light of the interaction partners of ASAP1 and its role in the regulation of EGFR internalization and cell motility.

5.2 ASAP1 regulates EGF internalization.

It is known that EGF, its receptor and downstream signalling pathways are often deregulated in tumors. Several studies indicate that regulation of the internalization of EGFR also has an impact on cell migration, and thus in the context of a tumor cell alterations in the regulation of these process may affect invasion and metastasis

(Bremm et al., 2008; Roepstorff et al., 2008; Muller et al., 2009). As ASAP1 regulates the internalization of EGF (Nie et al., 2006), I first examined if the metastasis-promoting activity of ASAP1 could be mediated by its ability to regulate EGFR internalization.

To investigate the effects of ASAP1 on receptor uptake and vesicle trafficking, I first designed an assay based on the findings of Nie and colleagues who investigated the role of the BAR domain of ASAP1 in vesicle trafficking and uptake of EGFR (Nie et al., 2006). The procedure described in the paper used fluorescence microscopy as readout of the internalization rate of fluorescent EGF. This method has some weaknesses because the image analysis does not discriminate between unspecifically, surface bound EGF and the internalized growth factor-receptor complex. Other investigators performed an accurate analysis of the dynamics of EGFR internalization, and compared confocal microscopy with FACS analysis (Schmidt-Glenewinkel et al., 2009). Although confocal microscopy provided useful information about the kinetics of internalization, the FACS analysis resulted in a more accurate description of the process. This was due mainly to the increased sample size of the method: 10000 cells in the FACS analysis compared to 30 cells analysed with the microscope. The overall results coincided, but the FACS analysis proved to be a more sensitive tool to detect the trafficking of the receptor. Indeed, other authors have used the FACS method with analogous protocols to analyse EGFR internalization (Duan et al., 2003; Lidke et al., 2004; Wang et al., 2005). Given the advantages of the FACS analysis, I opted to use this procedure to analyse the effect of ASAP1 on the internalization of fluorescent EGF. An important improvement in the protocol that I developed was the use of a stripping step, which removes the surface-bound EGF and gives therefore a more specific indication about the amount of internalized EGF.

Using the optimized assay, I reproducibly observed that the specific and efficient silencing of ASAP1 resulted in an increase in the intracellular fluorescence after treatment with fluorescein-coupled EGF. At first sight this result is perhaps counterintuitive, because it would appear to suggest that silencing of ASAP1 increases uptake of EGF. However, published data indicate that the reverse is in fact true, because reduced ASAP1 activity slows vesicle trafficking, resulting in an accumulation of the growth factor intracellularly, thereby increasing the fluorescent signal. For

example, this has been demonstrated in studies that used mutant forms of ASAP1 to investigate its role in vesicle trafficking and EGF uptake (Nie et al., 2006). In these experiments, HeLa cells were transfected with a mutant form of ASAP lacking the BAR domain and treated with the same fluorescein-coupled EGF that I used. Compared to controls transfected with the full length ASAP1, cells transfected with a mutant ASAP1 lacking the BAR domain showed an increase in intracellular fluorescence, as measured by fluorescence microscopy. This is because reduced activity of ASAP1 causes a slow down of the internalization process, resulting in an accumulation of the EGF-receptor complex, and therefore in an increase in the fluorescent signal (Nie et al., 2006). In the control cells in which normal ASAP1 activity is present, the internalization of the receptor and clearance of the fluorescein-coupled EGF occurs more rapidly. Thus, the fluorescence intensity is lower.

Orth and colleagues have shown a link between the formation of circular dorsal ruffles (CDR, or "waves"), which are one of the cytoskeletal structures ASAP1 participates in (Randazzo et al., 2000), and the internalization of receptors such as EGFR (Orth et al., 2006). CDRs are formed in response to stimulation of the tyrosine kinase receptors for HGF, EGF and PDGF, and are found on the membrane of migratory cells. Although their precise function is not clear, it seems that they have a role in cell motility, as their appearance precedes the formation of lamellipodia (Buccione et al., 2004). These structures can be responsible of the sequestration and endocytosis of up to 50% of receptors such as EGFR (Orth et al., 2006). ASAP1 might therefore regulate the internalization of EGFR not only via the classical endocytotic process through its BAR domain, but also by contributing to this alternative pathway.

5.3 ASAP1 interaction with Nm23-H1 and h-prune in EGF recycling

The laboratory of Prof. Zollo found that h-prune and Nm23-H1, two proteins already known to interact with each other and to control cell motility and invasion, were able to co-immunoprecipitate with ASAP1. This observation led me to hypothesize that these three proteins might form a regulatory complex involved in the metastatic process. To verify whether Nm23-H1 and h-prune can indeed affect ASAP1 and its activities, I

investigated two functions of the ASAP1 protein, namely its role in vesicle trafficking and EGFR internalization, and its ability to promote motility, parameters that are highly relevant to metastasis formation. Loss- and gain-of-function experiments allowed me to investigate the influence of Nm23-H1 and h-prune on ASAP1 activity in these assays.

I used the EGF internalization assay that I developed to investigate if and how Nm23-H1 and h-prune affect ASAP1-dependent regulation of EGF internalization in MD MB 231 cells. The overexpression of h-prune did not affect the internalization rate of EGF in the presence or absence of ASAP1. In contrast, loss- and gain-of-function experiments with Nm23-H1 suggested a role for Nm23H1 in EGF internalization. While silencing of Nm23-H1 alone had no effect on EGF internalization, the increased fluorescence observed after silencing ASAP1 in these assays was abrogated by the concomitant silencing of Nm23-H1. Ectopic expression of Nm23-H1 also resulted in a small but significant increase in fluorescence. However, ectopic expression of Nm23-H1 in cells with silenced ASAP1 reduced the increase in fluorescence observed with ASAP1 silencing alone. Although these results do not provide any evidence that Nm23-H1 regulates ASAP1-mediated EGF recycling, they do suggest that Nm23-H1 participates in this process, and may serve as a "governor" that acts to maintain EGF internalization rates within normal boundaries.

Interestingly, Nm23-H1 has been linked with the regulation of endocytosis, albeit in other contexts. Palacios and colleagues showed that Nm23-H1 is recruited by Arf6-GTP to cell-cell contacts to facilitate dynamin–dependent vesicle fission (Palacios et al., 2002). ASAP1, an effector for Arf6, may participate in this complex, which could also be relevant in the internalization of EGF. Moreover, in *Drosophila* the homologue of Nm23-H1, *awd*, is recruited to the plasma membrane together with *shi*/dynamin to regulate the internalization of *Btl*/FGFR homologue, again linking Nm23-H1 with endocytosis (Dammai et al., 2003). Similarly it has been proposed that Nm23-H1 could act as an unconventional GEF for dynamin, facilitating its activation, because the inhibition of Nm23-H1 caused a reduction in dynamin-mediated endocytosis (Krishnan et al., 2001). Dynamin is a large GTPase that is inactivated by hydrolyzing GTP to GDP. This GTPase activity is enhanced by protein interaction partners that bind to the proline-rich region of dynamin via SH3 domains (Hinshaw, 2000), and ASAP1 may be

one of these. The GTPase effector domain (GED) of dynamin is responsible for the GTPase activity of dynamin, but ASAP1 with its GAP domain may also contribute to the hydrolysis of GTP, thereby facilitating the budding of the endocytotic vesicle. This would mean that ASAP1 not only binds to the membrane to bend it and facilitate endocytosis, but may also be involved directly in dynamin–mediated vesicle fission *(Figure 56)*. Moreover, it has been suggested that proteins with a BAR domain such as ASAP1 can destabilize the phospholipid bilayer and thereby influence the GTPase activity of dynamin (Ferguson and De Camilli, 2012).

5.4 Effects of Nm23-H1 and h-prune on ASAP1-mediated motility

A key feature of ASAP1 in promoting the metastatic process is its role in cell motility (Müller et al., 2010). Therefore I analysed the effects of Nm23-H1 on this activity. The silencing of ASAP1 in the MDA MB 231 cells resulted in a clear reduction in the motility of the cells, as expected. Silencing of Nm23-H1 also reduced motility to a similar degree, and concomitant silencing of both ASAP1 and Nm23-H1 did not lead to any further reduction in motility. Furthermore, ectopic expression of Nm23-H1 had no effect on cell motility, and also had no effect on reduced cell motility subsequent to ASAP1 silencing. These findings could in principle indicate that Nm23-H1 and ASAP1 cooperate to regulate motility, if one assumes that ASAP1 and Nm23-H1 interact stoichiometrically at steady state within MDA MB 231 cells. Further experiments would be required to investigate this possibility, for example using the wild-type and knockout MEFs I produced. However, it would seem unlikely that the levels of ASAP1 and Nm23-H1 are finely balanced in this way. Thus a tentative conclusion is that Nm23-H1 affects motility independently of its interaction with ASAP1. The fact that the SH3 binding domain of ASAP1 is critically required for ASAP1-mediated motility (Müller et al., 2010), whereas Nm23-H1 does not possess a SH3 domain and does not interfere with the interaction between ASAP1 and the SH3 domain-containing SLK protein provides further indirect support for this conclusion.

On first sight it is surprising that the silencing of Nm23-H1 resulted in a decrease in cell motility, as Nm23-H1 is known as a metastasis suppressor, and thus its knock down would be expected to cause an increase in the migratory potential of the cells.

Other authors however have linked the expression of Nm23-H1 with tumor progression and poor prognosis, despite its prominent role as a metastasis suppressor (Zeng et al., 1994; Müller et al., 1998; Xiao et al., 1998). These observations underscore the complex effects of Nm23-H1 in different contexts and cellular processes.

I also examined the effect of h-prune on cell motility, and whether this modulates ASAP1-mediated cell motility. Ectopic expression of h-prune resulted in a modest but significant reduction in the motility of MDA MB 231 cells. This result is surprising, as ectopic expression of h-prune has previously been reported to promote cell motility in breast cancer cells (D'Angelo et al., 2004). A possible explanation for this finding is that the effect of h-prune on cell motility is context dependent, and that it has different effects in different cells. Despite modestly reducing motility, ectopic h-prune expression had no effect on the much greater reduction in cell motility following silencing of ASAP1. These data therefore do not provide any evidence that h-prune regulates ASAP1-mediated cell motility, but further experiments would be needed to substantiate this conclusion.

5.5 SLK is a novel SH3 domain-containing interaction partner of ASAP1 that regulates cell motility independently of ASAP1

Previous studies in the laboratory of Prof. Sleeman showed that the SH3 binding domain of ASAP1 is necessary for this protein to exert its pro-motility and pro-metastatic effects, both *in vitro* and *in vivo* (Müller et al., 2010). The results I obtained with the ASAP1-knockout MEFs again confirmed the importance of the SH3 binding domain of ASAP1 in regulating motility. In these cells, enforced expression of wild type ASAP1 rescued the motility of the ASAP1 knockout MEFs, which was not the case for the SH3 binding domain mutant of ASAP1.

To gain further insight into how ASAP1 regulates tumor cell motility and metastasis at the molecular level, I used a commercially-available array of proteins containing SH3 domains to find potential new proteins that interact with ASAP1 via its SH3 binding domain. An interesting candidate that emerged from this screening was STE20-like kinase or SLK, which was then confirmed as an interaction partner for ASAP1 by

means of co-immunoprecipitation (Müller et al., 2010). SLK was of particular interest for my studies, as it has already been linked both to cell motility and to the promotion of tumor progression in the context of breast cancer. For example, it has been shown that the kinase activity of SLK is required for ErbB2-driven breast cancer cell motility (Roovers et al., 2009).

Human SLK has been cloned and characterized from a human lung carcinoma cell line (Yamada et al., 2000). It is a germinal centre kinase (GCK)-related kinase that is ubiquitously expressed in adult tissues, and which has a role in actin stress fibre dissolution and the induction of apoptosis (Sabourin et al., 2000). SLK is indirectly associated with the microtubules and is enriched at the leading edge of migrating cells (Wagner et al., 2002). It is activated by the FAK/Src/MAPK pathway, and subsequently promotes focal adhesion turnover and cell migration (Wagner et al., 2008) *(Figure 55)*. The disassembly of actin stress fibres caused by SLK is inhibited by inactive Rac1 (Wagner et al., 2002).

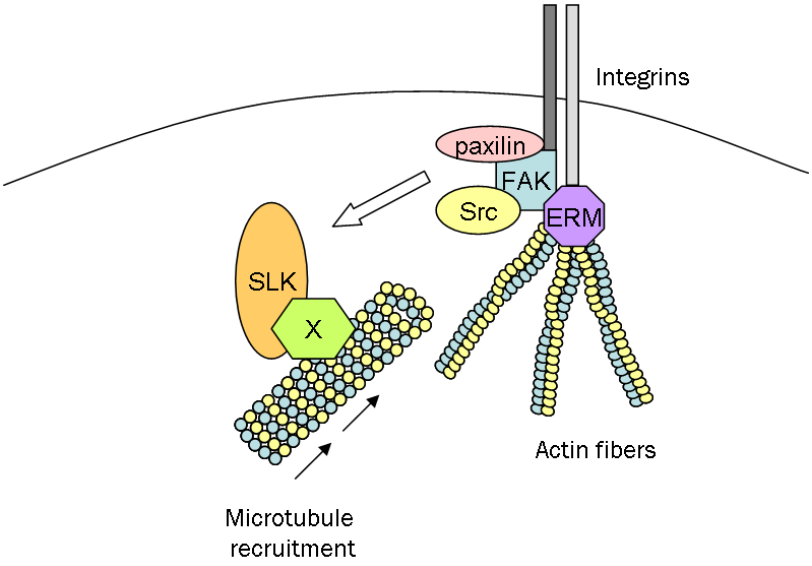

Figure 55: **The role of SLK in focal adhesions.** SLK associates with microtubules via a binding protein that remains to be identified (X). The activation of the integrin-Src-FAK pathways leads to the recruitment and activation of the microtubule-SLK complex (adapted from Wagner and Sabourin 2009).

In MDA MB 231 cells, I found that ectopic expression of SLK resulted in increased cell motility as expected. Consistently, SLK knockdown reduced the motility of the cells, but to a lesser extent than ASAP1 knockdown, which may reflect the different

efficiency of the silencing. Importantly, ectopic expression of SLK was able to rescue the reduction in motility caused by the knockdown of ASAP1, and restored cell motility to normal basal levels. The silencing of the two proteins together did not show an additive effect in inhibiting motility. In both the knockout and in the wild type MEFs, ectopic expression of SLK resulted in an increase of cell motility. Together these data confirm the roles of ASAP1 and SLK proteins in regulating cell motility, but suggest that SLK exerts its motility-promoting activities independently of ASAP1.

Both ASAP1 and SLK have been described as being part of focal adhesions, and are involved in FAK signalling that promotes motility *(Figure 56)* (Wagner et al., 2008; Roovers et al., 2009; Brown et al., 2000; Liu et al., 2002). FAK signalling is a very important regulator of cell motility, and it has been linked with cancer in various reports (McLean et al., 2005). As SLK and ASAP1 both play a role in cell motility and migration, and have been implicated in tumor progression, it is tempting to speculate that they may share a common upstream signal, namely FAK-Src phosphorylation, but then independently affect different downstream pathways upon activation. This would reflect the redundancy of signals that is often found in cells (Kafri et al., 2009).

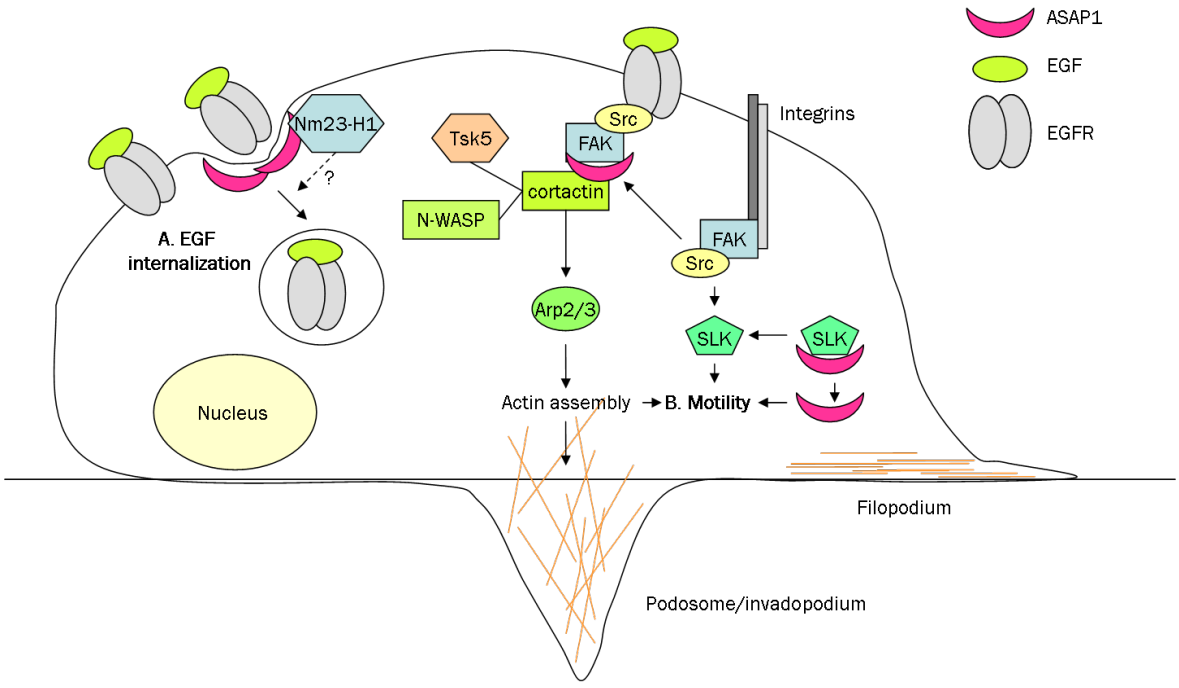

Figure 56: **Schematic diagram showing the effects of ASAP1 in the cell and the possible role of its interaction partners in these processes. A.** ASAP1 dimerizes, and promotes the internalization of EGF. Nm23-H1 might participate in this process by interacting both with ASAP1 and dynamin. **B.**

ASAP1 and SLK might be commonly activated by FAK-Src signalling to promote motility. The two proteins subsequently act through independent mechanisms to regulate motility, despite that fact that they can interact with each other.

5.6 What is the relevance of the interaction of Nm23-H1 and h-prune with ASAP1 *in vivo*?

The cell motility and metastasis-promoting effects of ASAP1 are dependent on its SH3 binding domain (Müller et al., 2010), as I also demonstrate here with the rescue experiments in the ASAP1 knockdown MEFs. Neither h-prune nor Nm23-H1 were able to impair the binding of ASAP1 to SLK, suggesting that h-prune and Nm23-H1 do not interact with ASAP1 via its SH3 binding domain (note that neither protein contains an SH3 domain), and also do not interfere with its ability to interact with proteins that contain SH3 domains. Furthermore, I did not obtain any substantial data to support the notion that h-prune or Nm23-H1 regulates ASAP1-mediated EGF internalization or cell motility. The question therefore arose as to whether the interaction between ASAP1 and Nm23-H1 and h-prune as evidenced by co-immunoprecipitation is relevant to the cell motility and metastasis promoting activity of ASAP1. To begin to address this issue I used size exclusion chromatography to determine the degree to which h-prune and Nm23-H1 are present in ASAP1-containing protein complexes extracted from MDA MB 231 cells. I found that Nm23-H1 and h-prune eluted in similarly-sized protein complexes, consistent with their reported interaction. However, little if any ASAP1 was present in these fractions. Furthermore, the majority of ASAP1 was found in high molecular weight protein complexes that eluted in fractions that contained little h-prune or Nm23-H1. This result has several putative explanations. First, concomitant over expression of Nm23-H1 and h-prune may result in these two proteins preferentially binding to each other and excluding ASAP1 from their complex. Second, the strength of the interaction between ASAP1 and Nm23-H1 or h-prune to ASAP1 may not be enough to keep the complex intact through the chromatographic separation. As the lysis and buffer conditions used for the co-immunoprecipitation experiments are different to those required for the size exclusion chromatography, this might lead to contrasting results. Alternatively, the results may reflect that although ASAP1 can co-immunoprecipate with both h-prune and Nm23-H1, these interactions represent only a

small minority of ASAP1 protein complexes found in MDA MB 231 cells. Either way, the size exclusion chromatography results clearly show that virtually all mature ASAP1 protein is present in high molecular weight complexes in MDA MB 231 cells, reflecting the multidomain nature of the protein and its ability to interact with a wide variety of other proteins. In further work, size exclusion chromatography will also be used to investigate whether SLK co-elutes with ASAP1-containing protein complexes.

5.7 Conclusions

In my thesis work I have substantiated the notion that ASAP1 regulates EGF internalization and cell motility, processes that likely underlie the ability of ASAP1 to promote metastasis formation. I have also confirmed that the SH3 binding domain of ASAP1 is important for its ability to promote cell motility, and have identified a number of new SH3 domain-containing proteins that interact with ASAP1, including SLK whose interaction with ASAP1 I could confirm using co-immunoprecipitation. Overall, my studies showed that three interacting partners of ASAP1, namely Nm23-H1, h-prune and SLK do not play fundamental roles in regulating the motility-promoting activity of ASAP1, and therefore probably also do not affect its ability to induce metastasis formation *in vivo*. I was also unable to find any substantial evidence to suggest that Nm23-H1 and h-prune modulate ASAP1-dependent EGF internalization. Together with the analysis of ASAP1-containing protein complexes using size exclusion chromatography, these data suggest that Nm23-H1 and h-prune probably do not contribute to any significant extent to ASAP1-dependent EGF internalization and cell motility. Future work will capitalize on the availability of wild type and ASAP1 knockout MEFs to substantiate these preliminary conclusions. Further analysis of other possible interaction partners, particularly those that emerged from the SH3 domain screening I undertook, should shed light on the proteins that regulate the motility-promoting activity of ASAP1 and its role in EGF internalization.

BIBLIOGRAPHY

Aaronson, S.A. (1991). Growth factors and cancer. Science 254, 1146-1153.

Aktary, Z., Chapman, K., Lam, L., Lo, A., Ji, C., Graham, K., Cook, L., Li, L., Mackey, J.R., and Pasdar, M. (2010). Plakoglobin interacts with and increases the protein levels of metastasis suppressor Nm23-H2 and regulates the expression of Nm23-H1. Oncogene 29, 2118-2129.

Allan, A.L., Vantyghem, S.A., Tuck, A.B., and Chambers, A.F. (2006). Tumor dormancy and cancer stem cells: implications for the biology and treatment of breast cancer metastasis. Breast Dis 26, 87-98.

Almog, N. (2010). Molecular mechanisms underlying tumor dormancy. Cancer Lett. 294, 139-146.

Anderson, K.I., Wang, Y.L., and Small, J.V. (1996). Coordination of protrusion and translocation of the keratocyte involves rolling of the cell body. J. Cell Biol. 134, 1209-1218.

Baeriswyl, V., and Christofori, G. (2009). The angiogenic switch in carcinogenesis. Semin. Cancer Biol. 19, 329-337.

Balch, W.E., Dunphy, W.G., Braell, W.A., and Rothman, J.E. (1984). Reconstitution of the transport of protein between successive compartments of the Golgi measured by the coupled incorporation of N-acetylglucosamine. Cell 39, 405-416.

Balch, W.E., Glick, B.S., and Rothman, J.E. (1984). Sequential intermediates in the pathway of intercompartmental transport in a cell-free system. Cell 39, 525-536.

Bergers, G., and Benjamin, L.E. (2003). Tumorigenesis and the angiogenic switch. Nat Rev Cancer 3, 401-410.

Bernards, A., and Settleman, J. (2004). GAP control: regulating the regulators of small GTPases. Trends Cell Biol. 14, 377-385.

Bharti, S., Inoue, H., Bharti, K., Hirsch, D.S., Nie, Z., Yoon, H., Artym, V., Yamada, K.M., Mueller, S.C., Barr, V.A., and Randazzo, P.A. (2007). Src-dependent phosphorylation of ASAP1 regulates podosomes. Mol. Cell. Biol. 27, 8271-8283.

Biggs, J., Hersperger, E., Steeg, P.S., Liotta, L.A., and Shearn, A. (1990). A Drosophila gene that is homologous to a mammalian gene associated with tumor metastasis codes for a nucleoside diphosphate kinase. Cell 63, 933-940.

Biswas, S.K., Sica, A., and Lewis, C.E. (2008). Plasticity of macrophage function during tumor progression: regulation by distinct molecular mechanisms. J. Immunol. 180, 2011-2017.

Boissan, M., Dabernat., S, Peuchant, E., Schlattner, U., Lascu, I, Lacombe, ML. (2009). The mammalian NM23/NDPK family: from metastasis control to cilia movement. Mol Cell Biochem 329, 51-62

Bonifacino, J.S., and Glick, B.S. (2004). The mechanisms of vesicle budding and fusion. Cell 116, 153-166.

Boulay, P., Schlienger, S., Lewis-Saravalli, S., Vitale, N., Ferbeyre, G., and Claing, A. (2011). ARF1 controls proliferation of breast cancer cells by regulating the retinoblastoma protein. Oncogene 30, 3846-3861.

Boulay, P.L., Cotton, M., Melançon, P., and Claing, A. (2008). ADP-ribosylation factor 1 controls the activation of the phosphatidylinositol 3-kinase pathway to regulate epidermal growth factor-dependent growth and migration of breast cancer cells. J Biol Chem 283:36425–36434

Bowden, E.T., Barth, M., Thomas, D., Glazer, R.I., and Mueller, S.C. (1999). An invasion-related complex of cortactin, paxillin and PKCmu associates with invadopodia at sites of extracellular matrix degradation. Oncogene 18, 4440-4449.

Brabletz, T., Jung, A., Spaderna, S., Hlubek, F., and Kirchner, T. (2005). Opinion: migrating cancer stem cells - an integrated concept of malignant tumour progression. Nat Rev Cancer 5, 744-749.

Brazil, D.P., and Hemmings, B.A. (2001). Ten years of protein kinase B signalling: a hard Akt to follow. Trends Biochem. Sci. 26, 657-664.

Bremm, A., Walch, A., Fuchs, M., Mages J., Duyster J., Keller G., Hermannstädter C., Becker K., Rauser S., Langer R., Hann von Weyhern C., Höfler H. and Luber B (2008). Enhanced Activation of Epidermal Growth Factor Receptor Caused by Tumor-Derived E-Cadherin Mutations. Cancer Res 68,707-714.

Broussard, J.A., Webb, D.J., and Kaverina, I. (2008). Asymmetric focal adhesion disassembly in motile cells. Curr. Opin. Cell Biol. 20, 85-90.

Brown, M.T., Andrade, J., Radhakrishna, H., Donaldson, J.G., Cooper, J.A., and Randazzo, P.A. (1998). ASAP1, a phospholipid-dependent arf GTPase-activating protein that associates with and is phosphorylated by Src. Mol. Cell. Biol. 18, 7038-7051.

Buccione, R., Orth, J.D., and Mcniven, M.A. (2004). Foot and mouth: podosomes, invadopodia and circular dorsal ruffles. Nat. Rev. Mol. Cell Biol. 5, 647-657.

Cairns, R.A., Harris, I.S., and Mak, T.W. (2011). Regulation of cancer cell metabolism. Nat Rev Cancer 11, 85-95.

Calle, Y., Carragher, N.O., Thrasher, A.J., and Jones, G.E. (2006). Inhibition of calpain stabilises podosomes and impairs dendritic cell motility. J. Cell. Sci. 119, 2375-2385.

Che, M.M., Boja, E.S., Yoon, H., Gruschus, J., Jaffe, H., Stauffer, S., Schuck, P., Fales, H.M., and Randazzo, P.A. (2005). Regulation of ASAP1 by phospholipids is dependent on the interface between the PH and Arf GAP domains. Cell. Signal. 17, 1276-1288. Cherfils, J., and Chardin, P. (1999). GEFs: structural basis for their activation of small GTP-binding proteins. Trends Biochem. Sci. 24, 306-311.

Christofori, G. (2006). New signals from the invasive front. Nature 441, 444-450.

Coghlin, C., and Murray, G.I. (2010). Current and emerging concepts in tumour metastasis. J. Pathol. 222, 1-15.

Colicelli, J. (2004). Human RAS superfamily proteins and related GTPases. Science's STKE 2004, RE13.

Colotta, F., Allavena, P., Sica, A., Garlanda, C., and Mantovani, A. (2009). Cancer-related inflammation, the seventh hallmark of cancer: links to genetic instability. Carcinogenesis 30, 1073-1081.

Cotton, M., and Claing, A. (2009). G protein-coupled receptors stimulation and the control of cell migration. Cell. Signal. 21, 1045-1053.

Cougoule, C., Cabec, V.L., Poincloux, R., Saati, T.A., Mege, J., Tabouret, G., Lowell, C.A., Laviolette-Malirat, N., and Maridonneau-Parini, I. (2010). Three-dimensional migration of macrophages requires Hck for podosome organization and extracellular matrix proteolysis. Blood 115, 1444-1452.

Cristofano, A.D., and Pandolfi, P.P. (2000). The multiple roles of PTEN in tumor suppression. Cell 100, 387-390.

Cully, M., You, H., Levine, A.J., and Mak, T.W. (2006). Beyond PTEN mutations: the PI3K pathway as an integrator of multiple inputs during tumorigenesis. Nat Rev Cancer 6, 184-192.

Curtis, C.D., Likhite, V.S., McLeod, I.X., Yates, J.R., and Nardulli, A.M. (2007). Interaction of the tumor metastasis suppressor nonmetastatic protein 23 homologue H1 and estrogen receptor alpha alters estrogen-responsive gene expression. Cancer Res. 67, 10600-10607.

D'Angelo, A., Garzia, L., André, A., Carotenuto, P., Aglio, V., Guardiola, O., Arrigoni, G., Cossu, A., Palmieri, G., Aravind, L., and Zollo, M. (2004). Prune cAMP phosphodiesterase binds nm23-H1 and promotes cancer metastasis. Cancer Cell 5, 137-149.

D'souza-Schorey, C., and Chavrier, P. (2006). ARF proteins: roles in membrane traffic and beyond. Nat. Rev. Mol. Cell Biol. 7, 347-358.

Dammai, V., Adryan, B., Lavenburg, K.R., and Hsu, T. (2003). Drosophila awd, the homolog of human nm23, regulates FGF receptor levels and functions synergistically with shi/dynamin during tracheal development. Genes & Development 17, 2812-2824.

De Palma, M.D., Venneri, M.A., Galli, R., Sergi, L.S., Politi, L.S., Sampaolesi, M., and Naldini, L. (2005). Tie2 identifies a hematopoietic lineage of proangiogenic monocytes required for tumor vessel formation and a mesenchymal population of pericyte progenitors. Cancer Cell 8, 211-226.

Donaldson, J.G. (2003). Multiple roles for Arf6: sorting, structuring, and signaling at the plasma membrane. J. Biol. Chem. 278, 41573-41576.

Downward, J. (2003). Targeting RAS signalling pathways in cancer therapy. Nat Rev Cancer 3, 11-22.

Duan, L., Miura, Y., Dimri, M., Majumder, B., Dodge, I.L, Reddi, A.L., Ghosh, A., Fernandes, N., Zhou, P., Mullane-Robinson, K., Rao, N., Donoghue, S., Rogers, R.A., Bowtell, D., Naramura, M., Gu, H., Band, V., and Band, H. (2003). Cbl-mediated

Ubiquitinylation Is Required for Lysosomal Sorting of Epidermal Growth Factor Receptor but Is Dispensable for Endocytosis. J Biol Chem 278, 28950-28960.

East, M.P., and Kahn, R.A. (2011). Models for the functions of Arf GAPs. Semin. Cell Dev. Biol. 22, 3-9.

Ehlers, J.P., Worley, L., Onken, M.D., and Harbour, J.W. (2005). DDEF1 is located in an amplified region of chromosome 8q and is overexpressed in uveal melanoma. Clin. Cancer Res. 11, 3609-3613.

Fan, Z., Beresford, P.J., Oh, D.Y., Zhang, D., and Lieberman, J. (2003). Tumor suppressor NM23-H1 is a granzyme A-activated DNase during CTL-mediated apoptosis, and the nucleosome assembly protein SET is its inhibitor. Cell 112, 659-672.

Fantl, V., Smith, R., Brookes, S., Dickson, C., and Peters, G. (1993). Chromosome 11q13 abnormalities in human breast cancer. Cancer Surv. 18, 77-94.

Ferguson, S.M., and Camilli, P.D. (2012). Dynamin, a membrane-remodelling GTPase. Nat. Rev. Mol. Cell Biol. 13, 75-88.

Fernandez-Medarde, A., and Santos, E. (2011). Ras in cancer and developmental diseases. Genes {\&} Cancer 2, 344-358.

Fidler, I.J. (1970). Metastasis: quantitative analysis of distribution and fate of tumor embolilabeled with 125 I-5-iodo-2'-deoxyuridine. J. Natl. Cancer Inst. 45, 773-782.

Fidler, I.J., and Kripke, M.L. (1977). Metastasis results from preexisting variant cells within a malignant tumor. Science 197, 893-895.

Fogelgren, B., Polgár, N., Szauter, K.M., Ujfaludi, Z., Laczkó, R., Fong, K.S.K., and Csiszar, K. (2005). Cellular fibronectin binds to lysyl oxidase with high affinity and is critical for its proteolytic activation. J. Biol. Chem. 280, 24690-24697.

Folkman, J. (1971). Tumor angiogenesis: therapeutic implications. N. Engl. J. Med. 285, 1182-1186.

Forus, A., D'angelo, A., Henriksen, J., Merla, G., Maelandsmo, G.M., Fl\orenes, V.A., Olivieri, S., Bjerkehagen, B., Meza-Zepeda, L.A., Blanco, F.d.V., et al. (2001). Amplification and overexpression of PRUNE in human sarcomas and breast carcinomas-a possible mechanism for altering the nm23-H1 activity. Oncogene 20, 6881-6890.

Fournier, H., Dupé-Manet, S., Bouvard, D., Lacombe, M., Marie, C., Block, M.R., and Albiges-Rizo, C. (2002). Integrin cytoplasmic domain-associated protein 1alpha (ICAP-1alpha) interacts directly with the metastasis suppressor nm23-H2, and both proteins are targeted to newly formed cell adhesion sites upon integrin engagement. J. Biol. Chem. 277, 20895-20902.

Fridman, J.S., and Lowe, S.W. (2003). Control of apoptosis by p53. Oncogene 22, 9030-9040.

Friedl, P., and Gilmour, D. (2009). Collective cell migration in morphogenesis, regeneration and cancer. Nat. Rev. Mol. Cell Biol. 10, 445-457.

Friedl, P., and Wolf, K. (2003). Tumour-cell invasion and migration: diversity and escape mechanisms. Nat Rev Cancer 3, 362-374.

Furman, C., Short, S.M., Subramanian, R.R., Zetter, B.R., and Roberts, T.M. (2002). DEF-1/ASAP1 is a GTPase-activating protein (GAP) for ARF1 that enhances cell motility through a GAP-dependent mechanism. J. Biol. Chem. 277, 7962-7969.

Garzia, L., D'angelo, A., Amoresano, A., Knauer, S.K., Cirulli, C., Campanella, C., Stauber, R.H., Steegborn, C., Iolascon, A., and Zollo, M. (2008). Phosphorylation of nm23-H1 by CKI induces its complex formation with h-prune and promotes cell motility. Oncogene 27, 1853-1864.

Geiger, B., Spatz, J.P., and Bershadsky, A.D. (2009). Environmental sensing through focal adhesions. Nat. Rev. Mol. Cell Biol. 10, 21-33.

Giaccone, G., and Rodriguez, J.A. (2005). EGFR inhibitors: what have we learned from the treatment of lung cancer? Nat Clin Prac Oncol 2, 554-561.

Gialeli, C., Theocharis, A.D. and Karamanos, N.K. (2011). Roles of matrix metalloproteinases in cancer progression and their pharmacological targeting. FEBS Jan;278(1):16-27

Gillingham, A.K., and Munro, S. (2007). The small G proteins of the Arf family and their regulators. Annu. Rev. Cell Dev. Biol. 23, 579-611.

Goldberg, J. (1999). Structural and functional analysis of the ARF1-ARFGAP complex reveals a role for coatomer in GTP hydrolysis. Cell 96, 893-902.

Gozuacik, D., and Kimchi, A. (2004). Autophagy as a cell death and tumor suppressor mechanism. Oncogene 23, 2891-2906.

Gschwind, A., Fischer, O.M., and Ullrich, A. (2004). The discovery of receptor tyrosine kinases: targets for cancer therapy. Nat Rev Cancer 4, 361-370.

Haglund, K., Shimokawa, N., Szymkiewicz, I., and Dikic, I. (2002). Cbl-directed monoubiquitination of CIN85 is involved in regulation of ligand-induced degradation of EGF receptors. Proc. Natl. Acad. Sci. USA 99, 12191-12196.

Hahn, W.C., and Weinberg, R.A. (2002). Rules for making human tumor cells. N. Engl. J. Med. 347, 1593-1603.

Hammerman, P.S., Jänne, P.A., and Johnson, B.E. (2009). Resistance to Epidermal Growth Factor Receptor Tyrosine Kinase Inhibitors in Non-Small Cell Lung Cancer. Clin. Cancer Res. 15, 7502-7509.

Hanahan, D., and Weinberg, R.A. (2011). Hallmarks of cancer: the next generation. Cell 144, 646-674.

Hartsough, M.T., Morrison, D.K., Salerno, M., Palmieri, D., Ouatas, T., Mair, M., Patrick, J., and Steeg, P.S. (2002). Nm23-H1 metastasis suppressor phosphorylation of kinase suppressor of Ras via a histidine protein kinase pathway. J. Biol. Chem. 277, 32389-32399.

Hashimoto, S., Hashimoto, A., Yamada, A., Onodera, Y., and Sabe, H. (2005). Assays and properties of the ArfGAPs, AMAP1 and AMAP2, in Arf6 function.

Hayakawa, Y., and Smyth, M.J. (2006). Innate immune recognition and suppression of tumors. Adv. Cancer Res. 95, 293-322.

Hinshaw, J.E. (2000). Dynamin and its role in membrane fission. Annu. Rev. Cell Dev. Biol. 16, 483-519.

Horwitz, R., and Webb, D. (2003). Cell migration. Curr. Biol. 13, R756-9.

Huang, F., Goh, L.K., and Sorkin, A. (2007). EGF receptor ubiquitination is not necessary for its internalization. Proc. Natl. Acad. Sci. USA 104, 16904-16909.

Inoue, H., Ha, V.L., Prekeris, R., and Randazzo, P.A. (2008). Arf GTPase-activating protein ASAP1 interacts with Rab11 effector FIP3 and regulates pericentrosomal localization of transferrin receptor-positive recycling endosome.Mol Biol Cell 19:4224–4237

Iwashita, S., Fujii, M., Mukai, H., Ono, Y., and Miyamoto, M. (2004). Lbc proto-oncogene product binds to and could be negatively regulated by metastasis suppressor nm23-H2. Biochem. Biophys. Res. Commun. 320, 1063-1068.

Jackson, A.L., and Loeb, L.A. (1998). The mutation rate and cancer. Genetics 148, 1483-1490.

Jay, P.Y., Pham, P.A., Wong, S.A., and Elson, E.L. (1995). A mechanical function of myosin II in cell motility. J. Cell. Sci. 108 (Pt 1), 387-393.

Jemal, A., Siegel, R., Ward, E., Hao, Y., Xu, J., Murray, T., and Thun, M.J. (2008). Cancer statistics, 2008. CA Cancer. J. Clin. 58, 71-96.

Jian, X., Brown, P., Schuck, P., Gruschus, J.M., Balbo, A., Hinshaw, J.E., and Randazzo, P.A. (2009). Autoinhibition of Arf GTPase-activating protein activity by the BAR domain in ASAP1. J. Biol. Chem. 284, 1652-1663.

Jones, R.G., and Thompson, C.B. (2009). Tumor suppressors and cell metabolism: a recipe for cancer growth. Genes & Development 23, 537-548.

Joyce, J.A., and Pollard, J.W. (2009). Microenvironmental regulation of metastasis. Nat Rev Cancer 9, 239-252.

Kafri, R., Springer, M., and Pilpel, Y. (2009). Genetic redundancy: new tricks for old genes. Cell 136:389–392

Kahn, R.A., and Gilman, A.G. (1984). Purification of a protein cofactor required for ADP-ribosylation of the stimulatory regulatory component of adenylate cyclase by cholera toxin. J. Biol. Chem. 259, 6228-6234.

Kaplan, R.N., Riba, R.D., Zacharoulis, S., Bramley, A.H., Vincent, L., Costa, C., Macdonald, D.D., Jin, D.K., Shido, K., Kerns, S.A., et al. (2005). VEGFR1-positive haematopoietic bone marrow progenitors initiate the pre-metastatic niche. Nature 438, 820-827.

Karlseder, J., Zeillinger, R., Schneeberger, C., Czerwenka, K., Speiser, P., Kubista, E., Birnbaum, D., Gaudray, P., and Theillet, C. (1994). Patterns of DNA amplification at band q13 of chromosome 11 in human breast cancer. Genes Chromosomes Cancer 9, 42-48.

Kerbel, R.S. (2008). Tumor angiogenesis. N. Engl. J. Med. 358, 2039-2049.

Kessenbrock, K., Plaks, V., and Werb, Z. (2010). Matrix metalloproteinases: regulators of the tumor microenvironment. Cell 141, 52-67.

Klein, C.A. (2009). Parallel progression of primary tumours and metastases. Nat Rev Cancer 9, 302-312.

Klionsky, D.J., and Emr, S.D. (2000). Autophagy as a regulated pathway of cellular degradation. Science 290, 1717-1721.

Kobayashi, T., Hino, S., Oue, N., Asahara, T., Zollo, M., Yasui, W., and Kikuchi, A. (2006). Glycogen synthase kinase 3 and h-prune regulate cell migration by modulating focal adhesions. Mol. Cell. Biol. 26, 898-911.

Kölsch, V., Charest, P.G., and Firtel, R.A. (2008). The regulation of cell motility and chemotaxis by phospholipid signaling. J. Cell. Sci. 121, 551-559.

Kowanetz, K., Husnjak, K., H\oller, D., Kowanetz, M., Soubeyran, P., Hirsch, D., Schmidt, M.H.H., Pavelic, K., Camilli, P.D., Randazzo, P.A., and Dikic, I. (2004). CIN85 associates with multiple effectors controlling intracellular trafficking of epidermal growth factor receptors. Mol. Biol. Cell 15, 3155-3166.

Krishnan, K.S., Rikhy, R., Rao, S., Shivalkar, M., Mosko, M., Narayanan, R., Etter, P., Estes, P.S., and Ramaswami, M. (2001). Nucleoside diphosphate kinase, a source of GTP, is required for dynamin-dependent synaptic vesicle recycling. Neuron 30, 197-210.

Kruljac-Letunic, A., Moelleken, J., Kallin, A., Wieland, F., and Blaukat, A. (2003). The tyrosine kinase Pyk2 regulates Arf1 activity by phosphorylation and inhibition of the Arf-GTPase-activating protein ASAP1. J. Biol. Chem. 278, 29560-29570.

Lacombe, M.L., Milon, L., Munier, A., Mehus, J.G., and Lambeth, D.O. (2000). The human Nm23/nucleoside diphosphate kinases. J. Bioenerg. Biomembr. 32, 247-258.

Levine, A.J. (1997). p53, the cellular gatekeeper for growth and division. Cell 88, 323-331.

Lidke, D.S., Nagy, P., Heintzmann, R., Arndt-Jovin, D.J., Post, J.N., Grecco, H.E., Jares-Erijman,. E.A., and Jovin, T.M. (2004). Quantum dot ligands provide new insights into erbB/HER receptor-mediated signal transduction. Nat Biotechnol 22:198–203.

Lin, D., Watahiki, A., Bayani, J., Zhang, F., Liu, L., Ling, V., Sadar, M.D., English, J., Fazli, L., So, A., et al. (2008). ASAP1, a gene at 8q24, is associated with prostate cancer metastasis. Cancer Res. 68, 4352-4359.

Liu, Y., Loijens, J.C., Martin, K.H., Karginov, A.V., and Parsons, J.T. (2002). The association of ASAP1, an ADP ribosylation factor-GTPase activating protein, with focal adhesion kinase contributes to the process of focal adhesion assembly. Mol Biol Cell 13:2147–2156

Liu, Y., Yerushalmi, G.M., Grigera, P.R., and Parsons, J.T. (2005). Mislocalization or reduced expression of Arf GTPase-activating protein ASAP1 inhibits cell spreading and DNA: an migration by influencing Arf1 GTPase cycling. J. Biol. Chem. 280, 8884-8892.

Lombardi, D., Sacchi, A., D'Agostino, G., and Tibursi, G. (1995). The association of the Nm23-H1 protein and beta-tubulin correlates with cell differentiation. Exp. Cell Res. 217, 267-271.

Lukanidin, E., and Sleeman, J.P. (2012). Building the niche: The role of the S100 proteins in metastatic growth. Semin. Cancer Biol. 22, 216-225.

Lynch, D.K., Winata, S.C., Lyons, R.J., Hughes, W.E., Lehrbach, G.M., Wasinger, V., Corthals, G., Cordwell, S., and Daly, R.J. (2003). A Cortactin-CD2-associated protein (CD2AP) complex provides a novel link between epidermal growth factor receptor endocytosis and the actin cytoskeleton. J. Biol. Chem. 278, 21805-21813.

Ma, D., Mccorkle, J.R., and Kaetzel, D.M. (2004). The metastasis suppressor NM23-H1 possesses 3'-5' exonuclease activity. J. Biol. Chem. 279, 18073-18084.

MacDonald, N.J., Rosa, A.D.l., Benedict, M.A., Freije, J.M., Krutsch, H., and Steeg, P.S. (1993). A serine phosphorylation of Nm23, and not its nucleoside diphosphate kinase activity, correlates with suppression of tumor metastatic potential. J. Biol. Chem. 268, 25780-25789.

Mandiyan, V., Andreev, J., Schlessinger, J., and Hubbard, S.R. (1999). Crystal structure of the ARF-GAP domain and ankyrin repeats of PYK2-associated protein beta. EMBO J. 18, 6890-6898.

Mani, S.A., Guo, W., Liao, M., Eaton, E.N., Ayyanan, A., Zhou, A.Y., Brooks, M., Reinhard, F., Zhang, C.C., Shipitsin, M., et al. (2008). The epithelial-mesenchymal transition generates cells with properties of stem cells. Cell 133, 704-715.

Marino, N., Marshall, J., and Steeg, P.S. (2011). Protein-protein interactions: a mechanism regulating the anti-metastatic properties of Nm23-H1. Naunyn Schmiedebergs Arch. Pharmacol. 384, 351-362.

Matsuya, M., Sasaki, H., Aoto, H., Mitaka, T., Nagura, K., Ohba, T., Ishino, M., Takahashi, S., Suzuki, R., and Sasaki T. (1998). Cell adhesion kinase beta forms a complex with a new member, Hic-5, of proteins localized at focal adhesions. J Biol Chem 273:1003–1014.

May, P., and May, E. (1999). Twenty years of p53 research: structural and functional aspects of the p53 protein. Oncogene 18, 7621-7636.

Mclean, G.W., Carragher, N.O., Avizienyte, E., Evans, J., Brunton, V.G., and Frame, M.C. (2005). The role of focal-adhesion kinase in cancer - a new therapeutic opportunity. Nat Rev Cancer 5, 505-515.

Miyamoto, S., Teramoto, H., Coso, O.A., Gutkind, J.S., Burbelo, P.D., Akiyama, S.K., and Yamada, K.M. (1995). Integrin function: molecular hierarchies of cytoskeletal and signaling molecules. J. Cell Biol. 131, 791-805.

Morishige, M., Hashimoto, S., Ogawa, E., Toda, Y., Kotani, H., Hirose, M., Wei, S., Hashimoto, A., Yamada, A., Yano, H., et al. (2008). GEP100 links epidermal growth factor receptor signalling to Arf6 activation to induce breast cancer invasion. Nat. Cell Biol. 10, 85-92.

Muller, P.A.J., Caswell, P.T., Doyle, B., Iwanicki, M.P., Tan, E.H., Karim, S., Lukashchuk, N., Gillespie, D.A., Ludwig, R.L., Gosselin, P., et al. (2009). Mutant p53 drives invasion by promoting integrin recycling. Cell 139, 1327-1341.

Müller, T., Stein, U., Poletti, A., Garzia, L., Rothley, M., Plaumann, D., Thiele, W., Bauer, M., Galasso, A., Schlag, P., et al. (2010). ASAP1 promotes tumor cell motility and invasiveness, stimulates metastasis formation in vivo, and correlates with poor survival in colorectal cancer patients. Oncogene 29, 2393-2403.

Mūller, W., Schneiders, A., Hommel, G., and Gabbert, H.E. (1998). Expression of nm23 in gastric carcinoma: association with tumor progression and poor prognosis. Cancer 83, 2481-2487.

Murakami, M., Meneses, P.I., Knight, J.S., Lan, K., Kaul, R., Verma, S.C., and Robertson, E.S. (2008). Nm23-H1 modulates the activity of the guanine exchange factor Dbl-1. Int. J. Cancer 123, 500-510.

Murakami, M., Meneses, P.I., Lan, K., and Robertson, E.S. (2008). The suppressor of metastasis Nm23-H1 interacts with the Cdc42 Rho family member and the pleckstrin homology domain of oncoprotein Dbl-1 to suppress cell migration. Cancer Biol Ther 7, 677-688.

Murdoch, C., Muthana, M., Coffelt, S.B., and Lewis, C.E. (2008). The role of myeloid cells in the promotion of tumour angiogenesis. Nat Rev Cancer 8, 618-631.

Murphy, D.A., and Courtneidge, S.A. (2011). The 'ins' and 'outs' of podosomes and invadopodia: characteristics, formation and function. Nat. Rev. Mol. Cell Biol. 12, 413-426.

Murphy, G., and Nagase, H. (2008). Progress in matrix metalloproteinase research. Mol. Aspects Med. 29, 290-308.

Nam, J., Onodera, Y., Mazaki, Y., Miyoshi, H., Hashimoto, S., and Sabe, H. (2007). CIN85, a Cbl-interacting protein, is a component of AMAP1-mediated breast cancer invasion machinery. EMBO J. 26, 647-656.

Nestl, A., Stein, O.D.V., Zatloukal, K., Thies, W.G., Herrlich, P., Hofmann, M., and Sleeman, J.P. (2001). Gene expression patterns associated with the metastatic phenotype in rodent and human tumors. Cancer Res. 61, 1569-1577.

Nie, Z., and Randazzo, P.A. (2006). Arf GAPs and membrane traffic. J. Cell. Sci. 119, 1203-1211.

Nie, Z., Hirsch, D.S., Luo, R., Jian, X., Stauffer, S., Cremesti, A., Andrade, J., Lebowitz, J., Marino, M., Ahvazi, B., Hinshaw, J.E., and Randazzo, P.A. (2006). A BAR domain in the N terminus of the Arf GAP ASAP1 affects membrane structure and trafficking of epidermal growth factor receptor. Curr. Biol. 16, 130-139.

Oakes, P.W., Beckham, Y., Stricker, J., and Gardel, M.L. (2012). Tension is required but not sufficient for focal adhesion maturation without a stress fiber template. J. Cell Biol. 196, 363-374.

Oda, A., Wada, I., Miura, K., Okawa, K., Kadoya, T., Kato, T., Nishihara, H., Maeda, M., Tanaka, S., Nagashima, K., et al. (2003). CrkL directs ASAP1 to peripheral focal adhesions. J. Biol. Chem. 278, 6456-6460.

Onder, T.T., Gupta, P.B., Mani, S.A., Yang, J., Lander, E.S., and Weinberg, R.A. (2008). Loss of E-cadherin promotes metastasis via multiple downstream transcriptional pathways. (2008). Loss of E-cadherin promotes metastasis via multiple downstream transcriptional pathways. Cancer Research 68:3645-3654

Onodera, Y., Hashimoto, S., Hashimoto, A., Morishige, M., Mazaki, Y., Yamada, A., Ogawa, E., Adachi, M., Sakurai, T., Manabe, T., et al. (2005). Expression of AMAP1, an ArfGAP, provides novel targets to inhibit breast cancer invasive activities. EMBO J. 24, 963-973.

Orimo, A., Gupta, P.B., Sgroi, D.C., Arenzana-Seisdedos, F., Delaunay, T., Naeem, R., Carey, V.J., Richardson, A.L., and Weinberg, R.A. (2005). Stromal fibroblasts present in invasive human breast carcinomas promote tumor growth and angiogenesis through elevated SDF-1/CXCL12 secretion. Cell 121, 335-348.

Orth, J.D., Krueger, E. W., Weller, S.G., and McNiven M.A. (2006). A Novel Endocytic Mechanism of Epidermal Growth Factor Receptor Sequestration and Internalization. Cancer Res 66,3603-3610.

Otero, A.S. (1997). Copurification of vimentin, energy metabolism enzymes, and a MER5 homolog with nucleoside diphosphate kinase. Identification of tissue-specific interactions. J. Biol. Chem. 272, 14690-14694.

Otero, A.S. (2000). NM23/nucleoside diphosphate kinase and signal transduction. J. Bioenerg. Biomembr. 32, 269-275.

Otsuki, Y., Tanaka, M., Yoshii, S., Kawazoe, N., Nakaya, K., and Sugimura, H. (2001). Tumor metastasis suppressor nm23H1 regulates Rac1 GTPase by interaction with Tiam1. Proc. Natl. Acad. Sci. USA 98, 4385-4390.

Palacios, F., Schweitzer, J.K., Boshans, R.L., and D'souza-Schorey, C. (2002). ARF6-GTP recruits Nm23-H1 to facilitate dynamin-mediated endocytosis during adherens junctions disassembly. Nat. Cell Biol. 4, 929-936.

Palecek, S.P., Huttenlocher, A., Horwitz, A.F., and Lauffenburger, D.A. (1998). Physical and biochemical regulation of integrin release during rear detachment of migrating cells. J. Cell. Sci. 111 (Pt 7), 929-940.

Palmer, T.D., Ashby, W.J., Lewis, J.D., and Zijlstra, A. (2011). Targeting tumor cell motility to prevent metastasis. Adv. Drug Deliv. Rev. 63, 568-581.

Paravicini, G., Steinmayr, M., André, E., and Becker-André, M. (1996). The metastasis suppressor candidate nucleotide diphosphate kinase NM23 specifically interacts with members of the ROR/RZR nuclear orphan receptor subfamily. Biochem. Biophys. Res. Commun. 227, 82-87.

Parsons, J.T., Horwitz, A.R., and Schwartz, M.A. (2010). Cell adhesion: integrating cytoskeletal dynamics and cellular tension. Nat. Rev. Mol. Cell Biol. 11, 633-643.

Pasqualato, S., Renault, L., and Cherfils, J. (2002). Arf, Arl, Arp and Sar proteins: a family of GTP-binding proteins with a structural device for 'front-back' communication. EMBO 11:1035–1041

Peinado, H., Lavotshkin, S., and Lyden, D. (2011). The secreted factors responsible for pre-metastatic niche formation: Old sayings and new thoughts. Semin. Cancer Biol. 21, 139-146.

Peinado, H., Portillo, F., and Cano, A. (2004). Transcriptional regulation of cadherins during development and carcinogenesis. Int. J. Dev. Biol. 48, 365-375.

Pellegrin, S., and Mellor, H. (2007). Actin stress fibres. J. Cell. Sci. 120, 3491-3499.

206.

Peters, G., Fantl, V., Smith, R., Brookes, S., and Dickson, C. (1995). Chromosome 11q13 markers and D-type cyclins in breast cancer. Breast Cancer Res. Treat. 33, 125-135.

Petit, V., and Thiery, J.P. (2000). Focal adhesions: structure and dynamics. Biol. Cell. 92, 477-494.

Pinon, V.P., Millot, G., Munier, A., Vassy, J., Linares-Cruz, G., Capeau, J., Calvo, F., and Lacombe, M.L. (1999). Cytoskeletal association of the A and B nucleoside diphosphate kinases of interphasic but not mitotic human carcinoma cell lines: specific nuclear localization of the B subunit. Exp. Cell Res. 246, 355-367.

Psaila, B., and Lyden, D. (2009). The metastatic niche: adapting the foreign soil. Nat Rev Cancer 9, 285-293.

Randazzo, P.A., and Hirsch, D.S. (2004). Arf GAPs: multifunctional proteins that regulate membrane traffic and actin remodelling. Cell. Signal. 16, 401-413.

Randazzo, P.A., Andrade, J., Miura, K., Brown, M.T., Long, Y.Q., Stauffer, S., Roller, P., and Cooper, J.A. (2000). The Arf GTPase-activating protein ASAP1 regulates the actin cytoskeleton. Proc. Natl. Acad. Sci. USA 97, 4011-4016.

Randazzo, P.A., Inoue, H., and Bharti, S. (2007). Arf GAPs as regulators of the actin cytoskeleton. Biol. Cell. 99, 583-600.

Reymond, A., Volorio, S., Merla, G., Al-Maghtheh, M., Zuffardi, O., Bulfone, A., Ballabio, A., and Zollo, M. (1999). Evidence for interaction between human PRUNE and nm23-H1 NDPKinase. Oncogene 18, 7244-7252.

Roepstorff, K., Grøvdal, L., Grandal, M., Lerdrup, M., van Deurs, B. (2008). Endocytic downregulation of ErbB receptors: mechanisms and relevance in cancer. Histochem Cell Biol 129:563–578

Roovers, K., Wagner, S., Storbeck, C.J., O'Reilly, P., Lo, V., Northey, J.J., Chmielecki, J., Muller, W.J., Siegel, P.M., and Sabourin, L.A. (2009). The Ste20-like kinase SLK is required for ErbB2-driven breast cancer cell motility. Oncogene 28, 2839-2848.

Rottiers, P., Saltel, F., Daubon, T., Chaigne-Delalande, B., Tridon, V., Billottet, C., Reuzeau, E., and G\'enot, E. (2009). TGFbeta-induced endothelial podosomes mediate basement membrane collagen degradation in arterial vessels. J. Cell. Sci. 122, 4311-4318.

Roussos, E.T., Condeelis, J.S., and Patsialou, A. (2011). Chemotaxis in cancer. Nat Rev Cancer 11, 573-587.

Sabe, H., Onodera, Y., Mazaki, Y., and Hashimoto, S. (2006). ArfGAP family proteins in cell adhesion, migration and tumor invasion. Curr. Opin. Cell Biol. 18, 558-564.

Sabourin, L.A., Tamai, K., Seale, P., Wagner, J., and Rudnicki, M.A. (2000). Caspase 3 cleavage of the Ste20-related kinase SLK releases and activates an apoptosis-inducing kinase domain and an actin-disassembling region. Mol. Cell. Biol. 20, 684-696.

Schaller, M.D., and Parsons, J.T. (1994). Focal adhesion kinase and associated proteins. Curr. Opin. Cell Biol. 6, 705-710.

Schmidt-Glenewinkel, H., Reinz, E., Eils, R., and Nathan R Brady. (2009). Systems biological analysis of epidermal growth factor receptor internalization dynamics for altered receptor levels. J Biol Chem 284:17243–17252.

Schuuring, E., Verhoeven, E., Mooi, W.J., and Michalides, R.J. (1992). Identification and cloning of two overexpressed genes, U21B31/PRAD1 and EMS1, within the amplified chromosome 11q13 region in human carcinomas. Oncogene 7, 355-361.

Sheetz, M.P., Felsenfeld, D., Galbraith, C.G., and Choquet, D. (1999). Cell migration as a five-step cycle. Biochem. Soc. Symp. 65, 233-243.

Sherr, C.J., and McCormick, F. (2002). The RB and p53 pathways in cancer. Cancer Cell 2, 103-112.

Shiba, Y., and Randazzo, P.A. (2011). GEFH1 binds ASAP1 and regulates podosome formation. Biochem. Biophys. Res. Commun. 406, 574-579.

Sims, A.M., Shephard, N., Carter, K., Doan, T., Dowling, A., Duncan, E.L., Eisman, J., Jones, G., Nicholson, G., Prince, R., et al. (2008). Genetic analyses in a sample of individuals with high or low BMD shows association with multiple Wnt pathway genes. J. Bone Miner. Res. 23, 499-506.

Sleeman, J.P., Christofori, G., Fodde, R., Collard, J.G., Berx, G., Decraene, C., and R\uegg, C. (2012). Concepts of metastasis in flux: The stromal progression model. Semin. Cancer Biol. 22, 174-186.

Sleeman, J.P., Nazarenko, I., and Thiele, W. (2011). Do all roads lead to Rome? Routes to metastasis development. Int. J. Cancer 128, 2511-2526.

Solinas, G., Germano, G., Mantovani, A., and Allavena, P. (2009). Tumor-associated macrophages (TAM) as major players of the cancer-related inflammation. J. Leukoc. Biol. 86, 1065-1073.

Steeg, P.S., Bevilacqua, G., Kopper, L., Thorgeirsson, U.P., Talmadge, J.E., Liotta, L.A., and Sobel, M.E. (1988). Evidence for a novel gene associated with low tumor metastatic potential. J. Natl. Cancer Inst. 80, 200-204.

Steeg, P.S., Horak, C.E., and Miller, K.D. (2008). Clinical-translational approaches to the Nm23-H1 metastasis suppressor. Clin Cancer Res 14:5006–5012

Stossel, T.P. (1993). On the crawling of animal cells. Science 260, 1086-1094.

Stylli, S.S., Kaye, A.H., and Lock, P. (2008). Invadopodia: at the cutting edge of tumour invasion. J. Clin. Neurosci. 15, 725-737.

Subramanian, C., Cotter, M.A., and Robertson, E.S. (2001). Epstein-Barr virus nuclear protein EBNA-3C interacts with the human metastatic suppressor Nm23-H1: a molecular link to cancer metastasis. Nat. Med. 7, 350-355.

Talmadge, J.E., and Fidler, I.J. (2010). AACR centennial series: the biology of cancer metastasis: historical perspective. Cancer Res. 70, 5649-5669.

Tammenkoski, M., Koivula, K., Cusanelli, E., Zollo, M., Steegborn, C., Baykov, A.A., and Lahti, R. (2008). Human metastasis regulator protein H-prune is a short-chain exopolyphosphatase. Biochemistry (N. Y.) 47, 9707-9713.

Tarone, G., Cirillo, D., Giancotti, F.G., Comoglio, P.M., and Marchisio, P.C. (1985). Rous sarcoma virus-transformed fibroblasts adhere primarily at discrete protrusions of the ventral membrane called podosomes. Exp. Cell Res. 159, 141-157.

Thiery, J.P., and Sleeman, J.P. (2006). Complex networks orchestrate epithelial-mesenchymal transitions. Nat. Rev. Mol. Cell Biol. 7, 131-142.

Thompson, E.W., Newgreen, D.F., and Tarin, D. (2005). Carcinoma invasion and metastasis: a role for epithelial-mesenchymal transition? Cancer Res. 65, 5991-5; dsusson 5995.

Timmons, L., and Shearn, A. (1996). Germline transformation using a prune cDNA rescues prune/killer of prune lethality and the prune eye color phenotype in Drosophila. Genetics 144, 1589-1600.

Tokarska-Schlattner, M., Boissan, M., Munier, A., Borot, C., Mailleau, C., Speer, O., Schlattner, U., and Lacombe, M. (2008). The nucleoside diphosphate kinase D (NM23-H4) binds the inner mitochondrial membrane with high affinity to cardiolipin and couples nucleotide transfer with respiration. J. Biol. Chem. 283, 26198-26207.

Toyokuni, S., Okamoto, K., Yodoi, J., and Hiai, H. (1995). Persistent oxidative stress in cancer. FEBS Lett. 358, 1-3.

Tseng, Y.H., Vicent, D., Zhu, J., Niu, Y., Adeyinka, A., Moyers, J.S., Watson, P.H., and Kahn, C.R. (2001). Regulation of growth and tumorigenicity of breast cancer cells by the low molecular weight GTPase Rad and nm23. Cancer Res. 61, 2071-2079.

Tsuiki, H., Nitta, M., Furuya, A., Hanai, N., Fujiwara, T., Inagaki, M., Kochi, M., Ushio, Y., Saya, H., and Nakamura, H. (1999). A novel human nucleoside diphosphate (NDP) kinase, Nm23-H6, localizes in mitochondria and affects cytokinesis. J. Cell. Biochem. 76, 254-269.

Turner, C.E., West, K.A., and Brown, M.C. (2001). Paxillin-ARF GAP signaling and the cytoskeleton. Curr. Opin. Cell Biol. 13, 593-599.

Uhr, J.W., and Pantel, K. (2011). Controversies in clinical cancer dormancy. Proc. Natl. Acad. Sci. USA 108, 12396-12400.

Verkhovsky, A.B., Svitkina, T.M., and Borisy, G.G. (1999). Self-polarization and directional motility of cytoplasm. Curr. Biol. 9, 11-20.

Wagner, P.D., and Vu, N.D. (1995). Phosphorylation of ATP-citrate lyase by nucleoside diphosphate kinase. J. Biol. Chem. 270, 21758-21764.

Wagner, P.D., and Vu, N.D. (2000). Histidine to aspartate phosphotransferase activity of nm23 proteins: phosphorylation of aldolase C on Asp-319. Biochem. J. 346 Pt 3, 623-630.

Wagner, S., Flood, T.A., O'Reilly, P., Hume, K., and Sabourin, L.A. (2002). Association of the Ste20-like kinase (SLK) with the microtubule. Role in Rac1-mediated regulation of actin dynamics during cell adhesion and spreading. J. Biol. Chem. 277, 37685-37692.

Wagner, S., Storbeck, C.J., Roovers, K., Chaar, Z.Y., Kolodziej, P., Mckay, M., and Sabourin, L.A. (2008). FAK/src-family dependent activation of the Ste20-like kinase SLK is required for microtubule-dependent focal adhesion turnover and cell migration. PLoS ONE 3, e1868.

Wagner, S.M., and Sabourin, L.A. (2009). A novel role for the Ste20 kinase SLK in adhesion signaling and cell migration. Cell Adh Migr 3, 182-184.

Wallet, V., Mutzel, R., Troll, H., Barzu, O., Wurster, B., Veron, M., and Lacombe, M.L. (1990). Dictyostelium nucleoside diphosphate kinase highly homologous to Nm23 and Awd proteins involved in mammalian tumor metastasis and Drosophila development. J. Natl. Cancer Inst. 82, 1199-1202.

Wang, Q., Villeneuve, G., and Wang, Z. (2005). Control of epidermal growth factor receptor endocytosis by receptor dimerization, rather than receptor kinase activation. EMBO 6,10

Wang, W., Goswami, S., Sahai, E., Wyckoff, J.B., Segall, J.E., and Condeelis, J.S. (2005). Tumor cells caught in the act of invading: their strategy for enhanced cell motility. Trends Cell Biol. 15, 138-145.

Warburg, O.H., and Biologie, K.f. (1926). Über den Stoffwechsel der Tumoren.263.

Webb, D.J., Zhang, H., and Horwitz, A.F. (2005). Cell migration: an overview. Methods Mol. Biol. 294, 3-11.

Wennerberg, K., Rossman, K.L., and Der, C.J. (2005). The Ras superfamily at a glance. J. Cell. Sci. 118, 843-846.

White, E., and Dipaola, R.S. (2009). The Double-Edged Sword of Autophagy Modulation in Cancer. Clinical Cancer Research 15, 5308-5316.

Williams, M.E., Gaffey, M.J., Weiss, L.M., Wilczynski, S.P., Schuuring, E., and Levine, P.A. (1993). Chromosome 11Q13 amplification in head and neck squamous cell carcinoma. Arch Otolaryngol Head Neck Surg. 119:1238-1243

Xiao, C., Dai, Y., Yu, H., Wang, J., and Ni, C. (1998). Relationship between expression of CD44v6 and nm23-H1 and tumor invasion and metastasis in hepatocellular carcinoma. World J Gastroenterol 4, 412-414.

Yamada, E., Tsujikawa, K., Itoh, S., Kameda, Y., Kohama, Y., and Yamamoto, H. (2000). Molecular cloning and characterization of a novel human STE20-like kinase, hSLK. Biochim. Biophys. Acta 1495, 250-262.

Yang, L., and Moses, H.L. (2008). Transforming growth factor beta: tumor suppressor or promoter? Are host immune cells the answer? Cancer Res. 68, 9107-9111.

Yilmaz, M., and Christofori, G. (2010). Mechanisms of motility in metastasizing cells. Molecular Cancer Research 8, 629-642.

Zaidel-Bar, R., Cohen, M., Addadi, L., and Geiger, B. (2004). Hierarchical assembly of cell-matrix adhesion complexes. Biochem. Soc. Trans. 32, 416-420.

Zeng, Z.S., Hsu, S., Zhang, Z.F., Cohen, A.M., Enker, W.E., Turnbull, A.A., and Guillem, J.G. (1994). High level of Nm23-H1 gene expression is associated with local colorectal cancer progression not with metastases. Br. J. Cancer 70, 1025-1030.

Zhang, Q., Mccorkle, J.R., Novak, M., Yang, M., and Kaetzel, D.M. (2011). Metastasis suppressor function of NM23-H1 requires its 3'-5' exonuclease activity. Int. J. Cancer 128, 40-50.

ACKNOWLEGMENTS

My PhD was a long battle that I could not have won without the help and the support of many people, first of all my supervisor Prof. Sleeman. His incredible patience and optimism, as well of course his scientific knowledge and technical skills have been precious resources for my life as PhD student. I wish to thank him for all the support, help and the many handkerchiefs. It has been a privilege to be a PhD in his lab.

Anke welcomed me warmly since the very first day, and always had time for me and my complaints (scientific and not): without her I would have been lost, not only in the German bureaucracy. She is a real friend.

Having started to work in the lab since its very first days, I had the luck to encounter all its members, and each newcomer added a smile and friendship to my life in the lab. Some people, though, deserve a special mention. Annette helped me from the very beginning, the pillar of the lab! Vanessa, with whom I first shared my office, despite the many things to do, always had time to listen to me and give me precious suggestions. It was great to have you as a colleague and friend! Then, of course, Caro and Natascha, the best postdocs one could have: thank you. Justyna and her apples will also stay in my memories: no one can cut them thinner then you without a cryostat! A special thanks goes in particular to Hani and Luca, with whom I shared a great time also outside of the lab. Both of them, together with the incredible amounts of cups of coffee, chatting, laughing and complaining that we shared made my PhD time unforgettable: thank you! Tina, Ingrid, Diego, Flavia, Martin: my half-colleagues! Thank you for the nice time we shared together, I am very happy to have met you!

My family and my in-laws gave me a special, constant support and encouraged me during bad times. Their affection despite 600km distance was very important for me.

I was very lucky because during my stay in Germany I encountered and got to know many nice and interesting people that made my staying abroad easier. Some of them, though, are particularly special: Arne Herr Bartolini, flavonoids-Stefan and loquace Lucas, soon followed by DIE Mara and Daniela, really made the difference. Their friendship is very precious to me, and I will never forget the fun we had together! You cheered up the long, cold German winter helped creating the famous "Husarenpartystrasse" and joined enthusiastically all the crazy stuff Ste and I proposed! Thank you!

Last mention, but most important person, without whom I am lost. I love you.